December 2020

Discrete-time Stable Geometric Controller and Observer Designs for Unmanned Vehicles

Reza Hamrah
Syracuse University

Abstract

In the first part of this dissertation, we consider tracking control of underactuated systems on the tangent bundle of the six-dimensional Lie group of rigid body motions, $\mathrm{SE}(3)$. We formulate both asymptotically and finite-time stable tracking control schemes for underactuated rigid bodies that have one translational and three rotational degrees of freedom actuated, in discrete time. Rigorous stability analyses of the tracking control schemes presented here guarantee the nonlinear stability of these schemes. The proposed schemes here are developed in discrete time as it is more convenient for onboard computer implementation and ensures stability irrespective of the sampling period. A stable convergence of translational and rotational tracking errors to the desired trajectory is guaranteed for both asymptotically and finite-time stable schemes. In the second part, a nonlinear finite-time stable attitude estimation scheme for a rigid body that does not require knowledge of the dynamics is developed. The proposed scheme estimates the attitude and constant angular velocity bias vector from a minimum of two known linearly independent vectors for attitude, and biased angular velocity measurements made in the body-fixed frame. The constant bias in angular velocity measurements is also estimated. The estimation scheme is proven to be almost globally finite time stable in the absence of measurement errors using a Lyapunov analysis. In addition, the behavior of this estimation scheme is compared with three state-of-the-art filters for attitude estimation, and the comparison results are presented.

Discrete-time Stable Geometric Controller and Observer Designs for Unmanned Vehicles

by

Reza Hamrah

B.Sc., MUT University of Technology, 2009

M.Sc., Shahid Beheshti University, 2012

Dissertation

Submitted in partial fulfillment of the requirements for the degree of

Doctor of Philosophy in Mechanical and Aerospace Engineering

Syracuse University

December 2020

Dedication

I dedicate my dissertation work to my parents, and my brothers Hamed and Hadid, and my beloved sister Yeganeh.

Acknowledgements

I would like to thank the following people, without whom I would not have been able to complete this research, and without whom I would not have made it through.

Above all, I would like to express my sincere gratitude to my advisor, Dr. Amit K. Sanyal, for his consistent support, timely guidance, and encouragement which have been invaluable throughout this research. I deeply appreciate the amount of time he spent to share his knowledge and teach me many skills in research that maybe not every graduate student is blessed enough to learn from their advisor.

I would like to thank our former postdoc fellow, my mentor in Akrobotix LLC, and my friend Dr. Sasi Prabhakaran who was very instrumental in shaping my experimental skills. I appreciate the opportunity I have had to learn from him that has made a substantial change in my skills.

Further, my sincere thanks go to Dr. Qiu for the opportunity to work collaboratively with her students who brought different skill sets and backgrounds to the table, especially her PhD student Krittaphat Pugdeethosapol with whom I conducted many experiments on autonomous trajectory generation/tracking in AUSLab and learned from each other.

I would also like to thank all the instructors I had here at Syracuse University, specifically, I am grateful to Dr. Fardad for the amazing way he teaches, and Dr. Duenas who was my TA advisor for the Control Systems course and I learned a lot from him.

I would especially like to thank my amazing family for the love, support, and encouragement I have received over the years. Undoubtedly, this could not have been done without them. Thanks also to all the amazing fellow teammates during my doctoral studies; Dr. Hossein Eslamiat, Dr. Rakesh Warier, Mani Dhullipalla, Ningshan Wang, and

Abhijit Dongare, as well as other significant friends who accompanied me throughout my journey. Thanks for being there for me when I really needed you.

Finally, I am grateful to the kind staff of the MAE department, Kathy Datthyn-Madigan, Hind Bin Gabr, and Linda Manzano, for their support with the paperwork ensuring the smooth completion of my doctoral studies.

Contents

List of Figures

Chapter 1

Introduction

Unmanned aerial vehicles (UAVs) are finding an increasing set of applications such as security, inspection of civilian infrastructure, agriculture and aquaculture, space and underwater exploration, wildlife tracking, package delivery, and remote sensing, all of which can benefit from reliable autonomous operations. Autonomous operations, including autonomous trajectory tracking for unmanned vehicles, is a challenging problem that has attracted the attention of many researchers, especially in applications where it is difficult or impossible to do remote piloting. The key objective of reliable operations of UAVs is stable and robust guidance and control, particularly for operations that need safety and reliability in the presence of external disturbances.

Estimation of rigid body motion is also a long-standing problem of interest for a wide variety of mechanical systems such as aerial and under-water vehicles, spacecraft, or any other moving objects in three dimensions. Motion estimation for rigid bodies is challenging primarily because this motion is described by nonlinear dynamics and the state space is nonlinear. This nonlinearity arises from the intrinsic nature of rigid body attitude, which is represented by the special orthogonal group, $\mathrm{SO}(3)$. One adverse consequence of unstable estimation and control schemes is that they end up taking longer to converge

compared with stable schemes under similar initial conditions and initial transient behavior (Izadi, 2015).

In the first phase of this work, which includes Chapters 2 and 3, nonlinearly stable tracking control schemes are proposed for rigid body motion. The literature on tracking control of UAVs includes many linear control methods that fail to work for large maneuvers due to the nonlinearities in the dynamics. A variety of nonlinear controllers using methods such as sliding-mode, back-stepping, dynamic inversion (Wang et al., 2013), and feedback-linearization (Lee, Kim, and Sastry, 2009), have also been proposed as solutions to this problem. Another important issue in control of rigid body systems is the characterization of the configuration space, and therefore the state space. The configuration space for a rigid body is not a linear (vector) space. Therefore, the literature on attitude control can be divided into two categories in the sense of configuration space and attitude representation (Chaturvedi, Sanyal, and McClamroch, 2011). In the first category, attitude control is studied using representations of attitude in $\mathbb{R}^3$ or $\mathbb{S}^3$ (the unit hypersphere embedded in $\mathbb{R}^4$). For example, commonly used attitude representations for rigid body rotational dynamics and control are Euler angles on $\mathbb{R}^3$ and unit quaternions on $\mathbb{S}^3 \subset \mathbb{R}^4$. Euler angles are not unique at certain orientations where the angular rates become unbounded, a phenomenon called "gimbal lock". Unit quaternions can represent all possible attitudes, but are known to be ambiguous: an antipodal pair of unit quaternions represents a single attitude. This leads to a type of instability called "unwinding" in continuous state feedback (Bhat and Bernstein, 2000a; Chaturvedi, Sanyal, and McClamroch, 2011). The second category avoids the aforementioned drawbacks, by studying attitude control within a geometric framework as in this research. This framework represents rigid body attitude or reduced attitude (pointing direction) as an element of $\mathrm{SO}(3)$

or $\mathbb{S}^2$ (an ordinary 2-dimensional sphere in 3-dimensional Euclidean space), respectively. The set of rigid rotations are uniquely and globally represented by the special orthogonal matrices of order three, commonly represented as $\mathrm{SO}(3)$. The set $\mathrm{SO}(3)$ is a matrix manifold and forms a Lie group under the operation of matrix multiplication. Similarly, the set of rigid body rotations and translations is represented by the Special Euclidean group $\mathrm{SE}(3)$ which is also a Lie group, and a manifold with the semi-direct product structure $\mathrm{SO}(3) \rtimes \mathbb{R}^3$. An early work using geometric control on Lie groups to treat the trajectory tracking problem for a fully-actuated system on $\mathrm{SE}(3)$ was presented in (Bullo and Murray, 1999), which generalized the classical proportional derivative (PD) control in a coordinate-free way. Geometric tracking controllers based on the Special Euclidean group $\mathrm{SE}(3)$ that avoid singularities and instabilities of other control laws, were reported in (Shi, Zhang, and Zhou, 2015; Lee, Leok, and McClamroch, 2010; Mellinger and Kumar, 2011; Kushleyev et al., 2013; Rudin et al., 2011; Fernando et al., 2011; Lee, Leok, and McClamroch, 2012; Lee et al., 2013; Goodarzi, Lee, and Lee, 2015; Invernizzi and Lovera, 2017). It is worth mentioning that all these controllers are obtained in continuous time.

Absence of nonlinear stability in the presence of perturbations can lead to failure and crash of even remotely piloted vehicles in LOS (line of sight) operations. A continuous-time integrated guidance and feedback tracking control scheme is presented in (Prabhakaran, Sanyal, and Samiei, 2018; Prabhakaran, Sanyal, and Izadi, 2017) as a solution to this problem, and the continuous equations of motion are discretized in the form of a Lie Group Variational Integrator (LGVI) for computer implementation, by applying the discrete Lagrange-d'Alembert principle. Prior related research on LGVI discretization includes (Lee, Leok, and McClamroch, 2005; Nordkvist and Sanyal, 2010; Sanyal, Nordkvist, and Chyba, 2011; Marsden and West, 2001; Hussein et al., 2006; Izadi and Sanyal,

2014; Izadi and Sanyal, 2016). However, *implementing a discretization of a continuous-time stable tracking control scheme does not guarantee the discrete-time stability of the resulting control*. This has been demonstrated convincingly for the case of nonlinear observer design for attitude dynamics in (Izadi and Sanyal, 2014; Izadi and Sanyal, 2016; Izadi et al., 2015c). In addition, discrete-time tracking control scheme enables onboard computer implementation with a variety of discrete-time input data frequencies. This problem motivates the research presented here to design *discrete-time* tracking control schemes.

This work presents a systematic treatment of *discrete-time* stable geometric control for tracking position and attitude trajectories of unmanned vehicles that have four independent control inputs for the six degrees of freedom of translational and rotational motion in three dimensional Euclidean space. The control inputs actuate the three degrees of rotational motion and one degree of translational motion in a vehicle body-fixed coordinate frame. For ease of onboard computer implementation, the trajectory tracking problem is posed in discrete-time and a discrete-time stable trajectory tracking control algorithm is obtained for an underactuated vehicle. This actuation model covers a wide range of unmanned vehicles like fixed-wing and rotorcraft unmanned aerial vehicles, underwater vehicles, and spacecraft. In this research work, the vehicle's position and orientation are represented globally and its dynamics analyzed in the framework of geometric mechanics. The configuration space is the Lie group $\mathrm{SE}(3)$, which is the group of translations and rotations of the vehicle in three-dimensional Euclidean space (Bloch et al., 2003; Bullo and Lewis, 2004). To the best of our knowledge, a discrete-time stable tracking control scheme as outlined above for a rigid body with this actuation model on $\mathrm{SE}(3)$ has not been reported in prior literature.

Discrete-time tracking control with asymptotic stability: In the first part of this research work, a discrete-time tracking control scheme is obtained using discrete-time Lyapunov analysis that provides stable asymptotic convergence of actual states to desired states, as in (Haddad and Chellaboina, 2008). It is shown that the total energy-like quantity of the tracking errors for both desired translational and rotational motions is decreasing in discrete time. This leads to discrete-time tracking error dynamics behaving as a dissipative system; therefore the state tracking errors are dissipated in discrete time. The stable discrete-time control laws are then obtained from these discrete-time error dynamics equations as well as the LGVI-based discretized dynamics model of the vehicle. This discrete-time stable tracking control algorithm utilizes the trajectory generation scheme presented in (Prabhakaran, Sanyal, and Samiei, 2018; Prabhakaran, Sanyal, and Izadi, 2017) and a method that is similar to that of (Lee, Leok, and McClamroch, 2010) that tracks the given desired trajectory for the translational motion, and the desired trajectory for the attitude based on the desired thrust direction to achieve the translational motion trajectory.

Discrete-time tracking control with finite-time stability: Finite-time stable control has the advantage of providing guaranteed convergence to a desired state (or trajectory) in finite time, as well as being more robust to bounded temporary and persistent disturbances than asymptotic stability (Bhat and Bernstein, 2000b). Furthermore, low-level persistent disturbances are better rejected by a finite-time stable system in comparison to an asymptotically stable system, because the ultimate bound on the state is of higher order than the bound on the disturbance (Sanyal and Bohn, 2015). A finite-time stable control scheme for simple mechanical systems in generalized coordinates is designed

and presented in (Sanyal and Bohn, 2015). In (Sanyal, Bohn, and Bloch, 2013), continuous finite-time stable control (FTS) schemes are shown to be effective especially when there are bounded disturbance inputs. Continuous FTS control systems have been analyzed in (Shi, Zhang, and Zhou, 2015; Bhat and Bernstein, 1998; Bhat and Bernstein, 2000b; Dorato, 2006; Haddad, Nersesov, and Du, 2008; Yan et al., 2015; Harshavarthini, Rathinasamy, and Ahn, 2019). An almost global finite time stabilization of rigid body attitude motion to a desired attitude is studied in (Sanyal, Bohn, and Bloch, 2013; Bohn and Sanyal, 2015). Continuous-time FTS integrated guidance and feedback tracking control schemes for pose tracking of rigid bodies were reported in (Prabhakaran, Sanyal, and Samiei, 2018; Prabhakaran, Sanyal, and Izadi, 2017; Prabhakaran, Sanyal, and Warier, 2017), which ensure finite-time stability of the overall feedback system. In these papers, the continuous equations of motion were discretized in the form of LGVI by applying the discrete Lagrange-d'Alembert principle, and the continuous-time control scheme was sampled at a constant sampling rate for computer implementation. Prior related research on LGVI discretization of rigid body dynamics includes (Lee, Leok, and McClamroch, 2005; Nordkvist and Sanyal, 2010; Sanyal, Nordkvist, and Chyba, 2011; Marsden and West, 2001; Hussein et al., 2006; Izadi and Sanyal, 2014; Izadi and Sanyal, 2016).

The second phase of this treatise (including Chapters 4 and 5) focuses on estimation of attitude motion of a rigid body in three-dimensional Euclidean space, which is vital for a number of applications including unmanned aerial vehicles, spacecraft and underwater vehicles. The set of possible rotations of a rigid body is again given by the set of 3×3 real orthogonal matrices of determinant 1, the Special Orthogonal group $\mathrm{SO}(3)$. The nonlinear nature of the configuration space $\mathrm{SO}(3)$, makes the problem of attitude estimation an inherently nonlinear problem. As the attitude of the rigid body cannot be directly

measured, the objective of an attitude estimator is to compute the orientation of the rigid body from vector measurements obtained from sensors mounted on the rigid body.

Attitude estimation schemes have a long history with early work, such as (Black, 1964; Wahba, 1965), proposing static attitude estimation schemes. The performance of the static determination schemes are often unsatisfactory in the presence of noise and bias components in measurements. Often, estimation schemes like modified Kalman Filter (Shuster, 1990; Choukroun, Bar-Itzhack, and Oshman, 2006) and Multiplicative Extended Kalman Filter (Markley, 1988) are used for attitude estimation. However, the implicit linearization in the Kalman filter-like schemes may cause poor performance (Crassidis, Markley, and Cheng, 2007). More recent approaches have focused on nonlinear estimation schemes such as (Bonnabel, Martin, and Rouchon, 2009; Mahony, Hamel, and Pflimlin, 2008; Vasconcelos et al., 2010) where the attitude estimate evolves on the nonlinear state space $\mathrm{SO}(3)$ (or its tangent bundle $\mathrm{TSO}(3)$, if angular velocity is also being estimated). Other prior work on nonlinear deterministic estimation schemes on $\mathrm{SO}(3)$ include (Rehbinder and Ghosh, 2003; Markley, 2006; Sanyal, 2006; Aguiar and Hespanha, 2006; Bonnabel, Martin, and Rouchon, 2009; Lageman, Trumpf, and Mahony, 2010; Vasconcelos et al., 2010; Moutinho, Figueirôa, and Azinheira, 2015; Barrau and Bonnabel, 2017; Mahony and Hamel, 2017) and (Hashim, Brown, and Mcisaac, 2019). Recent work on attitude observer on $\mathrm{SO}(3)$ with exponential stability are (Gamagedara, Lee, and Chang, 2019), in which the observer is developed with time varying reference directions, and (Reis et al., 2018) that proposed an attitude observer based on single body-vector measurement. Attitude estimation schemes based on the Lagrange-d'Alembert principle from variational mechanics were first introduced in (Izadi and Sanyal, 2014) and subsequently developed in (Izadi et al., 2015a; Izadi et al., 2015b).

As mentioned before, due to the topological properties of the manifold $SO(3)$, no continuous attitude observer defined on the tangent space of $SO(3)$ can guarantee convergence of the attitude estimation error to identity from all initial attitude and angular velocity estimation errors. This is shown in prior work like (Bhat and Bernstein, 2000a) and (Chaturvedi, Sanyal, and McClamroch, 2011). A continuous observer at best can be almost global in terms of the region of attraction. For an attitude estimator, almost global stability means that the attitude estimate stabilizes to the actual attitude from almost all values of initial attitude estimate except those in a set of zero measure in the tangent space of $SO(3)$. An attitude estimation scheme presented in (Izadi et al., 2016) follows the variational framework of the estimation scheme reported in (Izadi and Sanyal, 2014) but includes bias in angular velocity measurements and estimates a constant bias vector. It is also shown that the proposed scheme is almost globally asymptotically stable, like the variational attitude estimator for the bias-free case.

In practice, the measured value of angular velocity often has bias. In the literature, separate schemes for bias estimation are employed to compensate for this bias. For example, in the estimation schemes provided in (Mahony, Hamel, and Pflimlin, 2008; Tayebi, Roberts, and Benallegue, 2011; Izadi et al., 2016), an unknown constant bias is estimated along with the attitude. However, most of the proposed attitude estimation schemes and the bias estimation schemes are only asymptotically stable. There are advantages in having finite time stable estimation schemes: they have been shown to be more robust to disturbances and noise, and provide faster convergence than an asymptotically stable scheme with similar initial transience. Additionally, a finite time stable estimation scheme makes the case for a "separation principle" easier in case that estimated state variables are used for control. Finite time estimation schemes in the absence of bias using sliding mode

controller and neural networks are proposed in (Li et al., 2015), which are not continuous. Prior work by (Bohn and Sanyal, 2014) and (Sanyal, Izadi, and Bohn, 2014) proposed an almost global finite time stable attitude observer. However, the exact dynamical model including the moment of inertia is assumed to be available for estimation and the angular velocity bias was not considered. The algorithm in (Warier, Sanyal, and Prabhakaran, 2019) provides finite time stable attitude estimation in the absence of bias without requiring the dynamics model of the rigid body.

The contributions in this dissertation have been submitted or published in the following conference proceedings and journals.

- R. Hamrah and A. K. Sanyal, "Finite-time stable tracking control for an underactuated system in SE(3) in discrete time," to appear in International Journal of Control, 2020.

- R. Hamrah, A. K. Sanyal, and S. P. Viswanathan, "Discrete finite-time stable attitude tracking control of unmanned vehicles on SO(3)," in 2020 American Control Conference (ACC), Denver, CO, USA, July 1-3, 2020.

- R. Hamrah, R. Warier, and A. K. Sanyal, "Finite-time stable estimator for attitude motion in the presence of bias in angular velocity measurements," Submitted in Automatica, 2019 (under 2nd review)

- R. Hamrah, A. K. Sanyal, and S. P. Viswanathan, "Discrete finite-time stable position tracking control of unmanned vehicles," in 58th IEEE Conference on Decision and Control (CDC), Nice, France, December 11-13, 2019.

- A. K. Sanyal, R. R. Warier, and R. Hamrah, "Finite time stable attitude and angular velocity bias estimation for rigid bodies with unknown dynamics," in 18th European Control Conference (ECC), June 2019, pp. 4047–4052.

- R. Hamrah, R. R. Warier, and A. K. Sanyal, "Discrete-time stable tracking control of underactuated rigid body systems on SE(3)," in 57th IEEE Conference on Decision and Control, CDC 2018, Miami, FL, USA, December 17-19, 2018, pp. 2932–2937.

The remainder of this dissertation is structured as follows. Chapter 2 gives problem formulations and some mathematical preliminaries, and also presents a discrete-time stable tracking control scheme for an underactuated vehicle modeled as a rigid body that guarantees asymptotically discrete-time stability of the feedback system. Chapter 3 deals with a finite-time stable tracking control scheme for underactuated systems that is developed in discrete time. This scheme is based on our recently developed theory for finite-time stability for discrete-time systems using discrete Lyapunov analysis. In Chapter 4, we design a nonlinear finite-time stable attitude estimation scheme for a rigid body with unknown dynamics. Attitude is estimated from a minimum of two linearly independent known vectors measured in the body-fixed frame, and the angular velocity vector is assumed to have a constant bias in addition to measurement errors. Furthermore, the advantages of finite-time stabilization in discrete time over finite-time stabilization of a sampled continuous-time tracking control system is addressed in this chapter. In Chapter 5, we derive and analyze the stability and robustness of the proposed, nonlinear geometric estimator presented in Chapter 4, and the behavior of this estimation scheme is compared with three state-of-the-art filters for attitude estimation. Chapter 6 describes the details of experimental verification of the discrete finite-time stable tracking control

presented in Chapter 3. Finally, Chapter 7 concludes the dissertation and outlines possible future directions.

Chapter 2

Discrete-Time Stable Tracking Control with Asymptotic Convergence

This chapter is adapted from the paper (Hamrah, Warier, and Sanyal, 2018) published in Proceeding of the 57^{th} IEEE Conference on Decision and Control (CDC 2018) . The author gratefully acknowledges Dr. Amit Sanyal for his participation.

Abstract This chapter presents a discrete-time stable tracking control scheme for an underactuated vehicle modeled as a rigid body. This energy-based control scheme guarantees discrete-time asymptotic stability of the feedback system. The underactuated vehicle is characterized by four control inputs for the six degrees of freedom of rigid body motion. These control inputs actuate the three degrees of freedom (DOF) of rotational motion and one degree of freedom of translational motion in a vehicle body-fixed coordinate frame. The actuated translational DOF corresponds to a body-fixed thrust direction. The stability analysis of translational and rotational motion of the vehicle are addressed separately, and it is shown that the total energy-like quantity of the system is decreasing in discrete time. This leads to discrete-time control laws that achieve asymptotically

stable tracking of desired position and attitude trajectories.

2.1 Coordinate Frame Definition

We denote the set of real numbers by $\mathbb{R}$ and the set of natural numbers by $\mathbb{N}$. The set of all possible attitudes of a rigid body is the set of 3×3 real orthogonal matrices with determinant 1, commonly referred to as the special orthogonal group $\mathrm{SO}(3)$ (Murray, 2017). This is a Lie group represented in matrix form as follows:

$$\mathrm{SO}(3) = \left\{ R \in \mathbb{R}^{3\times 3} | R^{\mathrm{T}} R = R R^{\mathrm{T}} = I, \det(R) = 1 \right\}.$$

The Lie algebra (tangent space at identity) of $\mathrm{SO}(3)$ is denoted as $\mathfrak{so}(3)$ and defined as,

$$\mathfrak{so}(3) = \left\{ S \in \mathbb{R}^{3\times 3} \mid S = -S^{\mathrm{T}} \right\}.$$

The configuration of an unmanned vehicle modeled as a rigid body is given by its position and orientation, which are together referred to as its pose. To define the pose of the vehicle, we fix a coordinate frame $\mathcal{B}$ to its body and another coordinate frame $\mathcal{I}$ that is fixed in space and takes the role of an inertial coordinate frame. Let $b \in \mathbb{R}^3$ denote the position vector of the origin of frame $\mathcal{B}$ with respect to frame $\mathcal{I}$ represented in frame $\mathcal{I}$. Let $R \in \mathrm{SO}(3)$ denote the orientation, defined as the rotation matrix from frame $\mathcal{B}$ to frame $\mathcal{I}$. The pose of the vehicle can be represented in matrix form as follows:

$$\mathrm{g} = \begin{bmatrix} R & b \\ 0 & 1 \end{bmatrix} \in \mathrm{SE}(3), \tag{2.1}$$

where SE(3) is the six-dimensional Lie group of rigid body motions (translational and rotational) that is obtained as the semi-direct product of $\mathbb{R}^3$ with SO(3) (Varadarajan, 1984). A conceptual diagram of guidance on SE(3) through a set of waypoints is given in Fig. 2.1.

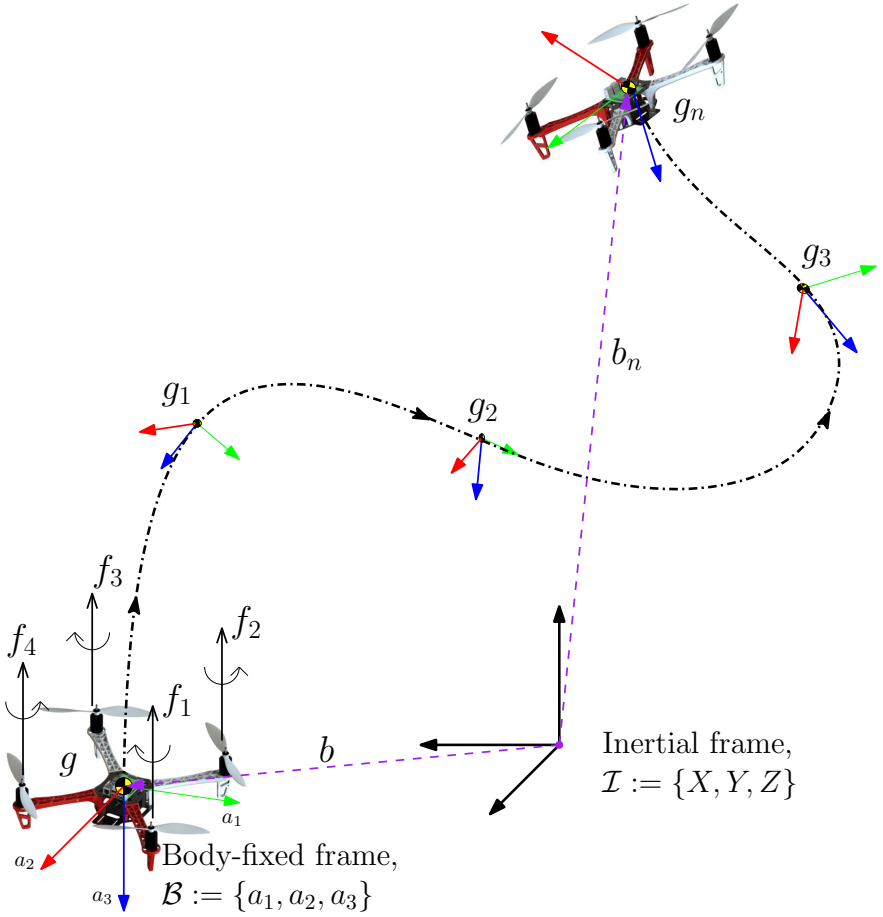

FIGURE 2.1: Guidance through a set of finite waypoints between initial and final configurations on SE(3).

2.1.1 Trajectory Generation for Underactuated Vehicle

The trajectory generation problem consists of creating an appropriately smooth position trajectory that is continuous and twice differentiable (i.e., $b^d(t) = C^2(\mathbb{R}, \mathbb{R}^3)$), where $b^d(t)$ gives the desired position trajectory on $\mathbb{R}^3$. Such a time trajectory for the position through given waypoints could be generated using one of several techniques (Lee, Leok, and McClamroch, 2010; Mellinger, Michael, and Kumar, 2012). Once the desired position trajectory over time has been generated for the underactuated vehicle with body-fixed thrust direction, a desired attitude trajectory $R^d(t)$ is generated such that the position trajectory is tracked.

Let $g^d(t) \in SE(3)$ be the desired pose (position and attitude) generated by the guidance scheme (Prabhakaran, Sanyal, and Izadi, 2017; Prabhakaran, Sanyal, and Samiei, 2018). Then the desired velocities (translational and rotational) are given by $\xi^d(t)$ that satisfies the kinematics

$$\dot{g}^d(t) = g^d(t)\xi^d(t)^\vee, \text{ with } (\xi^d)^\vee = \begin{bmatrix} (\Omega^d)^\times & v^d \\ 0 & 0 \end{bmatrix} \in \mathfrak{se}(3) \subset \mathbb{R}^{4\times 4}$$
$$\text{for } \xi^d = \begin{bmatrix} \Omega^d \\ v^d \end{bmatrix} \in \mathbb{R}^6. \tag{2.2}$$

Here v^d, Ω^d are the body's desired translational and angular velocities respectively, and $(\cdot)^\times : \mathbb{R}^3 \to \mathfrak{so}(3) \subset \mathbb{R}^{3\times 3}$ is the skew-symmetric cross-product operator giving the

vector space isomorphism between $\mathbb{R}^3$ and $\mathfrak{so}(3)$:

$$x^{\times} = \begin{bmatrix} x_1 \\ x_2 \\ x_3 \end{bmatrix}^{\times} = \begin{bmatrix} 0 & -x_3 & x_2 \\ x_3 & 0 & -x_1 \\ -x_2 & x_1 & 0 \end{bmatrix}. \tag{2.3}$$

In addition to the desired waypoints, the vehicle has to satisfy its known dynamics. Consider the “nominal" model of the dynamics for the underactuated vehicle as given by

$$\mathbb{I}\dot{\xi} = \mathrm{ad}^*_{\xi}\mathbb{I}\xi + \varphi(g,\xi) + Bu,\ u \in \mathcal{C} \subset \mathbb{R}^4,\ B \in \mathbb{R}^{6\times 4}, \tag{2.4}$$

where $\mathbb{I}$ denotes the mass (m) and inertia (J) properties of the vehicle given as

$$\mathbb{I} = \begin{bmatrix} J & 0 \\ 0 & mI_3 \end{bmatrix} \in \mathbb{R}^{6\times 6}, \tag{2.5}$$

and I_3 is the 3×3 identity matrix. The vector of known (modeled) moments and forces is denoted $\varphi(g,\xi) \in \mathbb{R}^6$; usually this is obtained from a known model. Note that the vehicle has four inputs for the six degrees of freedom of translational and rotational motion, as given by the control influence matrix B, which can be expressed in block matrix form as follows:

$$B = \begin{bmatrix} I_4 \\ 0_{2\times 4} \end{bmatrix},$$

where I_4 is the 4×4 identity matrix. The co-adjoint operator (ad^*_ξ) is defined in matrix form as

$$\mathrm{ad}^*_\xi = (\mathrm{ad}_\xi)^{\mathrm{T}} = \begin{bmatrix} -\Omega^\times & -\nu^\times \\ 0 & -\Omega^\times \end{bmatrix}, \tag{2.6}$$

where $\Omega, \nu \in \mathbb{R}^3$ denote the rotational and translational velocities of the underactuated vehicle, respectively, in frame $\mathcal{B}$. The vector of control inputs $u \in \mathcal{C} \subset \mathbb{R}^4$ has to be in the set of admissible controls $\mathcal{C}$ and directly actuates the three degrees of rotational motion and one degree of translational motion. This actuation model is applicable to aerial, space and underwater vehicles and it is known that a rigid body is controllable with such actuation (Prabhakaran, Sanyal, and Samiei, 2018).

2.1.2 Tracking errors expressed in inertial and body frames

Define pose and desired pose of the vehicle on $\mathrm{SE}(3)$ as follows

$$\mathrm{g} = \begin{bmatrix} R & b \\ 0 & 1 \end{bmatrix}, \quad \mathrm{g}^d = \begin{bmatrix} R^d & b^d \\ 0 & 1 \end{bmatrix}. \tag{2.7}$$

Tracking error on $\mathrm{SE}(3)$ is given by

$$h = (g^d)^{-1} g = \begin{bmatrix} Q & x \\ 0 & 1 \end{bmatrix}, \tag{2.8}$$

where $Q = (R^d)^{\mathrm{T}} R$ is the attitude tracking error, and $x = (R^d)^{\mathrm{T}}(b - b^d) = (R^d)^{\mathrm{T}} \tilde{b}$ is the position tracking error, both in body fixed frame. Therefore, the kinematics for the pose

tracking error is:

$$\dot{h} = h\bar{\xi}^{\vee}, \tag{2.9}$$

where

$$\bar{\xi}^{\vee} = \begin{bmatrix} \omega^{\times} & v \\ 0 & 0 \end{bmatrix}, \tag{2.10}$$

and $\omega = \Omega - Q^{\mathrm{T}}\Omega^{d}$ is the angular velocity tracking error, and $v = \nu - Q^{\mathrm{T}}(\nu^{d} + (\Omega^{d})^{\times}x)$ is the translational velocity tracking error expressed in the body frame. The tracking errors for translational motion are expressed with respect to inertial frame as $\tilde{b} := b - b^{d}$ and $\tilde{v} := v - v^{d}$, which are position and velocity tracking errors, respectively.

2.2 Discrete-time Stable Position Tracking Control on $\mathbb{R}^3$

For onboard computer implementation, the continuous time stable tracking control scheme (Prabhakaran, Sanyal, and Samiei, 2018) has to be discretized such that discrete-time stability of the resulting control is guaranteed. Consider tracking a known trajectory $b^{d}(t)$, and $v^{d}(t) = \dot{b}^{d}$ in interval of time $[t_0,\ t_f] \in \mathbb{R}^{+}$ divided into N equal-length subintervals $[t_k,\ t_{k+1}]$ for $k = 0, 1, ..., N$, with $t_N = t_f$ and $t_{k+1} - t_k = \Delta t$ where Δt is the time step size. Define the trace inner product on $\mathbb{R}^{n_1 \times n_2}$ as

$$\langle A_1, A_2 \rangle := \mathrm{trace}(A_1^{\mathrm{T}} A_2). \tag{2.11}$$

Theorem 2.2.1. *Let E_k denote a total energy-like quantity for the desired translational motion at*

instant k as the sum of kinetic and potential energy-like terms that are quadratic in velocity and position tracking errors, respectively. The total energy function is expressed as

$$E_k = T_k + U_k,$$

where

$$T_k = \frac{1}{2}\langle m\tilde{v}_k, \tilde{v}_k\rangle \;\; \textit{and} \;\; U_k = \frac{1}{2}\langle P\tilde{b}_k, \tilde{b}_k\rangle,$$

where $P \in \mathbb{R}^{3\times 3}$ is a positive definite control gain matrix. Then the position and velocity tracking errors are dissipated in discrete time, and the following discrete-time control law guarantees the stability of translational motion tracking,

$$\begin{aligned}\varphi_k = \frac{m}{\Delta t}\Big\{&\Delta t\; g\; e_3 + v_k - v_{k+1}^d \\ &- (M + D + \frac{\Delta t^2}{4}P)^{-1}\big[(M - D - \frac{\Delta t^2}{4}P)\tilde{v}_k - \Delta t P\tilde{b}_k\big]\Big\}.\end{aligned} \tag{2.12}$$

where where $e_3 = [0\ 0\ 1]^T$ is one of the standard basis vectors of $\mathbb{R}^3$, $D \in \mathbb{R}^{3\times 3}$ is a positive definite control gain matrix, and $M = mI_3$.

Proof. Since a natural candidate Lyapunov function is obtained from the total energy of a system, one can write the candidate Lyapunov function for translational position tracking as

$$V_k^{tr}(\tilde{b}_k, \tilde{v}_k) = E_k = \frac{1}{2}\langle m\tilde{v}_k, \tilde{v}_k\rangle + \frac{1}{2}\langle P\tilde{b}_k, \tilde{b}_k\rangle. \tag{2.13}$$

As mentioned in section 2.1.2, $\tilde{b}_k$ and $\tilde{v}_k$ are the position and velocity tracking errors in

inertial frame $\mathcal{I}$, respectively. By looking at how the energy-like function V_{tr} changes over time, one can conclude the condition for the stability of the system. Define $\Delta V_k^{tr} = \Delta T_k + \Delta U_k$, where

$$\begin{aligned}\Delta T_k &= T_{k+1} - T_k \\ &= \frac{1}{2}\langle m\tilde{v}_{k+1}, \tilde{v}_{k+1}\rangle - \frac{1}{2}\langle m\tilde{v}_k, \tilde{v}_k\rangle \\ &= \frac{1}{2}m\langle(\tilde{v}_{k+1} - \tilde{v}_k), (\tilde{v}_{k+1} + \tilde{v}_k)\rangle,\end{aligned} \tag{2.14}$$

and

$$\begin{aligned}\Delta U_k &= U_{k+1} - U_k \\ &= \frac{1}{2}\langle P\tilde{b}_{k+1}, \tilde{b}_{k+1}\rangle - \frac{1}{2}\langle P\tilde{b}_k, \tilde{b}_k\rangle \\ &= \frac{1}{2}\langle P(\tilde{b}_{k+1} - \tilde{b}_k), (\tilde{b}_{k+1} + \tilde{b}_k)\rangle.\end{aligned} \tag{2.15}$$

Therefore, the increment in the Lyapunov function is obtained as

$$\begin{aligned}\Delta V_k^{tr} &= \frac{1}{2}m\langle(\tilde{v}_{k+1} - \tilde{v}_k), (\tilde{v}_{k+1} + \tilde{v}_k)\rangle \\ &\quad + \frac{1}{2}\langle P(\tilde{b}_{k+1} - \tilde{b}_k), (\tilde{b}_{k+1} + \tilde{b}_k)\rangle.\end{aligned} \tag{2.16}$$

Now, consider

$$\tilde{b}_{k+1} \approx \tilde{b}_k + \frac{\Delta t}{2}(\tilde{v}_k + \tilde{v}_{k+1}). \tag{2.17}$$

Substituting (2.17) into (2.16), one can obtain

$$\Delta V_k^{tr} = \frac{1}{2}(\tilde{v}_{k+1} + \tilde{v}_k)^{\mathrm{T}}\big[m(\tilde{v}_{k+1} - \tilde{v}_k) + \frac{\Delta t}{2}P(\tilde{b}_{k+1} + \tilde{b}_k)\big]. \tag{2.18}$$

ΔV_k^{tr} has to be a negative semi-definite expression to show that the total energy of the system is decreasing and therefore system is stable (Haddad and Chellaboina, 2008; Murray, 2017). Thus, we set

$$m(\tilde{v}_{k+1} - \tilde{v}_k) + \frac{\Delta t}{2}P(\tilde{b}_{k+1} + \tilde{b}_k) = -D(\tilde{v}_{k+1} + \tilde{v}_k)$$

to get $\Delta V_k^{tr} \leq 0$. As a result, one can obtain the discrete-time dynamics equation of this dissipative system in terms of position and velocity tracking errors in the inertial frame $\mathcal{I}$ as follows:

$$(M + D)\tilde{v}_{k+1} = (M - D)\tilde{v}_k - \frac{\Delta t}{2}P(\tilde{b}_{k+1} + \tilde{b}_k). \tag{2.19}$$

Substituting (2.17) in above expression, one obtains

$$\tilde{v}_{k+1} = (M + D + \frac{\Delta t^2}{4}P)^{-1}\big[(M - D - \frac{\Delta t^2}{4}P)\tilde{v}_k - \Delta t P\tilde{b}_k\big], \tag{2.20}$$

which is the velocity tracking error at instant $k + 1$. Note that

$$\tilde{v}_{k+1} = v_{k+1} - v_{k+1}^d, \tag{2.21}$$

where v_{k+1}, the velocity in inertial frame $\mathcal{I}$, is given by

$$v_{k+1} = R_{k+1} \nu_{k+1}. \tag{2.22}$$

The equations of motion are discretized in the form of a Lie Group Variational Integrator (LGVI). In contrast to general purpose numerical integrators, a LGVI preserves the structure of the configuration space without parameterization or re-projection. The LGVI scheme used in this work was first proposed in (Nordkvist and Sanyal, 2010). This integrator are also used in other research such as (Prabhakaran, Sanyal, and Izadi, 2017; Izadi and Sanyal, 2016; Karthikeyan, Simha, and Priyadarshan, 2016; Xiang et al., 2015). Therefore, the velocity in body frame $\mathcal{B}$, ν_{k+1}, is obtained in the form of an LGVI-based discretization of the system's dynamics as

$$\nu_{k+1} = F_k^{\mathrm{T}} \nu_k + \Delta t \; g \, R_{k+1}^{\mathrm{T}} e_3 - \frac{\Delta t}{m} f_k \, e_3. \tag{2.23}$$

where $F_k = R_k^{\mathrm{T}} R_{k+1}$.

Substituting (2.23) into (2.22) gives the discrete-time velocity vector in inertial frame

$$v_{k+1} = v_k + \Delta t \; g \, e_3 - \frac{\Delta t}{m} f_k R_{k+1} \, e_3, \tag{2.24}$$

Therefore, one can obtain the discrete-time control force vector of (3.40) by substituting (2.20) and (2.24) into (2.21). Note that $\varphi_k = f_k r_3$ can be considered as the control force vector acting on the body, expressed in inertial frame, where $r_3 = R_{k+1} e_3$ is the third column vector of the rotation matrix R_{k+1} from frame $\mathcal{B}$ to frame $\mathcal{I}$, which represents the true attitude of the body. Therefore, the magnitude of the vector φ_k is the control input

f_k, and is obtained as

$$f_k = e_3^{\mathrm{T}} R_{k+1}^{\mathrm{T}} \varphi_k. \tag{2.25}$$

■

In order to achieve discrete-time stable tracking of the desired translational motion, the attitude has to be controlled such that it tracks the desired thrust direction $r_3 = R_{k+1}e_3$, given by (3.40). The trajectory generation scheme will be described in section 2.4, which is also reported in (Prabhakaran, Sanyal, and Samiei, 2018).

2.3 Discrete-time Asymptotically Stable Attitude Tracking Control on $\mathrm{TSO}(3)$

In this section, an asymptotically stable attitude control scheme is provided that is discrete-time and can be implemented with actuators used in unmanned vehicles like rotorcraft and fixed-wing UAVs. Stability of the attitude tracking control can be analyzed by considering dynamical systems on the tangent bundle of $\mathrm{SO}(3)$, denoted by $\mathrm{TSO}(3)$. $\mathrm{TSO}(3)$ consists of all possible orientations and angular velocities.

Theorem 2.3.1. Consider the following total energy-like quantity at time t_k as the sum of kinetic and potential energy-like quantities for the desired rotational motion,

$$\mathcal{E}_k = \mathcal{U}_k + \mathcal{T}_k, \tag{2.26}$$

where

$$\mathcal{U}_k = k_p \langle I - Q_k, K \rangle, \;\; \mathcal{T}_k = \frac{1}{2} \langle J\omega_k, \omega_k \rangle,$$

$\langle I - Q_k, K \rangle$ is a Morse function on SO(3) (Milnor, 1963), and $\mathcal{T}_k$ is a rotational kinetic energy-like quantity that is quadratic in angular velocity tracking error. $K = \text{diag}(k_1, k_2, k_3)$, where $k_1 > k_2 > k_3$ and let $k_p > 1$. Then the discrete-time attitude control law

$$\begin{aligned} \tau_k = \frac{1}{\Delta t} \Big\{ J \Big((J + L_\omega)^{-1} \left[(J - L_\omega)\omega_k - \Delta t \; k_p \; S_K(Q_k) \right] \\ + Q_{k+1}^{\mathrm{T}} \Omega_{k+1}^d \Big) - F_k^{\mathrm{T}} \; J \Omega_k \Big\} \end{aligned} \tag{2.27}$$

leads to asymptotically stable tracking of the desired attitude trajectory in discrete time.

Proof. Consider the following candidate Morse-Lyapunov function, which can be interpreted as the total energy function that is sum of kinetic and potential energy-like terms for the desired rotational motion, as follows:

$$V_k^{rot}(Q_k, \omega_k) = \mathcal{E}_k = k_p \langle I - Q_k, K \rangle + \frac{1}{2} \langle J\omega_k, \omega_k \rangle. \tag{2.28}$$

The stability of attitude tracking error can be shown by analyzing $\Delta V_k^{rot} = \Delta \mathcal{U}_k + \Delta \mathcal{T}_k$, where

$$\begin{aligned} \Delta \mathcal{U}_k &= k_p \Big(\langle I - Q_{k+1}, K \rangle - \langle I - Q_k, K \rangle \Big) \\ &= k_p \langle Q_k - Q_{k+1}, K \rangle. \end{aligned} \tag{2.29}$$

and

$$\begin{aligned}\Delta\mathcal{T}_k &= \frac{1}{2}(\omega_{k+1}^{\mathrm{T}}\ J\omega_{k+1} - \omega_k^{\mathrm{T}}\ J\omega_k) \\ &= \frac{1}{2}(\omega_{k+1} - \omega_k)^{\mathrm{T}}\ J(\omega_{k+1} + \omega_k),\end{aligned} \tag{2.30}$$

Therefore, $\Delta V_k^{rot} = V_{k+1}^{rot} - V_k^{rot}$ is given as

$$\begin{aligned}\Delta V_k^{rot} &= \frac{1}{2}(\omega_{k+1} - \omega_k)^{\mathrm{T}}\ J(\omega_{k+1} + \omega_k) \\ &\quad + k_p\langle Q_k - Q_{k+1}, K\rangle.\end{aligned} \tag{2.31}$$

The kinematics of the attitude tracking error is discretized as follows:

$$\begin{aligned}Q_{k+1} &\approx Q_k\big[I + \frac{\Delta t}{2}(\omega_{k+1} + \omega_k)^{\times}\big] \\ &\approx Q_k + Q_k\frac{\Delta t}{2}(\omega_{k+1} + \omega_k)^{\times}.\end{aligned}$$

Thus,

$$Q_{k+1} - Q_k \approx \frac{\Delta t}{2}\ Q_k\ (\omega_{k+1} + \omega_k)^{\times}. \tag{2.32}$$

Substituting (2.32) into (2.29), the change in potential energy is obtained as:

$$\begin{aligned} k_p\langle Q_k - Q_{k+1}, K\rangle &= \frac{\Delta t}{2} k_p \langle -Q_k\ (\omega_{k+1} + \omega_k)^\times, K\rangle \\ &= \frac{\Delta t}{2} k_p \langle\ (\omega_{k+1} + \omega_k)^\times, -Q_k^{\mathrm{T}}\ K\rangle \\ &= \frac{\Delta t}{2} k_p \cdot \frac{1}{2}\langle (\omega_{k+1} + \omega_k)^\times, KQ_k - Q_k^{\mathrm{T}}\ K\rangle \\ &= \frac{\Delta t}{2} k_p\ (\omega_{k+1} + \omega_k)^{\mathrm{T}}\ S_K(Q_k), \end{aligned} \tag{2.33}$$

where

$$\begin{aligned} S_K(Q_k) &= \mathrm{vex}(KQ_k - Q_k^{\mathrm{T}}\ K) \\ &= \sum_{i=1}^{3} k_i (Q_k^{\mathrm{T}} e_i) \times e_i, \end{aligned} \tag{2.34}$$

and $\mathrm{vex}(\cdot) : \mathfrak{so}(3) \to \mathbb{R}$ is the inverse of the $(\cdot)^\times$ map.

Therefore, the change of the candidate Morse-Lyapunov function will be rewritten as

$$\begin{aligned} \Delta V_k^{rot} &= \frac{1}{2}(\omega_{k+1} - \omega_k)^{\mathrm{T}}\ J(\omega_{k+1} + \omega_k) \\ &\quad + \frac{\Delta t}{2} k_p \langle\ (\omega_{k+1} + \omega_k)^{\mathrm{T}}\ S_K(Q_k) \\ &= \frac{1}{2}(\omega_{k+1} + \omega_k)^{\mathrm{T}}\ \Big[J(\omega_{k+1} - \omega_k) + \Delta t\ k_p\ S_K(Q_k) \Big]. \end{aligned} \tag{2.35}$$

It can be shown that the attitude tracking control system is stable by setting

$$J(\omega_{k+1} - \omega_k) + \Delta t\ k_p\ S_K(Q_k) = -L_\omega(\omega_{k+1} + \omega_k), \tag{2.36}$$

so that

$$\Delta V_k^{rot} = -\frac{1}{2}(\omega_{k+1} + \omega_k)^{\mathrm{T}}\, L_\omega(\omega_{k+1} + \omega_k) \leq 0,$$

Where L_ω is a positive definite control gain matrix. Therefore, from (2.36) one can find the discrete-time attitude tracking error dynamics as

$$\omega_{k+1} = (J + L_\omega)^{-1}\Big[(J - L_\omega)\omega_k - \Delta t\; k_p\; S_K(Q_k)\Big]. \tag{2.37}$$

From the discretized dynamics equation of rotational motion obtained in the form of LGVI (Nordkvist and Sanyal, 2010; Prabhakaran, Sanyal, and Samiei, 2018), one finds that

$$J\,\Omega_{k+1} = F_k^{\mathrm{T}}\, J\Omega_k + \Delta t\tau_k, \tag{2.38}$$

where Ω_{k+1} can be written as

$$\Omega_{k+1} = \omega_{k+1} + Q_{k+1}^{\mathrm{T}}\, \Omega_{k+1}^d. \tag{2.39}$$

Substituting (2.37) into (3.72), and then solving (3.76) for the discrete-time control law τ_k, one obtains (2.27) for the control input torque for attitude tracking.

A generalization of LaSalle invariance theorem applicable to tracking control is given by Theorem 8.4 of (Khalil, 2001). A discrete-time version of this result completes the proof for both translational and attitude tracking schemes and allows us to conclude that the overall attitude and position tracking control system is asymptotically stable. ■

2.4 Generating desired attitude trajectory

Given the desired control force vector in inertial frame as given by (3.40), one can generate a desired trajectory for the third column of R^d (the desired attitude) as follows:

$$r_{3d} = \frac{\varphi_k}{\|\varphi_k\|} = R^d e_3. \tag{2.40}$$

Select an appropriate $s_d(t) \in \mathcal{C}^2(\mathbb{R}^3)$ such that it is transverse to r_{3d}. Now compute

$$\begin{aligned} r_{2d} =& \frac{r_{3d} \times s_d}{\|r_{3d} \times s_d\|} = R^d e_2, \\ \text{and } r_{1d} =& r_{2d} \times r_{3d} = R^d e_1. \end{aligned} \tag{2.41}$$

The desired attitude trajectory is then given by:

$$R^d = [r_{2d} \times r_{3d} \;\; r_{2d} \;\; r_{3d}] \in \mathrm{SO}(3). \tag{2.42}$$

The following statement gives a simpler choice of s_d in $\mathbb{R}^3$ that is transverse to $r_{3d} \in \mathbb{R}^3$ for all $t > 0$. It also gives a vector that is orthogonal to the given unit vector.

Proposition 2.4.1. Let $r_{3d} = \begin{bmatrix} a_1 & a_2 & a_3 \end{bmatrix}^{\mathrm{T}} \in \mathbb{S}^2 \subset \mathbb{R}^3$ be a known unit vector as given in (2.40). The vector

$$s_d = \begin{bmatrix} a_2 + a_3 \\ a_3 - a_1 \\ -a_1 - a_2 \end{bmatrix} \tag{2.43}$$

is orthogonal to r_{3d}.

Proof. This is easily verified by the property of scalar product (orthogonal projection) as follows:

$$\begin{aligned} r_{3d}^{\mathrm{T}} s_d &= a_1(a_2 + a_3) + a_2(a_3 - a_1) + a_3(-a_1 - a_2) \\ &= a_1(a_2 + a_3 - a_2 - a_3) + a_2(a_3 - a_3) = 0. \end{aligned}$$

This shows that the vector s_d as defined by (2.43) is orthogonal to the given vector r_{3d}. ■

2.5 Simulation Results

This section presents numerical simulation results for the discrete-time stable tracking control schemes for tracking position and attitude trajectories. The numerical simulation is performed for an UAV quadrotor of mass, $m = 4.34kg$, and a moment of inertia as

$$J = \mathrm{diag}[0.0820,\ 0.0845,\ 0.1377]kgm^2,$$

and for five seconds, $t = 5s$, with a time step size of $h = 0.01$, using the LGVI routine given in (2.23) and (3.76) and discrete-time control laws obtained in (2.25) and (2.27). The helical desired trajectory and the initial conditions are given as follows

$$\begin{aligned} b_k^d = b^d(t_k) &= \begin{bmatrix} 0.4\sin \pi t_k & 0.6\cos \pi t_k & 0.4\, t_k \end{bmatrix}^{\mathrm{T}}, \\ b_0 &= \begin{bmatrix} 1 & 0 & 0 \end{bmatrix}^{\mathrm{T}}, \ R_0 = \mathbf{I}_{3\times 3}, \\ v_0 = \Omega_0 &= \begin{bmatrix} 0 & 0 & 0 \end{bmatrix}^{\mathrm{T}}. \end{aligned}$$

and the gains are selected after trial and error as follows,

$$P = 48\ \mathbf{I}_{3\times 3}\ ; D = 0.15\ \mathbf{I}_{3\times 3},$$
$$L_\omega = 0.11\ \mathbf{I}_{3\times 3}\ ; k_p = 3\ .$$

and provide desirable transient response characteristics of the overall control scheme.

The time trajectory of the UAV tracking the desired trajectory is shown in Fig. 2.2 and it is inferred that the trajectory converges to the desired values and remains stable for all time, $t > 0$.

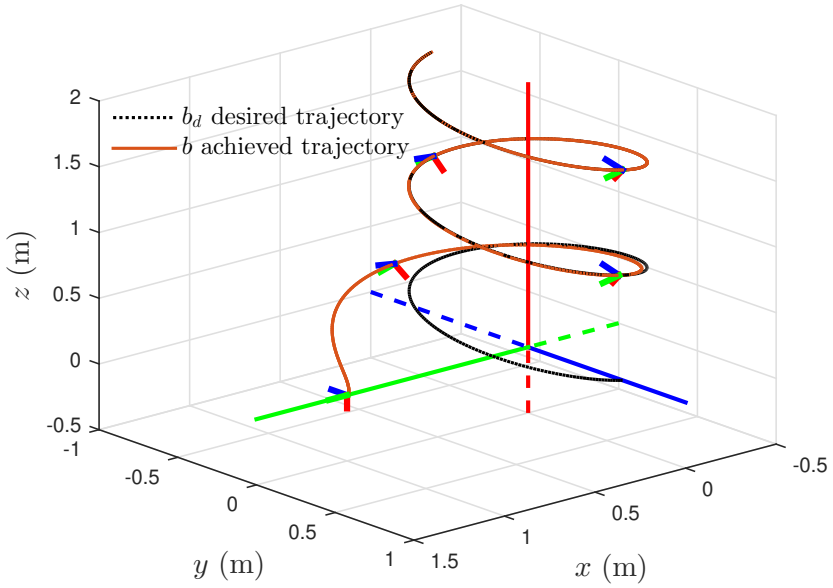

FIGURE 2.2: Time trajectory of UAV

The results of the numerical simulation for position and velocity tracking response of discrete-time control law obtained in eq. (2.25) are shown in Fig. 2.3 and Fig. 2.4, respectively. Fig. 2.3 indicates that the position tracking errors converge to zero and therefore

the discrete-time control scheme presented here is able to track the desired position trajectory and remains stable. It is also shown in Fig. 2.4 that the discrete-time control scheme guarantees that the UAV tracks the translation velocity too. The graphs of control laws are plotted in Fig. 2.5 and Fig. 2.6. As shown in Fig. 2.5, The total magnitude of the thrust force does not exceed 50 N , and Fig. 2.6 depicts the corresponding control torque inputs, which are within capabilities of the four propellers of the UAV. Moreover, Fig. 2.7 and Fig. 2.8 show that the total energy-like quantities for both desired translational motion and attitude tracking decrease over the time t, and ensure the stability of the system. These results show that the discrete-time tracking control scheme presented here takes the UAV from an initial pose to a desired final pose in SE(3), and the overall system is stable.

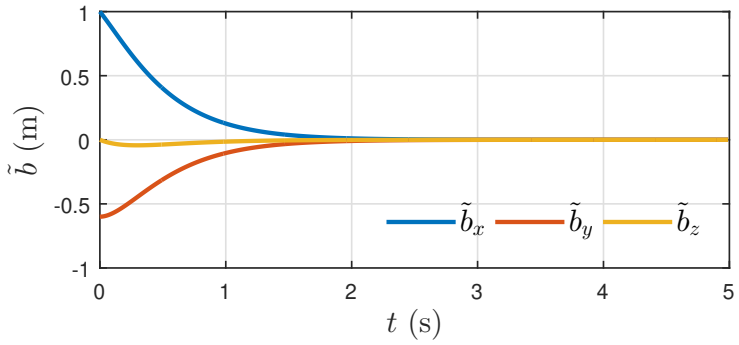

FIGURE 2.3: Position tracking error

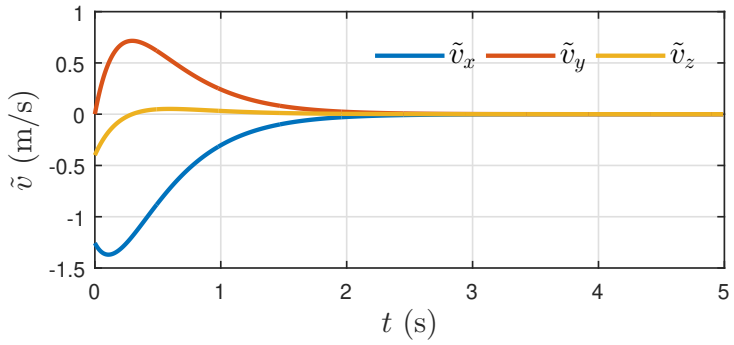

FIGURE 2.4: Velocity tracking error

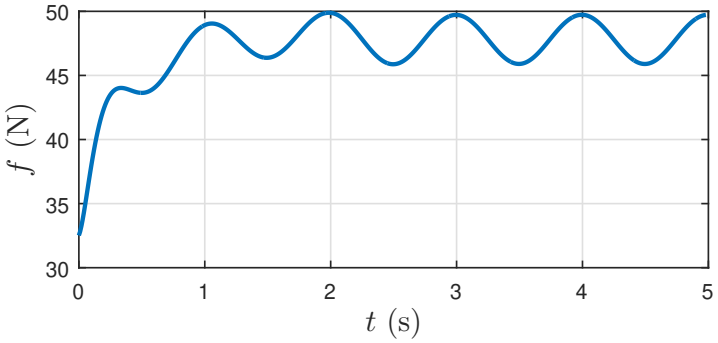

FIGURE 2.5: Total thrust force

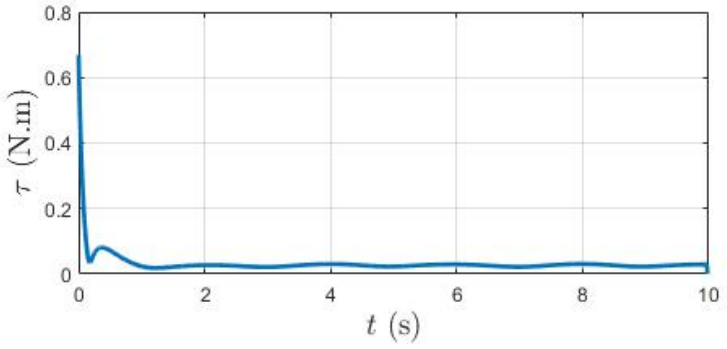

FIGURE 2.6: Control torque

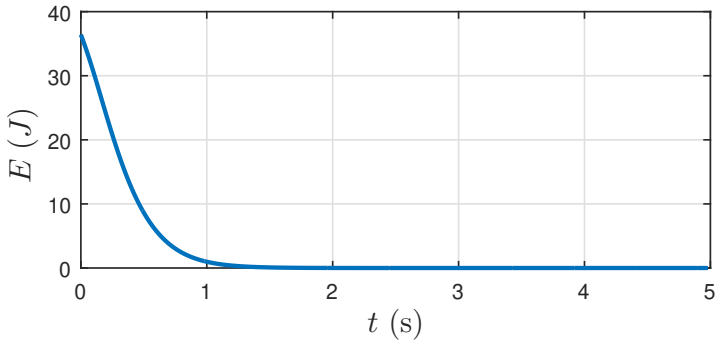

FIGURE 2.7: Total translational energy

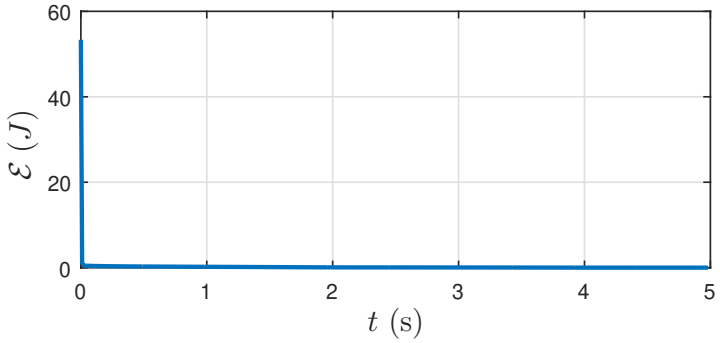

FIGURE 2.8: Total rotational energy

2.6 Conclusion

A discrete-time stable tracking control scheme for a rigid body with one actuated translational degree of freedom and three actuated rotational degrees of freedom, is presented in this chapter. This scheme is based on designing a discrete-time energy-based tracking control to obtain the desired discrete-time control force vector and control torque to asymptotically stabilize the desired translational motion and attitude trajectory. Discrete-time Lyapunov analysis shows that a tracking control scheme obtained provides stable

asymptotic convergence of actual states to desired states. It is also shown that the total energy-like quantity is decreasing in discrete time for both desired translational and desired rotational motions. The stable discrete-time control laws are then obtained from these discrete-time error dynamics equations as well as the LGVI-based discrete-time dynamics model of the vehicle. The overall discrete-time control scheme and trajectory generation is simulated numerically. Simulation results validate the stable performance of the overall tracking control scheme as well as discrete-time stability of the resulting control laws.

Chapter 3

Discrete Time Stable Tracking Control with Finite-time Convergence

This chapter is adapted from papers published in Proceedings of the 58^{th} IEEE Conference on Decision and Control (CDC 2019) (Hamrah, Sanyal, and Prabhakaran, 2019), the 2020 American Control Conference (ACC 2020) (Hamrah, Sanyal, and Prabhakaran, 2020), and a journal paper accepted to be published in International Journal of Control (Hamrah and Sanyal, 2020). The author gratefully acknowledges Dr. Amit Sanyal, and Dr. Sasi Prabhakaran for their participation.

Abstract We consider tracking control of a rigid body system with its three rotational degrees of freedom and one of its translational degrees of freedom actuated. This is an underactuated system on the tangent bundle of the six-dimensional Lie group of rigid body motions, $\mathrm{SE}(3)$. We formulate a finite-time stable tracking control scheme for this underactuated system in discrete time. This scheme is based on our recently developed theory for finite-time stability for discrete-time systems using discrete Lyapunov analysis. The proposed scheme here is developed in discrete time as it is more convenient for

onboard computer implementation and ensures stability irrespective of the sampling period. This tracking control scheme guarantees a stable convergence of translational and rotational tracking errors to the desired trajectory in finite time. Furthermore, the advantages of finite-time stabilization in discrete time over finite-time stabilization of a sampled continuous-time tracking control system is addressed in this Chapter through a numerical comparison. This comparison is performed using numerical simulations on continuous and discrete FTS tracking control schemes applied to an unmanned aerial vehicle model.

3.1 Problem Formulation

The coordinate frame definition and trajectory generation technique used in this research work is same as presented in Chapter 2. Tracking error kinematics and dynamics in continuous time are also as given in 2.1.2, where

$$Q = (R^d)^{\mathrm{T}} R \tag{3.1}$$

is the attitude tracking error in the desired body fixed frame, and

$$\omega = \Omega - Q^{\mathrm{T}}\Omega^d \tag{3.2}$$

is the angular velocity tracking error, and $v = \nu - Q^{\mathrm{T}}(\nu^d + (\Omega^d)^{\times}x)$ is the translational velocity tracking error expressed in the body frame. The tracking errors for translational motion are expressed with respect to inertial frame as $\tilde{b} := b - b^d$ and $\tilde{v} := v - v^d$, which are position and velocity tracking errors, respectively.

Therefore, in inertial frame $\mathcal{I}$, the translational error dynamics are expressed as

$$\dot{\tilde{b}} = \tilde{v} = v - v^d, \tag{3.3}$$

$$m\dot{\tilde{v}} = m\ g\ e_3 - (\varphi + \varphi_D) - v^d, \tag{3.4}$$

where φ is the control force vector, and φ_D is the disturbance force vector acting on the body, expressed in inertial frame. The magnitude of this vector is the control input f, which is designed as a feedback control law, and $e_3 = [0\ 0\ 1]^{\mathrm{T}}$ is the third standard basis of $\mathbb{R}^3$. The position trajectory control law gives a desired thrust direction, which is then used to generate a desired attitude trajectory, as described in (Prabhakaran, Sanyal, and Samiei, 2018). Let J denote inertia of a rigid body. The rotational dynamics of the rigid body is given by:

$$\dot{R} = R\,\Omega^{\times}, \tag{3.5}$$

$$J\dot{\Omega} = J\Omega \times \Omega + \tau + \tau_D. \tag{3.6}$$

where τ is the input torque, and τ_D is an unknown bounded disturbance torque. Therefore, the dynamics for the attitude tracking error is

$$J\dot{\omega} = \tau + J(\omega^{\times} Q^{\mathrm{T}}\Omega^d - Q^{\mathrm{T}}\dot{\Omega}^d) - (\omega + Q^{\mathrm{T}}\Omega^d)^{\times} J(\omega + Q^{\mathrm{T}}\Omega^d). \tag{3.7}$$

Since the translational error dynamics is expressed in the inertial frame, the rotational error dynamics is decoupled from the translational error dynamics such that the translation control force, f, is obtained in the inertial frame followed by the appropriate attitude control, τ, in body frame to track the desired trajectory, b^d.

Consider tracking a desired pose $g^d(t)$ in a time interval $[t_0,\ t_f] \in \mathbb{R}^+$ separated into N equal-length sub-intervals $[t_k,\ t_{k+1}]$ for $k = 0, 1, ..., N$, with $t_N = t_f$ and $t_{k+1} - t_k = \Delta t$ where Δt is the time step size. Therefore, one can express the discrete-time pose error kinematics and dynamics of an underactuated vehicle in the form of LGVI presented in (Nordkvist and Sanyal, 2010; Hamrah, Warier, and Sanyal, 2018) as

$$\begin{cases} \tilde{b}_{k+1} - \tilde{b}_k = \tilde{v}_k \Delta t, \\ m\tilde{v}_{k+1} = m\ v_k + \Delta t\ m\ g\ e_3 - (\bar{\varphi}_k + \bar{\varphi}_k^D) - m v_{k+1}^d, \\ R_{k+1} = R_k\ F_k, \\ J\,\Omega_{k+1} = F_k^{\mathrm{T}}\, J\Omega_k + u_k + u_k^D, \end{cases} \tag{3.8}$$

where $v_{k+1} = \tilde{v}_{k+1} + v_{k+1}^d$, $\bar{\varphi}_k = \Delta t \varphi_k$ is the force control input, $\bar{\varphi}_k^D$ is the disturbance force, $u_k = \Delta t \tau_k$ is the torque control input, u_k^D is the disturbance moment in addition to the control torque u_k, and $F_k \approx \exp(\Delta t\ \Omega_k^{\times}) \in \mathrm{SO}(3)$ guarantees that R_k evolves on $\mathrm{SO}(3)$. Using the discretized rotational kinematics equation given in (3.8) and attitude racking error of (3.1) in discrete form, one can write

$$Q_{k+1} = (R_{k+1}^d)^{\mathrm{T}} R_{k+1} = (R_{k+1}^d)^{\mathrm{T}} R_k\ F_k, \tag{3.9}$$

where $R_{k+1}^d = R_k^d\ F_k^d$. Then,

$$\begin{aligned} Q_{k+1} &= (F_k^d)^{\mathrm{T}} (R_k^d)^{\mathrm{T}} R_k\ F_k \\ &= (F_k^d)^{\mathrm{T}} Q_k\ F_k. \end{aligned} \tag{3.10}$$

Using the definitions for F_k and F_k^d given earlier into the above expression and carrying out some algebraic simplifications, one obtains

$$\begin{aligned} Q_{k+1} &\approx Q_k\left[I + \Delta t\ (\Omega_k - Q_k^{\mathrm{T}}\Omega_k^d)^{\times}\right] \\ &= Q_k(I + \varpi_k{}^{\times}), \end{aligned} \tag{3.11}$$

where $\varpi_k = \Delta t\ \omega_k$, and ω_k is the angular velocity tracking error at time instant t_k.

3.2 Finite-time Stability of Discrete-time Systems

The following result is a basic result on finite-time stability and convergence for discrete-time systems, and it was first reported in (Sanyal, 2019; Hamrah, Sanyal, and Prabhakaran, 2019).

Lemma 3.2.1. *Consider a discrete-time system with inputs $u_k \in \mathbb{R}^m$ and outputs $y_k \in \mathbb{R}^l$. Define a corresponding positive definite (Lyapunov) function $V : \mathbb{R}^l \to \mathbb{R}$ and let $V_k = V(y_k)$. Let α be a constant as $0 < \alpha < 1$, $\eta \in \mathbb{R}^+$ a constant, and let $\gamma_k := \gamma(V_k)$ where $\gamma : \mathbb{R}_0^+ \to \mathbb{R}_0^+$ is a positive definite function of V_k. Let γ_k satisfy the condition:*

$$\gamma_k \geq \eta \ \text{ for all } \ V_k \geq \varepsilon, \tag{3.12}$$

for some (possibly small) constant $\varepsilon \in \mathbb{R}^+$. Then, if V_k satisfies the relation

$$V_{k+1} - V_k \leq -\gamma_k V_k^{\alpha}, \tag{3.13}$$

the discrete system is (Lyapunov) stable at $y = 0$ *and* y_k *converges to* $y = 0$ *for* $k > N$*, where* $N \in \mathbb{W}$ *is finite.*

Proof. The proof of this Lemma is given in (Hamrah, Sanyal, and Prabhakaran, 2019; Sanyal, 2019), and omitted here for brevity.

■

The following statement presents the conditions under which a discrete-time system is finite-time stable using a Lyapunov function that is quadratic in terms of states.

Lemma 3.2.2. *Consider the discrete-time system*

$$x_{k+1} = \mathscr{B}(x_k)x_k, \tag{3.14}$$

where $x_k \in \mathbb{R}^n$ *and* $\mathscr{B} : \mathbb{R}^n \to \mathbb{R}$ *is a* $\mathcal{C}^o$ *function. Define* $V_k := V(x_k)$ *as follows:*

$$V_k := V(x_k) = x_k^T P x_k, \;\; P = P^T > 0, \tag{3.15}$$

and denote $\mathscr{B}_k := \mathscr{B}(x_k)$*. The system* (3.14) *is finite-time stable under following conditions:*

$$\begin{cases} \mathscr{B}_k^2 \leq 1 - \dfrac{\gamma_k}{V_k^{1-\alpha}}, \\ V_k \geq \epsilon = \eta^{\frac{1}{1-\alpha}}, \end{cases} \tag{3.16}$$

where V_k*,* γ_k*, and* η *are as defined in Lemma 3.2.1.*

Proof. Evaluating the first finite difference of V_k, one obtains

$$\begin{aligned} V_k^{(1)} := V_{k+1} - V_k &= (x_{k+1} - x_k)^{\mathrm{T}} P(x_k + x_{k+1}) \\ &= x_k^{\mathrm{T}}(\mathscr{B}_k + 1)P(\mathscr{B}_k - 1)x_k \\ &= (\mathscr{B}_k^2 - 1)x_k^{\mathrm{T}} P x_k \\ &= (\mathscr{B}_k^2 - 1)V_k. \end{aligned} \tag{3.17}$$

According to Lemma 3.2.1, finite-time stability of system (3.14) requires that

$$V_{k+1} - V_k \leq -\gamma_k V_k^{\alpha} \;\text{ for }\; 0 < \alpha < 1,$$

where γ_k is defined as in Lemma 3.2.1 and satisfies the condition (3.12). From (3.13) and (3.17), we have

$$\begin{aligned} V_{k+1} - V_k \leq -\gamma_k V_k^{\alpha} &\Leftrightarrow (\mathscr{B}_k^2 - 1)V_k \leq -\gamma_k V_k^{\alpha} \\ &\Leftrightarrow \mathscr{B}_k^2 \leq 1 - \frac{\gamma_k}{V_k^{1-\alpha}}. \end{aligned} \tag{3.18}$$

Noting that $\mathscr{B}^2 \geq 0$, we conclude from (3.18) that

$$V_k^{1-\alpha} \geq \gamma_k = \gamma(V_k). \tag{3.19}$$

It is also clear from above that if inequality (3.19) is reversed, i.e., if $\gamma_k \geq V_k^{1-\alpha}$ for finite k, then that would lead to a contradiction of (3.18) whereby $\mathscr{B}_k^2 \leq 0$, which can only happen if $\mathscr{B}_k = 0$. This, in turn, would result in finite-time stability of system (3.14) as $x_{k+1} = \mathscr{B}_k x_k = 0$. This leads us to the conclusion that if γ_k satisfies condition (3.12) in

Lemma 3.2.1, then system (3.14) will be finite-time stable. ■

Note that inequality (3.18) can be used to design $\mathscr{B}_k$ if, for example, it is evaluated as an equality with a $\gamma_k = \gamma(V_k)$ designed to meet the above requirement. In fact, $\gamma(.)$ can be positive definite function (not-necessary class-$\mathcal{K}$) that meets this requirement, i.e., $\gamma_k \geq \eta$ for all $V_k \geq \eta^{\frac{1}{1-\alpha}}$, $\eta > 0$. Following Lemma presents a design for γ which satisfies the conditions given in 3.16.

Lemma 3.2.3. *Consider the conditions* (3.16)*, under which the system* (3.14) *is shown that is finite-time stable. One possible design for* γ_k *and* $\mathscr{B}_k$ *as a function of* V_k *can be as*

$$\gamma_k = 4c\Big(\frac{V_k^{1-\alpha}}{V_k^{1-\alpha} + c}\Big)^2, \tag{3.20}$$

and

$$\mathscr{B}_k = \frac{V_k^{1-\alpha} - c}{V_k^{1-\alpha} + c}, \tag{3.21}$$

where $c \geq 0$ *is a constant, and* γ_k *and* $\mathscr{B}_k$ *satisfy both conditions in* (3.16)*.*

Proof. Consider

$$\gamma_k = f(V_k).\Big(\frac{V_k^{1-\alpha}}{V_k^{1-\alpha} + c}\Big)^2, \tag{3.22}$$

where $f(V_k)$ is a positive and bounded function. Then, to satisfy the condition (3.19), it is required to have

$$V_k^{1-\alpha} \geq f(V_k).\Big(\frac{V_k^{1-\alpha}}{V_k^{1-\alpha} + c}\Big)^2. \tag{3.23}$$

One can find $f(V_k)$ such that above inequality as well as (3.18) hold for the designed γ_k, and then the best expression for $\mathscr{B}_k$ will be determined accordingly.

Substituting (3.22) into (3.18), one finds

$$\begin{aligned}\mathscr{B}_k^2 &\leq 1 - f(V_k).\frac{V_k^{1-\alpha}}{(V_k^{1-\alpha}+c)^2} \\ &\leq \frac{(V_k^{1-\alpha}+c)^2 - f(V_k).V_k^{1-\alpha}}{(V_k^{1-\alpha}+c)^2} \\ &\leq \frac{(V_k^{1-\alpha})^2 + 2c\ V_k^{1-\alpha} - f(V_k).V_k^{1-\alpha} + c^2}{(V_k^{1-\alpha}+c)^2}.\end{aligned} \tag{3.24}$$

As noted in Lemma 3.2.2, $\mathscr{B}^2 \geq 0$ leads to $V_k^{1-\alpha} \geq \gamma_k$, and satisfies the condition (3.22). Therefore, for $\mathscr{B}^2 \geq 0$, it is required to have

$$\big(f(V_k) - 2c\big)\ V_k^{1-\alpha} \leq (V_k^{1-\alpha})^2 + c^2. \tag{3.25}$$

One solution to the above inequality is

$$\big(f(V_k) - 2c\big)\ V_k^{1-\alpha} = \pm 2c\ V_k^{1-\alpha}, \tag{3.26}$$

which gives $f(V_k) = 0\ , 4c$. Since γ_k is a positive definite function by definition, $f(V_k) = 4c$ would be the acceptable answer. Therefore, one obtains expressions for γ_k and $\mathscr{B}_k$ as

$$\begin{cases} \gamma_k = 4c\Big(\dfrac{V_k^{1-\alpha}}{V_k^{1-\alpha}+c}\Big)^2, \\ \mathscr{B}_k = \dfrac{V_k^{1-\alpha}-c}{V_k^{1-\alpha}+c}, \end{cases} \tag{3.27}$$

which satisfy the conditions given in (3.16) and guarantee the stability of the system (3.14).

■

3.3 Discrete-time Stable Position Tracking Control

Defining the discrete-time Lyapunov function quadratic in position tracking error as

$$V(\tilde{b}_k) = V_k = \frac{1}{2}\tilde{b}_k^{\mathrm{T}} P \tilde{b}_k, \tag{3.28}$$

where $P = P^{\mathrm{T}} \in \mathbb{R}^{3\times 3}$ is a positive definite control gain matrix. The total time difference of this discrete Lyapunov function in the time interval $[t_k,\ t_{k+1}]$ for $k = 0, 1, ..., N$ is then obtained as

$$\begin{aligned} \Delta V_k = V_{k+1} - V_k &= \frac{1}{2}\tilde{b}_{k+1}^{\mathrm{T}} P \tilde{b}_{k+1} - \frac{1}{2}\tilde{b}_k^{\mathrm{T}} P \tilde{b}_k \\ &= \frac{1}{2}(\tilde{b}_{k+1} - \tilde{b}_k)^{\mathrm{T}} P (\tilde{b}_k + \tilde{b}_{k+1}). \end{aligned} \tag{3.29}$$

A constructive method to obtain FTS position tracking control scheme in discrete time is provided here, which has two steps. In the first step, we develop a discrete vector-valued function of the position and velocity tracking errors that ensures that when this function converges to zero, the errors converge to zero as well. The following statement presents the first step of this method.

Lemma 3.3.1. *Define* $l(\tilde{b}_k, \tilde{v}_k)$ *as*

$$l(\tilde{b}_k, \tilde{v}_k) := \tilde{v}_k \Delta t + \frac{\beta(\tilde{b}_{k+1} + \tilde{b}_k)}{(\tilde{b}_k^T P \tilde{b}_k)^{1-1/p}}, \tag{3.30}$$

for the dynamics given in (3.8)*, where* $\beta > 0$, $1 < p < 2$ *and* $\tilde{v}_k = (\tilde{b}_{k+1} - \tilde{b}_k)/\Delta t$. *Let*

$$\begin{aligned} &\tilde{b}_{k+1} = \mathcal{B}(\tilde{b}_k)\tilde{b}_k, \text{ where} \\ &\mathcal{B}(\tilde{b}_k) := \frac{(\tilde{b}_k^T P \tilde{b}_k)^{1-1/p} - \beta}{(\tilde{b}_k^T P \tilde{b}_k)^{1-1/p} + \beta}. \end{aligned} \tag{3.31}$$

Then the tracking errors $(\tilde{b}_k, \tilde{v}_k)$ *converge to zero in finite time when* $l(\tilde{b}_k, \tilde{v}_k) = 0$.

Proof. One can rewrite (3.31) as

$$\tilde{b}_{k+1} = \tilde{b}_k \frac{(\tilde{b}_k^{\mathrm{T}} P \tilde{b}_k)^{1-1/p} - \beta}{(\tilde{b}_k^{\mathrm{T}} P \tilde{b}_k)^{1-1/p} + \beta}. \tag{3.32}$$

Hence, it can be simplified to

$$\tilde{b}_{k+1} - \tilde{b}_k = -\frac{\beta(\tilde{b}_{k+1} + \tilde{b}_k)}{(\tilde{b}_k^{\mathrm{T}} P \tilde{b}_k)^{1-1/p}}. \tag{3.33}$$

Note that this can be re-expressed as

$$-\frac{\beta(\tilde{b}_{k+1} + \tilde{b}_k)}{(\tilde{b}_k^{\mathrm{T}} P \tilde{b}_k)^{1-1/p}} = \tilde{v}_k \Delta t, \tag{3.34}$$

which holds when $l(\tilde{b}_k, \tilde{v}_k) = 0$.

Consider the discrete-time Lyapunov function V_k defined by (3.28). The difference between the values of this function at successive discrete instants is given by (3.29). From (3.33), substituting $\tilde{b}_{k+1} - \tilde{b}_k$ into (3.29), one gets

$$V_{k+1} - V_k = -\frac{\beta}{2} \frac{(\tilde{b}_{k+1} + \tilde{b}_k)^{\mathrm{T}} P (\tilde{b}_{k+1} + \tilde{b}_k)}{(\tilde{b}_k^{\mathrm{T}} P \tilde{b}_k)^{1-1/p}}. \tag{3.35}$$

Note that $\tilde{b}_{k+1} + \tilde{b}_k = \big(1 + \mathscr{B}(\tilde{b}_k)\big)\tilde{b}_k$, and the right side of expression (3.35) is zero if only if

$$\tilde{b}_{k+1} = -\tilde{b}_k,$$

which is possible if and only if $\mathcal{B}(\tilde{b}_k) = -1$ according to (3.31). From the expression for $\mathscr{B}(\tilde{b}_k)$ in (3.31), one can see that $\mathcal{B}(\tilde{b}_k) = -1$ if and only if $\tilde{b}_k = 0$. Therefore, we conclude that

$$V_{k+1} - V_k = 0 \;\Leftrightarrow\; \tilde{b}_k = 0.$$

Now substituting (3.32) into (3.35) and noting that $\tilde{b}_k^{\mathrm{T}} P \tilde{b}_k = 2V_k$, one obtains

$$V_{k+1} - V_k = -\gamma_k (V_k)^{1/p}, \tag{3.36}$$

where

$$\gamma_k = 4\beta \frac{2^{1-1/p}(V_k)^{2-2/p}}{\big((2V_k)^{1-1/p} + \beta\big)^2}. \tag{3.37}$$

Clearly, γ_k as given by eq. (3.37) is a class-$\mathcal{K}$ function of V_k. From eqs. (3.36) and (3.37), one can see that V_k is monotonously decreasing if $\gamma_k > 0$ and

$$0 < \gamma_k < \frac{4\beta}{2^{1-1/p}} \;\text{ for }\; 0 < 2V_k < \infty.$$

Therefore γ_k would lead to finite-time stability of tracking control system. Also from (3.37), one obtains the ratio:

$$a_k := \frac{\gamma_k}{\gamma_0} = \frac{(V_k)^{2-2/p}}{(V_0)^{2-2/p}} \frac{\big((2V_0)^{1-1/p} + \beta\big)^2}{\big((2V_k)^{1-1/p} + \beta\big)^2}. \tag{3.38}$$

This ratio in eq. (3.38) is bounded below by a positive number in the open interval $(0,1)$ for non-zero V_k and V_0. This guarantees the existence of $\varepsilon \in (0,1)$ and $0 < \chi < (V_0)^{1-1/p}$ that satisfy the condition (3.12) in the statement of Lemma 3.2.1 for V_k. Therefore, (3.36) guarantees that V_k converges to zero for $k > N$ for some finite $N \in \mathbb{N}$, and this ensures the finite-time stable convergence of tracking errors to zero. ■

In the second step of finding the FTS position tracking scheme in discrete time, one can create a control force for the error dynamics given in (3.8) that ensures convergence of the function $l(\tilde{b}_k, \tilde{v}_k)$ derived in the first step to zero in finite time. This will, in turn, ensure that $(\tilde{b}_k, \tilde{v}_k)$ converges to $(0,0)$ in finite time. In order to fulfill this objective, a positive definite Lyapunov function in terms of the obtained vector-valued $l(\tilde{b}_k, \tilde{v}_k)$ is constructed as

$$\mathscr{V}(\tilde{b}_k, \tilde{v}_k) = \frac{1}{2} l(\tilde{b}_k, \tilde{v}_k)^{\mathrm{T}} l(\tilde{b}_k, \tilde{v}_k), \tag{3.39}$$

which can be used to obtain the FTS tracking control scheme in discrete time. The following statement provides the main result on a finite-time stable position tracking control scheme.

Theorem 3.3.1. *Consider the translational kinematics and dynamics given by (3.8). Then, the discrete-time force control law given by*

$$\begin{aligned}\bar{\varphi}_k =& m\big(v_k + \Delta t\ g\ e_3 - \tilde{v}^d_{k+1}\big) \\ &- \frac{m}{\Delta t}\left[(1+\frac{\kappa}{(l_k^T l_k)^{1-1/p}})(1+\frac{\beta}{(\tilde{b}_{k+1}^T P \tilde{b}_{k+1})^{1-1/p}})\right]^{-1} \\ &\cdot \left\{\Big(1-\frac{\kappa}{(l_k^T l_k)^{1-1/p}}\Big)\tilde{v}_k \Delta t - \frac{2\beta}{(\tilde{b}_{k+1}^T P \tilde{b}_{k+1})^{1-1/p}}\Big(1+\frac{\kappa}{(l_k^T l_k)^{1-1/p}}\Big)\tilde{b}_{k+1}\right. \\ &\left. + \frac{\beta(\tilde{b}_{k+1}+\tilde{b}_k)}{(\tilde{b}_k^T P \tilde{b}_k)^{1-1/p}}\Big(1-\frac{\kappa}{(l_k^T l_k)^{1-1/p}}\Big)\right\}.\end{aligned} \tag{3.40}$$

where $\kappa > 0$, and p and β are as defined in Lemma 3.3.1, stabilizes the translational error dynamics in finite time.

Proof. Consider the Lyapunov function (3.39) quadratic in $l(\tilde{b}_k, \tilde{v}_k)$ as constructed in (3.30). Therefore, the time difference of this discrete-time Lyapunov function can be evaluated as follows:

$$\mathscr{V}_{k+1} - \mathscr{V}_k = \frac{1}{2}(l_{k+1}+l_k)^{\mathrm{T}}(l_{k+1}-l_k). \tag{3.41}$$

Similar to the definition for $\tilde{b}_{k+1}$ in Lemma 3.3.1, one can consider

$$l_{k+1} = \mathcal{L}(\tilde{b}_k, \tilde{v}_k)\ l_k, \tag{3.42}$$

where

$$\mathcal{L}(\tilde{b}_k, \tilde{v}_k) = \frac{(l_k^{\mathrm{T}} l_k)^{1-1/p} - \kappa}{(l_k^{\mathrm{T}} l_k)^{1-1/p} + \kappa}, \tag{3.43}$$

Substituting (3.43) in (3.42) gives

$$(l_{k+1} - l_k) = -\frac{\kappa}{(l_k^{\mathrm{T}} l_k)^{1-1/p}}(l_{k+1} + l_k). \tag{3.44}$$

Then according to Lemma 3.3.1, one can prove similarly that

$$\mathscr{V}_{k+1} - \mathscr{V}_k = -\lambda_k \mathscr{V}_k^{1/p}, \tag{3.45}$$

where

$$\lambda_k = 4\kappa \frac{2^{1-1/p}(\mathscr{V}_k)^{2-2/p}}{\left((2\mathscr{V}_k)^{1-1/p} + \kappa\right)^2} \tag{3.46}$$

is a class-$\mathcal{K}$ function of $\mathcal{V}_k$. Also, from (3.45) and (3.46), one can see that

$$0 < \lambda_k < \frac{4\kappa}{2^{1-1/p}} \quad \text{for} \quad 0 < 2\mathscr{V}_k < \infty.$$

Therefore, λ_k would lead to finite-time stability of tracking control system.

Now, by substituting $l(\tilde{b}_k, \tilde{v}_k)$ given in (3.30) into (3.44), one can obtain

$$\begin{aligned} &(\tilde{v}_{k+1} - \tilde{v}_k)\Delta t + \beta\Big[\frac{(\tilde{b}_{k+2} + \tilde{b}_{k+1})}{(\tilde{b}_{k+1}^{\mathrm{T}} P \tilde{b}_{k+1})^{1-1/p}} - \frac{(\tilde{b}_{k+1} + \tilde{b}_k)}{(\tilde{b}_k^{\mathrm{T}} P \tilde{b}_k)^{1-1/p}}\Big] \\ &= -\frac{\kappa}{(l_k^{\mathrm{T}} l_k)^{1-1/p}}\left\{(\tilde{v}_{k+1} + \tilde{v}_k)\Delta t + \beta\Big[\frac{(\tilde{b}_{k+2} + \tilde{b}_{k+1})}{(\tilde{b}_{k+1}^{\mathrm{T}} P \tilde{b}_{k+1})^{1-1/p}} + \frac{(\tilde{b}_{k+1} + \tilde{b}_k)}{(\tilde{b}_k^{\mathrm{T}} P \tilde{b}_k)^{1-1/p}}\Big]\right\}. \end{aligned} \tag{3.47}$$

Noting that $(\tilde{b}_{k+2} - \tilde{b}_{k+1})/\Delta t = \tilde{v}_{k+1}$, one can solve above expression for $\tilde{v}_{k+1}$ to obtain the discrete-time translational error dynamics equation as

$$\begin{aligned}
&\tilde{v}_{k+1} = \mathcal{F}(\tilde{b}_k, \tilde{b}_{k+1}, \tilde{v}_k, l_k) = \\
&\frac{1}{\Delta t}\left[(1 + \frac{\kappa}{(l_k^{\mathrm{T}} l_k)^{1-1/p}})(1 + \frac{\beta}{(\tilde{b}_{k+1}^{\mathrm{T}} P \tilde{b}_{k+1})^{1-1/p}})\right]^{-1} \\
&\cdot \left\{\left(1 - \frac{\kappa}{(l_k^{\mathrm{T}} l_k)^{1-1/p}}\right)\tilde{v}_k \Delta t - \frac{2\beta}{(\tilde{b}_{k+1}^{\mathrm{T}} P \tilde{b}_{k+1})^{1-1/p}}\left(1 + \frac{\kappa}{(l_k^{\mathrm{T}} l_k)^{1-1/p}}\right)\tilde{b}_{k+1}\right. \\
&\left. + \frac{\beta(\tilde{b}_{k+1} + \tilde{b}_k)}{(\tilde{b}_k^{\mathrm{T}} P \tilde{b}_k)^{1-1/p}}\left(1 - \frac{\kappa}{(l_k^{\mathrm{T}} l_k)^{1-1/p}}\right)\right\},
\end{aligned} \tag{3.48}$$

Then, noting that $\tilde{v}_{k+1} = v_{k+1} - v_{k+1}^d$, one can obtain the discrete-time control force vector given by (3.40) after substituting (3.48) in the second equation of (3.8). The discrete-time control force vector so obtained, guarantees the finite-time stability of the position tracking control. ■

The following section provides a finite-time stable feedback control law in discrete time to stabilize the attitude error dynamics (3.8).

3.4 Discrete Finite-time Stable Attitude Tracking Control

In this section, a finite-time stable attitude tracking control scheme in discrete time is provided. The following two Lemmas are also used to prove the main result.

Lemma 3.4.1. *Let x and y be non-negative real numbers and let p as defined in 3.3.1. Then*

$$x^{(1/p)} + y^{(1/p)} \geq (x + y)^{(1/p)}. \tag{3.49}$$

Moreover the above inequality is a strict inequality if both x and y are non-zero.

Lemma 3.4.2. *Let $K = \mathrm{diag}(k_1, k_2, k_3)$, where $k_1 > k_2 > k_3 \geq 1$. Define*

$$s_K(Q) = \sum_{i=1}^{3} k_i (Q^T e_i) \times e_i, \tag{3.50}$$

such that $\frac{\mathrm{d}}{\mathrm{d}t}\langle K, I - Q\rangle = \omega^T s_K(Q)$. Here $\langle A, B\rangle = \mathrm{tr}(A^T B)$, which makes $\langle K, I - Q\rangle$ a Morse function defined on $\mathrm{SO}(3)$. Let $\mathcal{S} \subset \mathrm{SO}(3)$ be a closed subset containing the identity in its interior, defined by

$$\mathcal{S} = \{Q \in \mathrm{SO}(3) \,:\, Q_{ii} \geq 0 \text{ and } Q_{ij}Q_{ji} \leq 0 \;\forall i,\; j \in \{1,2,3\},\; i \neq j\}. \tag{3.51}$$

Then for $Q \in \mathcal{S}$, we have

$$s_K(Q)^T s_K(Q) \geq \mathrm{tr}(K - KQ). \tag{3.52}$$

Proof. The proof of this Lemma is given in (Bohn and Sanyal, 2015), and omitted here for brevity. ■

The discrete finite-time attitude tracking control scheme and its proof of stability and domain of convergence are given as follows.

Theorem 3.4.1. *Consider the discretized rotational error kinematics and the real dynamics of an underactuated vehicle given in (3.8), with $s_K(Q_k)$ as defined in (3.50). Define*

$$z_K(Q_k) = \frac{s_K(Q_k)}{\left(s_K^T(Q_k) s_K(Q_k)\right)^{1-1/p}}, \tag{3.53}$$

where p is as defined in Lemma 3.4.1, and let k_l be a constant in the interval $(0,1]$. Then, the discrete-time control law given by

$$u_k = J\Bigg(\Big[\frac{(\psi_k^T J\psi_k)^{1-1/p} - \Gamma}{(\psi_k^T J\psi_k)^{1-1/p} + \Gamma}\Big]\left(\omega_k + k_l z_K(Q_k)\right) - k_l z_K(Q_{k+1}) + Q_{k+1}^T\,\Omega_{k+1}^d\Bigg) - F_k^T\,J\Omega_k, \tag{3.54}$$

stabilizes the rotational error dynamics

$$\omega_{k+1} = \left[\frac{(\psi_k^T J\psi_k)^{1-1/p} - \Gamma}{(\psi_k^T J\psi_k)^{1-1/p} + \Gamma}\right]\psi_k(\omega_k, Q_k) - k_l z_K(Q_{k+1}) \tag{3.55}$$

in finite time, where $\psi_k(\omega_k, Q_k)$ is defined as

$$\psi_k(\omega_k, Q_k) = \omega_k + k_l z_K(Q_k). \tag{3.56}$$

Proof. Consider $\omega_k = -k_l z_K(Q_k)$ and discretized error kinematics given in (3.8) and define the discrete-time Morse function $U_k = k_p \langle I - Q_k, K\rangle$ on SO(3) where $k_p > 1$. Then the first time difference of this discrete-time Morse function along the attitude kinematics

is given by

$$\begin{aligned} U_{k+1} - U_k &= k_p \langle Q_k - Q_{k+1}, K \rangle \\ &= k_p \langle -Q_k \, \varpi_k^{\times}, K \rangle \\ &= k_p \langle \, \varpi_k^{\times}, -Q_k^{\mathrm{T}} \, K \rangle \\ &= \frac{1}{2} k_p \langle \varpi_k^{\times}, K Q_k - Q_k^{\mathrm{T}} \, K \rangle \\ &= k_p \, \varpi_k^{\mathrm{T}} \, S_K(Q_k). \end{aligned} \tag{3.57}$$

Substituting $\varpi_k = \Delta t \; \omega_k$ in (3.57), one finds

$$\begin{aligned} k_p \, \varpi_k^{\mathrm{T}} \, S_K(Q_k) &= -\Delta t \; k_p \; k_l \; z_K(Q_k)^{\mathrm{T}} s_K(Q_k) \\ &= -k_p \; k_l \; \Delta t \; \left(s_K(Q_k)^{\mathrm{T}} s_K(Q_k) \right)^{1/p} \\ &\leq \; -k_p \; k_l \; \Delta t \; \left(\, \langle I - Q_k, K \rangle \, \right)^{1/p} \\ &\leq \; -k_l \; \Delta t \; \left(k_p \, \langle I - Q_k, K \rangle \, \right)^{1/p}. \end{aligned} \tag{3.58}$$

where we employed inequality (4.38) in Lemma 3.4.2. Therefore, when $\psi_k = 0$, one can conclude that $\langle I - Q_k, K \rangle \to 0$ in finite time for all initial Q_k in the subset $\mathcal{S} \subset \mathrm{SO}(3)$ defined in Lemma 3.4.1, which yields $Q_k \to I$ in finite time once $Q_k \in \mathcal{S}$. Moreover, as $\Delta U_k = U_{k+1} - U_k$ is negative definite when $\psi_k = 0$, it keeps decreasing in time and therefore Q_k will reach $\mathcal{S}$ in finite time. Therefore, $Q_k \to I$ in finite time.

The control law is then designed to ensure that $\psi_k(\omega_k, Q_k) \to 0$ in finite time. Define the Lyapunov function

$$\mathcal{V}_k(\omega_k, Q_k) = \frac{1}{2} \psi_k(\omega_k, Q_k)^{\mathrm{T}} \psi_k(\omega_k, Q_k) + k_p \, \langle I - Q_k, K \rangle \, . \tag{3.59}$$

The time difference of this discrete-time Lyapunov function can be evaluated as follows:

$$\begin{aligned}\mathcal{V}_{k+1} - \mathcal{V}_k &= \frac{1}{2}\psi_{k+1}^{\mathrm{T}} J \psi_{k+1} - \frac{1}{2}\psi_k^{\mathrm{T}} J \psi_k + k_p \left\langle Q_k - Q_{k+1}, K \right\rangle \\ &= \frac{1}{2}(\psi_{k+1} + \psi_k)^{\mathrm{T}} J (\psi_{k+1} - \psi_k) + k_p \left\langle Q_k - Q_{k+1}, K \right\rangle . \end{aligned} \tag{3.60}$$

One can consider

$$\psi_{k+1} = \Psi(\omega_k, Q_k)\psi_k, \tag{3.61}$$

where

$$\Psi(\omega_k, Q_k) = \frac{(\psi_k^{\mathrm{T}} J \psi_k)^{1-1/p} - \Gamma}{(\psi_k^{\mathrm{T}} J \psi_k)^{1-1/p} + \Gamma}, \tag{3.62}$$

and let $\Gamma > 0$.

Substituting (3.62) in (3.61) gives

$$(\psi_{k+1} - \psi_k) = -\frac{\Gamma}{(\psi_k^{\mathrm{T}} J \psi_k)^{1-1/p}}(\psi_{k+1} + \psi_k). \tag{3.63}$$

Therefore, one can rewrite (3.60) as

$$\mathcal{V}_{k+1} - \mathcal{V}_k = -\frac{\Gamma}{2}\frac{(\psi_{k+1} + \psi_k)^{\mathrm{T}} J (\psi_{k+1} + \psi_k)}{(\psi_k^{\mathrm{T}} J \psi_k)^{1-1/p}} + k_p\, \varpi_k^{\mathrm{T}} S_K(Q_k). \tag{3.64}$$

Note that the first term on the right-hand side of expression (3.64) is zero if and only if

$$\psi_{k+1} = -\psi_k,$$

which is possible if and only if $\Psi(\omega_k, Q_k) = -1$ according to (3.61). From (3.62), one can see that $\Psi(\omega_k, Q_k) = -1$ if and only if $\psi_k = 0$. Therefore, from (3.61) and (3.62) we conclude that

$$-\frac{\Gamma}{2}\frac{(\psi_{k+1}+\psi_k)^{\mathrm{T}} J(\psi_{k+1}+\psi_k)}{(\psi_k^{\mathrm{T}} J\psi_k)^{1-1/p}} = 0 \;\Leftrightarrow\; \psi_k = 0.$$

Therefore, the first term on the right side of expression (3.64) can be simplified as follows:

$$-\frac{\Gamma}{2}\frac{(\psi_{k+1}+\psi_k)^{\mathrm{T}} J(\psi_{k+1}+\psi_k)}{(\psi_k^{\mathrm{T}} J\psi_k)^{1-1/p}} = -\rho_k\,(\psi_k^{\mathrm{T}} J\psi_k)^{1/p}, \tag{3.65}$$

where

$$\rho_k = 4\Gamma\frac{(0.5)^{1-1/p}(\psi_k^{\mathrm{T}} J\psi_k)^{2-2/p}}{\left((\psi_k^{\mathrm{T}} J\psi_k)^{1-1/p}+\Gamma\right)^2}. \tag{3.66}$$

From equations (3.65) and (3.66), one can see that the first term on the right side of expression (3.64) is monotonously decreasing if

$$0 < \rho_k < \frac{4\Gamma}{2^{1-1/p}} \;\text{ for }\; 0 < \psi_k^{\mathrm{T}} J\psi_k < \infty,$$

Therefore, using (3.58) and (3.65), the expression (3.64) is evaluated as follows:

$$\begin{aligned}
\Delta\mathcal{V}_k &= -\rho_k(\psi_k^{\mathrm{T}} J\psi_k)^{1/p} - k_p k_l \Delta t\,\left(s_K(Q_k)^{\mathrm{T}} s_K(Q_k)\right)^{1/p} \\
&\le -(\psi_k^{\mathrm{T}} J\psi_k)^{1/p} - k_l\,\Delta t\,\left(k_p\,\langle I - Q_k, K\rangle\,\right)^{1/p} \\
&\le -k_l\,\Delta t\,\left((\psi_k^{\mathrm{T}} J\psi_k)^{1/p} + \left(k_p\,\langle I - Q_k, K\rangle\,\right)^{1/p}\right).
\end{aligned} \tag{3.67}$$

for $(Q_k, \omega_k) \in \mathcal{S} \times \mathbb{R}^3$. Finally, using inequality (4.36) in Lemma 3.4.1, one obtains

$$\begin{aligned}\Delta \mathcal{V}_k &\leq -k_l \, \Delta t \, \left(\psi_k^{\mathrm{T}} J \psi_k + k_p \, \langle I - Q_k, K \rangle \right)^{1/p} \\ &\leq -k_l \, \Delta t \, \mathcal{V}_k^{1/p}, \end{aligned} \tag{3.68}$$

where $k_p > 0$, and $0 < k_l \leq 1$. Therefore, all initial states of the feedback attitude system, which start in the domain of attraction of the equilibrium $(I, 0)$ and for which the value of the Lyapunov function $\mathcal{V}$ is finite, converge to $(I, 0)$ in finite time. Now, by substituting $\psi_k(\omega_k, Q_k)$ given in (3.56) into (3.61), one can obtain

$$\omega_{k+1} = \Psi(\omega_k, Q_k)\big(\omega_k + k_l z_K(Q_k)\big) - k_l z_K(Q_{k+1}), \tag{3.69}$$

or

$$\omega_{k+1} = \left[\frac{(\psi_k^{\mathrm{T}} J \psi_k)^{1-1/p} - \Gamma}{(\psi_k^{\mathrm{T}} J \psi_k)^{1-1/p} + \Gamma} \right] \psi_k(\omega_k, Q_k) - k_l z_K(Q_{k+1}). \tag{3.70}$$

From the discretized dynamics equation of rotational motion obtained in the form of a LGVI given in (3.8) as

$$J \, \Omega_{k+1} = F_k^{\mathrm{T}} \, J \Omega_k + u_k, \tag{3.71}$$

where

$$\Omega_{k+1} = \omega_{k+1} + Q_{k+1}^{\mathrm{T}} \, \Omega_{k+1}^d, \tag{3.72}$$

one can find the discrete-time control law u_k that guarantees the stability of the attitude tracking control in a finite time, as follows:

$$u_k = J\left(\left[\frac{(\psi_k^{\mathrm{T}} J \psi_k)^{1-1/p} - \Gamma}{(\psi_k^{\mathrm{T}} J \psi_k)^{1-1/p} + \Gamma}\right](\omega_k + k_l z_K(Q_k)) - k_l z_K(Q_{k+1}) + Q_{k+1}^{\mathrm{T}}\, \Omega_{k+1}^{d}\right) - F_k^{\mathrm{T}}\, J \Omega_k. \tag{3.73}$$

■

Remark 3.4.1. (**Almost global domain of attraction of the control scheme**) Analyzing the time difference of the Morse-Lyapunov function (3.59) showed that this function satisfies the sufficient condition for finite-time stability. From prior research on almost global asymptotic attitude stabilization and tracking in (Chaturvedi, Sanyal, and McClamroch, 2011; Sanyal, Nordkvist, and Chyba, 2011; Sanyal and Chaturvedi, 2008), we know that the subset of SO(3) where $s_K(Q_k) = 0$, which is also the set of critical points for $\langle I - Q_k, K\rangle$, is

$$C \triangleq \{I, \mathrm{diag}(1,-1,-1), \mathrm{diag}(-1,1,-1), \mathrm{diag}(-1,-1,1)\} \subset \mathrm{SO}(3).$$

Therefore, the subset of the state space where $V_{k+1} - V_k = 0$ is $\{(Q_k, \omega_k) : Q_k \in C$ and $\omega_k = 0\} \subset \mathrm{SO}(3) \times \mathbb{R}^3 \simeq \mathrm{TSO}(3)$. This subset is also the set of equilibria for tracking errors in the feedback attitude system, and its largest invariant set. Among the four equilibria in this set, the equilibrium $(Q_k, \omega_k) = (I, 0)$ is attractive as it corresponds to the minimum value of $V_k(Q_k, \omega_k)$. Other three equilibria are unstable equilibria. All trajectories that do not start on the stable manifolds of the other three equilibria converge to the stable equilibrium $(I, 0)$. The Lyapunov function along a state trajectory on any of

these stable manifolds increases in value when going backwards in time. A state trajectory on a stable manifold of any of these unstable equlibria cannot approach itself outside of a closed neighborhood containing the equilibrium. Therefore, the stable manifolds of these unstable equilibria form nowhere dense subsets of $\mathrm{SO}(3) \times \mathbb{R}^3$. Denote the union of these stable manifolds of the unstable equilibria as M. The complement of M is therefore dense and open in $\mathrm{TSO}(3) \simeq \mathrm{SO}(3) \times \mathbb{R}^3$. All initial states that are in the complement $\mathrm{SO}(3) \times \mathbb{R}^3 / M$ converge to the stable equilibrium $(I, 0)$, which makes its domain of attraction almost global.

3.5 Robustness Analysis of discrete-time FTS attitude tracking control scheme

The finite-time stability property of the attitude tracking control law given in Theorem 3.4.1 results in guaranteed convergence of almost any initial attitude state to the desired state, given by the tracking errors $(Q, \omega) = (I, 0)$, in finite time in the absence of any disturbances to the discretized dynamics model. In the presence of a bounded disturbance control input u_k^D in the dynamics, all attitude tracking errors will converge to a bounded neighborhood of $(I, 0)$ as well. The following result gives a conservative statement relating the bound of tracking errors that can be tolerated and bounds on the neighborhood of $(I, 0)$.

Corollary 3.5.1. *Consider the discretized feedback system given by the attitude kinematics and dynamics in the last two equations* (3.8)*, and the control law* (3.73)*. Let* $\mathcal{N} \subset S \times \mathbb{R}^3$*, where* S *is*

as defined in equation (4.37), be a closed neighborhood of $(I, 0)$ defined by

$$\mathcal{N} := \left\{(Q_k, \omega_k) : \ \|s_K(Q_k)\| \leq s_{max} \text{ and } \ \|\psi_k\| \leq \Psi_{max} < 1\right\}, \tag{3.74}$$

If the norm of the disturbance in control input, u_k^D, satisfies the following inequality,

$$\left\|u_k^D\right\| \leq \frac{k_l \ \Delta t \left(\Psi_{max}^{(2/p)} + s_{max}^{(2/p)}\right)}{\Psi_{max}}, \tag{3.75}$$

then, the tracking errors (Q, ω) converge to the neighborhood $\mathcal{N}$ in finite time.

Proof. Consider the discretized attitude dynamics of a rigid body in LGVI form given in (3.8) disturbed by a control input u_k^D,

$$J \ \Omega_{k+1} = F_k^{\mathrm{T}} \ J\Omega_k + u_k + u_k^D \tag{3.76}$$

which has an additional term (u_k^D) due to the disturbance control input, and noting that

$$\omega_{k+1} = \Omega_{k+1} - Q_{k+1}^{\mathrm{T}} \ \Omega_{k+1}^d,$$

and

$$\psi_k(\omega_k, Q_k) = \omega_k + k_l z_K(Q_k),$$

then, we can write

$$\begin{aligned}\psi_{k+1} - \psi_k &= \Omega_{k+1} - Q_{k+1}^{\mathrm{T}}\, \Omega_{k+1}^{d} - \Omega_k + Q_k^{\mathrm{T}}\, \Omega_k^{d} + k_l\Big(z_K(Q_{k+1}) - z_K(Q_k)\Big) \\ &= J^{-1}F_k^{\mathrm{T}}\, J\Omega_k + J^{-1}u_k + J^{-1}u_k^{D} - Q_{k+1}^{\mathrm{T}}\, \Omega_{k+1}^{d} \\ &- \Omega_k + Q_k^{\mathrm{T}}\, \Omega_k^{d} + k_l\Big(z_K(Q_{k+1}) - z_K(Q_k)\Big) \\ &= -\frac{\Gamma(\psi_{k+1} + \psi_k)}{(\psi_k^{\mathrm{T}} J \psi_k)^{1-1/p}} + J^{-1}u. \end{aligned} \tag{3.77}$$

Substituting (3.77) into the time difference of discrete-time Lyapunov function given in (3.60) and simplifying, we get

$$\begin{aligned}\mathcal{V}_{k+1} - \mathcal{V}_k &= \frac{1}{2}(\psi_{k+1} + \psi_k)^{\mathrm{T}} J\left[-\frac{\Gamma(\psi_{k+1} + \psi_k)}{(\psi_k^{\mathrm{T}} J \psi_k)^{1-1/p}} + J^{-1}u_k^{D}\right] + k_p\,\langle Q_k - Q_{k+1}, K\rangle \\ &= -\rho_k\,(\psi_k^{\mathrm{T}} J \psi_k)^{1/p} - k_p\, k_l\, \Delta t\, \left(s_K(Q_k)^{\mathrm{T}} s_K(Q_k)\right)^{1/p} + \frac{1}{2}(\psi_{k+1} + \psi_k)^{\mathrm{T}} u_k^{D}. \end{aligned} \tag{3.78}$$

Now, since $\|\psi_{k+1} + \psi_k\| \leq \|\psi_{k+1}\| + \|\psi_k\| \leq 2\Psi_{max}$, the last term on the right side of the above equation is upper bounded as follows:

$$\frac{1}{2}(\psi_{k+1} + \psi_k)u_k^{D} \leq \frac{1}{2}\,\|\psi_{k+1} + \psi_k\|\,\left\|u_k^{D}\right\| \leq \Psi_{max}\left\|u_k^{D}\right\|, \tag{3.79}$$

From $AB \leq \|A\| \, . \, \|B\|$, we can rewrite the time difference of Lyapunov function as

$$\begin{aligned}
\mathcal{V}_{k+1} - \mathcal{V}_k &\leq -\rho_k \, (\psi_k^{\mathrm{T}} J \psi_k)^{1/p} - k_p \, k_l \, \Delta t \, \left(\langle I - Q_k, K \rangle \right)^{1/p} + \frac{1}{2} \, \|\psi_{k+1} + \psi_k\| \, \left\| u_k^D \right\| \\
&\leq -(\psi_k^{\mathrm{T}} J \psi_k)^{1/p} - k_l \, \Delta t \, \left(k_p \, \langle I - Q_k, K \rangle \right)^{1/p} + \frac{1}{2} \, \|\psi_{k+1} + \psi_k\| \, \left\| u_k^D \right\| \\
&\leq -k_l \, \Delta t \, \left((\psi_k^{\mathrm{T}} J \psi_k)^{1/p} + \left(k_p \, \langle I - Q_k, K \rangle \right)^{1/p} \right) + \frac{1}{2} \, \|\psi_{k+1} + \psi_k\| \, \left\| u_k^D \right\| \\
&\leq -k_l \, \Delta t \, \left(\psi_{max}^{(1/p)} + s_{max}^{(1/p)} \right) + \Psi_{max} \left\| u_k^D \right\| . \qquad (3.80)
\end{aligned}$$

Therefore, $\mathcal{V}_{k+1} - \mathcal{V}_k$ is non-positive along the boundary of N if

$$-k_l \, \Delta t \, \left(\psi_{max}^{(1/p)} + s_{max}^{(1/p)} \right) + \Psi_{max} \left\| u_k^D \right\| \leq 0, \qquad (3.81)$$

which is a sufficient condition for all trajectories starting outside the boundary of neighborhood $\mathcal{N}$ to converge to this neighborhood of $(I, 0)$. Expression (3.81) leads to (4.65) for the bound on the norm of the disturbance u_k^D for which convergence of errors to the neighborhood $\mathcal{N}$ of $(I, 0)$ is guaranteed. ■

Remark 3.5.1. In the presence of bounded disturbances and internal parametric uncertainties in the dynamics of the rigid body, state trajectories will converge to a bounded neighborhood of $(Q, \omega) = (I, 0)$. On the other hand, based on a desired size of this neighborhood, one can find an upper bound on the norm of external disturbances and internal parametric uncertainties that can be tolerated for state trajectories to converge to this neighborhood. This can be done using the Lyapunov analysis presented in the proof of the almost global finite-time stability of the tracking control scheme given in Theorems 3.3.1 and 3.4.1.

3.6 Continuous finite-time stable tracking control on $\mathrm{SE}(3)$

A FTS tracking control scheme in continuous time has been reported in (Prabhakaran, Sanyal, and Warier, 2017). In this scheme, the error dynamics in continuous time is given by:

$$\begin{cases} m\dot{\tilde{v}} = m\, g\, e_3 - \varphi_c - v^d, \\ J\dot{\omega} = \tau_c + J(\omega^{\times} Q^{\mathrm{T}}\Omega^d - Q^{\mathrm{T}}\dot{\Omega}^d) - (\omega + Q^{\mathrm{T}}\Omega^d)^{\times} J(\omega + Q^{\mathrm{T}}\Omega^d), \end{cases} \tag{3.82}$$

where τ_c and $\varphi_c \in \mathbb{R}^3$ are obtained from the feedback control laws in continuous time as follows:

$$\begin{aligned} \tau_c = {} & J\left(Q^{\mathrm{T}}\dot{\Omega}^d - \frac{\kappa_r H(s_K(Q))}{\left(s_K^{\mathrm{T}}(Q)s_K(Q)\right)^{1-1/p}} w(Q,\omega)\right) \\ & + (Q^{\mathrm{T}}\Omega^d)^{\times} J\left(Q^{\mathrm{T}}\Omega^d - \kappa_r z_K(Q)\right) + \kappa_r J\left(z_K(Q) \times Q^{\mathrm{T}}\Omega^d\right) \\ & + \kappa_r J(\omega + Q^{\mathrm{T}}\Omega^d) \times z_K(Q) - k_p s_K(Q) - \frac{L_\Omega \Psi(Q,\omega)}{\left(\Psi(Q,\omega)^{\mathrm{T}} L_\Omega \Psi(Q,\omega)\right)^{1-1/p}}, \end{aligned} \tag{3.83}$$

and

$$\varphi_c = ge_3 - \dot{v}_d + \kappa_t(\dot{z} + \tilde{b}) + \frac{\kappa_t P_r(\tilde{v} + \kappa_t z)}{\left[(\tilde{v} + \kappa_t z)^{\mathrm{T}} P_r(\tilde{v} + \kappa_t z)\right]^{1-1/p}}. \tag{3.84}$$

In equations (3.83) and (3.84),

$$\Psi(Q,\omega) = \omega + \kappa z_K(Q), \tag{3.85}$$

$$H(x) = I - \frac{2(1-1/p)}{x^{\mathrm{T}}x} xx^{\mathrm{T}}, \tag{3.86}$$

$$z(t) = \frac{\tilde{b}}{(\tilde{b}^{\mathrm{T}}\tilde{b})^{1-1/p}}, \tag{3.87}$$

$$\dot{z} = \frac{(\tilde{b}^{\mathrm{T}}\tilde{b})^{1-1/p}\tilde{v} - (2-2/p)(\tilde{b}^{\mathrm{T}}\tilde{b})^{-1/p}(\tilde{b}^{\mathrm{T}}\tilde{v})\tilde{b}}{(\tilde{b}^{\mathrm{T}}\tilde{b})^{2-2/p}}, \tag{3.88}$$

where $P_r \in \mathbb{R}^{3\times 3}$ is a positive definite control gain matrix, and p is as defined in Lemma 3.4.1. Further, L_Ω is a positive definite control gain matrix such that $L_\Omega - J$ is positive semi-definite, $k_p > 1$ and the control gain κ is defined by

$$\kappa^p = \frac{\sigma_{L,\min}}{\sigma_{J,\max}} > 0.$$

These continuous control laws guarantee the finite-time stability of the feedback tracking error dynamics given by (3.82) at $(Q,\omega,\tilde{b},\tilde{v}) = (I,0,0,0)$. These control laws are then sampled over the time interval $[t_0,t_f]$ and with a time step size Δt.

The following section presents numerical results obtained by implementing this chapter's proposed FTS scheme in discrete time compared to the results of the sampled finite-time continuous scheme.

3.7 Simulation Results

This section presents numerical simulation results for the FTS tracking control scheme in discrete time. These simulation results are provided for a quadrotor UAV with a mass

$m = 4$ kg, for time period of $T = 5$s, and with time step size of $\Delta t = 0.01$s using discrete-time FTS control laws obtained in (3.40) and (3.73). Figure 3.1 shows the block diagram of a control system for controlling a quadrotor UAV to follow a time-varying desired position, b_k^d. This system has two loops: an inner loop for attitude control and an outer loop for position control. The desired attitude (R_k^d) that is to be tracked, is generated using the desired control force vector given by an outer loop position tracking scheme.

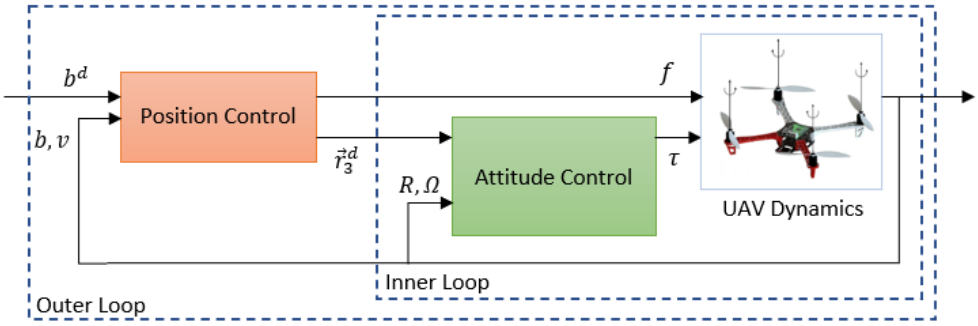

FIGURE 3.1: Block diagram of a quadrotor UAV control system.

3.7.1 Numerical simulation results for discrete-time FTS position and attitude tracking control schemes

A helical desired position trajectory with the following initial conditions is used for both control loops:

$$b_k^d = b^d(t_k) = \begin{bmatrix} 0.4\sin \pi t_k & 0.6\cos \pi t_k & 0.4\, t_k \end{bmatrix}^{\mathrm{T}},$$
$$b_0 = \begin{bmatrix} 1 & 0 & 0 \end{bmatrix}^{\mathrm{T}}, \; v_0 = \begin{bmatrix} 0 & 0 & 0 \end{bmatrix}^{\mathrm{T}},$$
$$R_0 = I, \; \Omega_0 = \begin{bmatrix} 0 & 0 & 0 \end{bmatrix}^{\mathrm{T}}, \; \Omega_0^d = \begin{bmatrix} 0 & 0 & 0 \end{bmatrix}^{\mathrm{T}}.$$

The gains are selected after trial and error for the FTS discrete-time attitude tracking scheme as follows:

$$P = 4\ \mathbf{I}_{3\times 3},\ \beta = 0.01,\ \kappa = 0.009,$$
$$k_l = 0.01,\ \Gamma = 0.1,$$

and for the FTS sampled continuous time scheme as follows:

$$P_r = 5\ \mathbf{I}_{3\times 3},\ \kappa_t = 0.8,$$
$$L_\Omega = 3.5\ \mathbf{I}_{3\times 3},\ k_p = 4.5,\ \kappa_r = 0.04,$$

which provide desirable and similar transient response characteristics of both tracking control schemes when $\Delta t = 0.01$. The time trajectory of the UAV tracking the desired trajectory is shown in Fig. 3.2 and it shows that the trajectory converges to the desired values in a finite time stable manner.

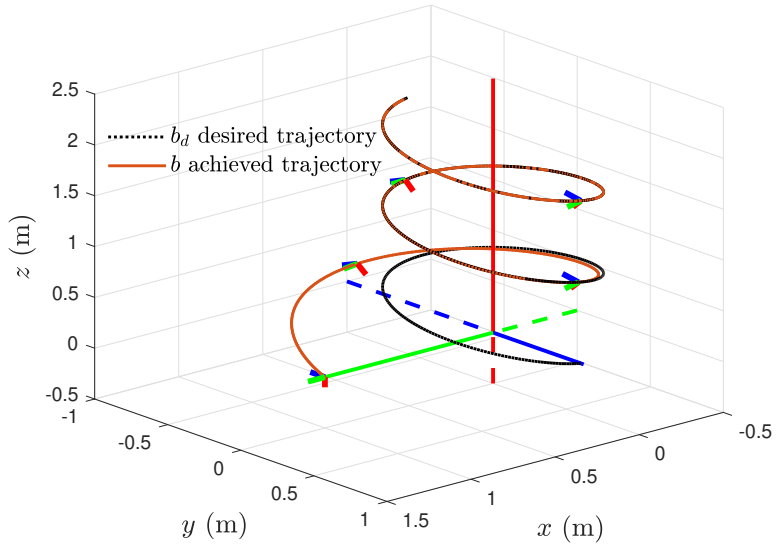

FIGURE 3.2: Time trajectory of UAV.

The results of the numerical simulation for the discrete-time FTS tracking control laws obtained in (3.40) and (3.73) for $\Delta t = 0.01$ and $t_f = 5s$ are shown in Figures 3.3 and 3.4. Figures 3.3a and 3.3b show that the translational motion tracking errors converge to zero in finite time. Figures 3.3c and 3.4a indicate the finite-time convergence of rotational motion tracking errors to zero. The attitude tracking error is parameterized by the principal rotation angle Φ of the attitude error matrix Q, and is given by

$$\Phi = \cos^{-1}\left(\frac{1}{2}(\text{tr}(Q) - 1)\right). \tag{3.89}$$

Convergence of the attitude tracking error Φ in finite time, as shown in Fig. 3.4a, implies that R tracks the desired trajectory R^d. The time plots of the control inputs f_k and τ_k in Figs. 3.4b and 3.4c respectively, show that the control effort is within reasonable bounds

and practically achievable for multi-rotor UAVs. Therefore the discrete-time tracking control scheme proposed here is able to track the desired trajectory in finite time.

3.7.2 Comparison with a sampled continuous-time tracking scheme

The performance of the proposed FTS tracking control scheme in discrete time is compared here to that of the sampled continuous-time FTS tracking scheme presented in section 3.6. Result of numerical simulations are provided for the same quadrotor UAV given above but for different time periods of $T = 5,\ 25$, and 50s, with different time step sizes of $\Delta t = 0.01,\ 0.05$, and 0.1s and the same total number of time steps, using discrete-time FTS control laws obtained in (3.40) and (3.73), and the sampled continuous-time control laws given in (Prabhakaran, Sanyal, and Warier, 2017). Simulation results are presented in Fig. 3.5 to Fig. 3.9 to compare the performance of the discrete-time FTS tracking scheme with a sampled continuous-time FTS tracking scheme for *different values of the time step size*. From these plots, one can conclude that the control law obtained by sampling the continuous FTS control input does not ensure the stability in tracking when the time step size changes. Moreover, to have a definite result of the comparison between results of these two schemes, a parameter study that was first proposed and used in (Hamrah, Sanyal, and Prabhakaran, 2019) is used here to confirm how the value of the Lyapunov function behaves at certain time instants. This tests whether the Lyapunov function increases in value between two successive sampling instants, and whether that increase is significant or is just an artifact of machine (float) precision. The results of this comparison are given in Table 3.1, where $\Delta\mathbb{V}_{\max}$ denotes the maximum positive value of the time difference

$\mathbb{V}_{k+1} - \mathbb{V}_k$ as:

$$\Delta\mathbb{V}_{\max} = \max\left[(\mathbb{V}_{k+1} - \mathbb{V}_k) > 0\right], \tag{3.90}$$

and $\mathbb{V}_k$ denotes the sum of the values of the Lyapunov functions for the position and attitude tracking errors as defined in (3.28) and (3.59), respectively. The value of $\mathbb{V}_{k+1} - \mathbb{V}_k$ is expected to be negative for a finite-time stable system until it converges to zero in finite time, which ensures the stability of the system in finite time. On the contrary, a significant increase in the value of $\Delta\mathbb{V}_{\max}$ occurs for the sampled continuous FTS tracking scheme as time step size increases, whereas $\Delta\mathbb{V}_{\max}$ has a negligible value (to machine precision) when the discrete-time FTS tracking control scheme is implemented.

Tracking Control Scheme	$\Delta t(s)$	$t_f(s)$	$\Delta\mathbb{V}_{max}$
Discrete-time FTS	0.01	5	1.0991×10^{-15}
	0.05	25	4.0776×10^{-25}
	0.1	50	4.1364×10^{-25}
Sampled Continuous FTS	0.01	5	2.3153×10^{-5}
	0.05	25	0.3166
	0.1	50	1.7888

TABLE 3.1: Stability performance of discrete-time FTS vs. sampled continuous-time FTS tracking control scheme on SO(3).

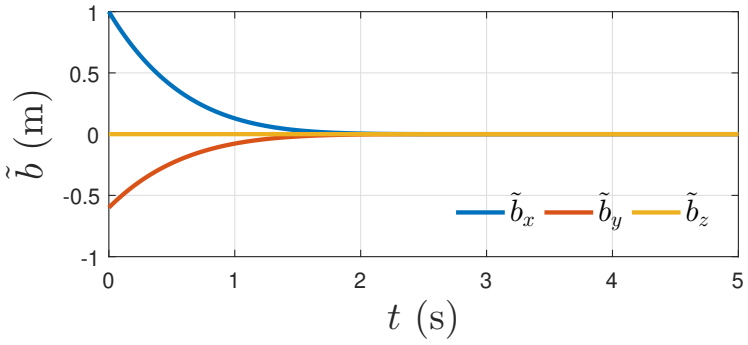

(A) Position tracking error

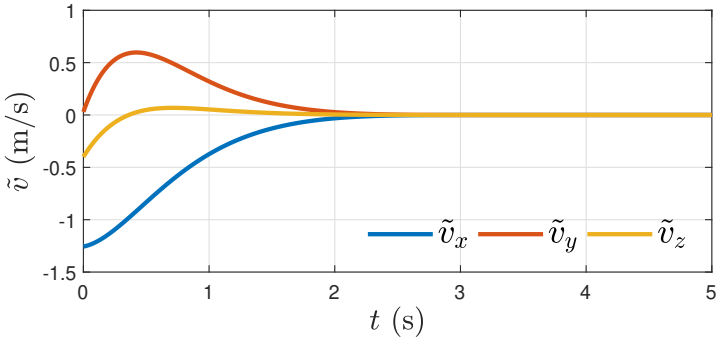

(B) Velocity tracking error

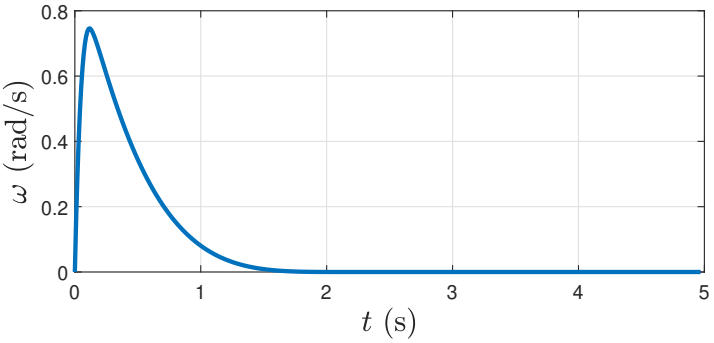

(C) Angular velocity error

FIGURE 3.3: Tracking errors and control laws for discrete-time FTS tracking control scheme for $\Delta t = 0.01$ and $t_f = 5$s.

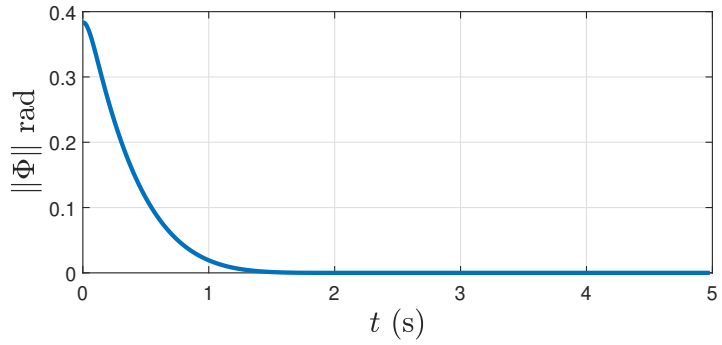

(A) Attitude tracking error function

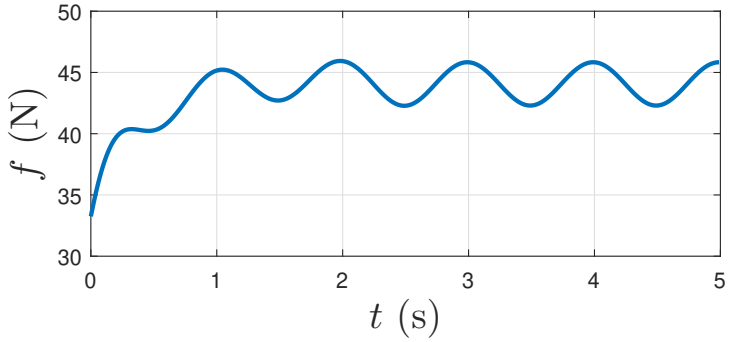

(B) Total thrust force

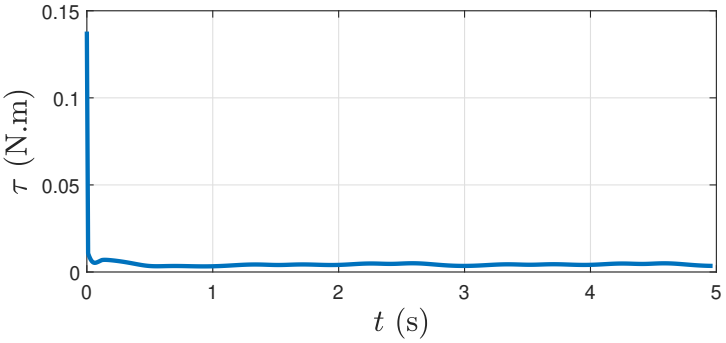

(C) Torque control

FIGURE 3.4: Tracking errors and control laws for discrete-time FTS tracking control scheme for $\Delta t = 0.01$ and $t_f = 5$s.

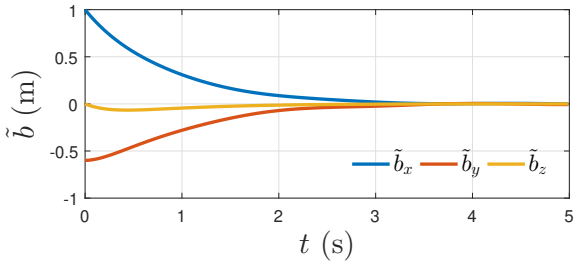

(A) Position tracking error

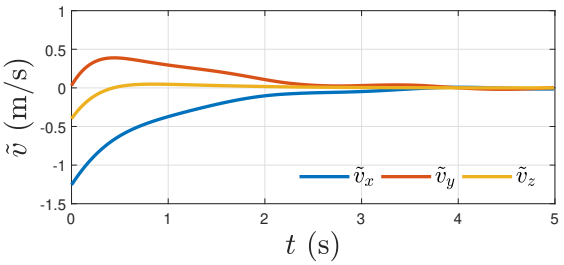

(B) Velocity tracking error

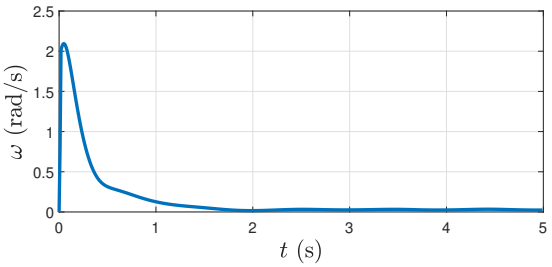

(C) Angular velocity error

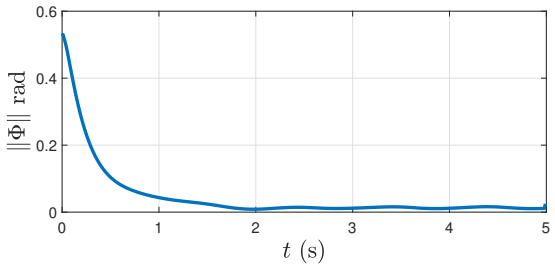

(D) Attitude tracking error function

FIGURE 3.5: Tracking errors for sampled FTS continuous tracking control scheme for $\Delta t = 0.01$ and $t_f = 5s$.

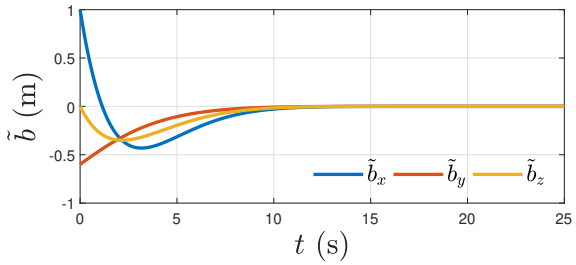

(A) Position tracking error

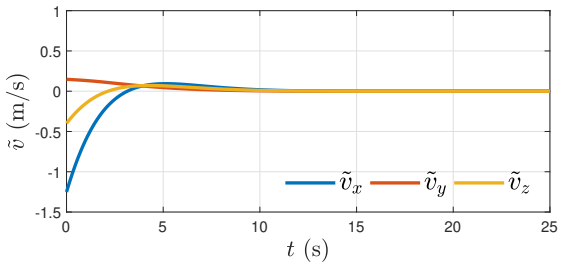

(B) Velocity tracking error

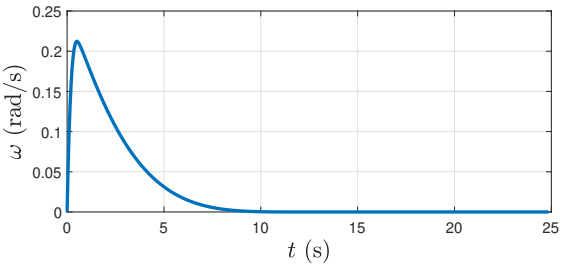

(C) Angular velocity error

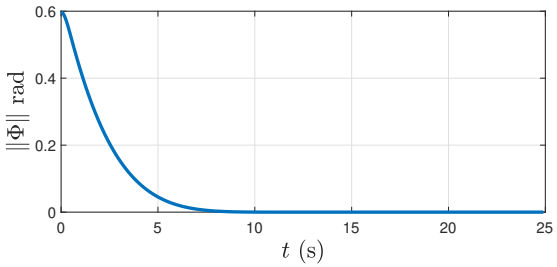

(D) Attitude tracking error function

FIGURE 3.6: Tracking errors for discrete-time FTS tracking control scheme for $\Delta t = 0.05$ and $t_f = 25s$.

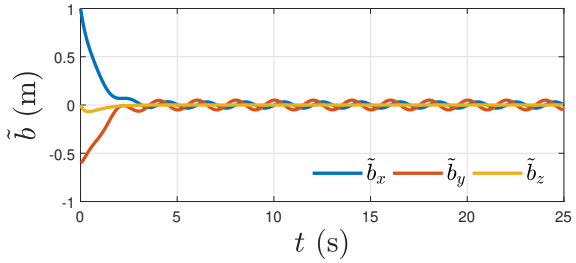

(A) Position tracking error

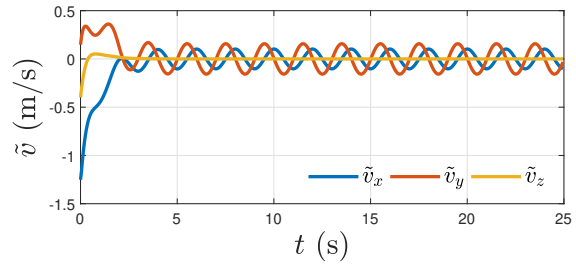

(B) Velocity tracking error

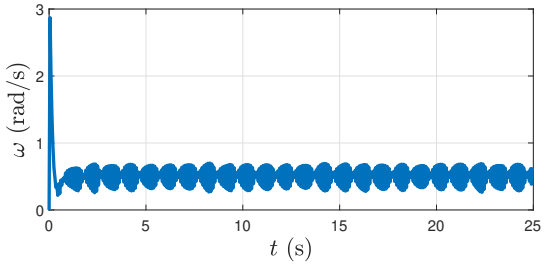

(C) Angular velocity error

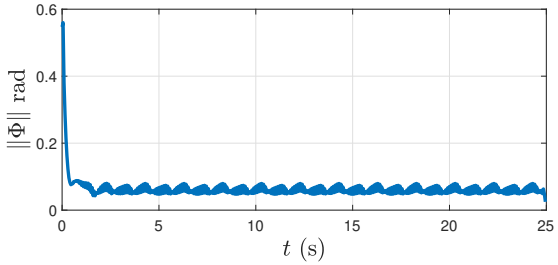

(D) Attitude tracking error

FIGURE 3.7: Tracking errors for sampled FTS continuous tracking control scheme for $\Delta t = 0.05$ and $t_f = 25s$.

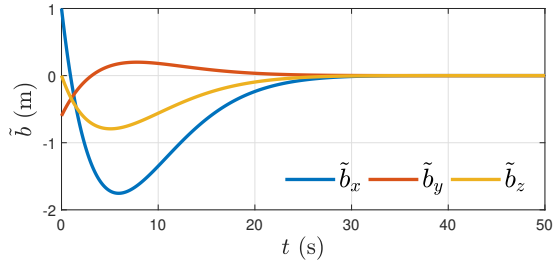

(A) Position tracking error

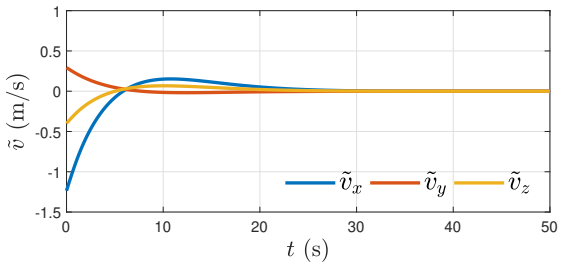

(B) Velocity tracking error

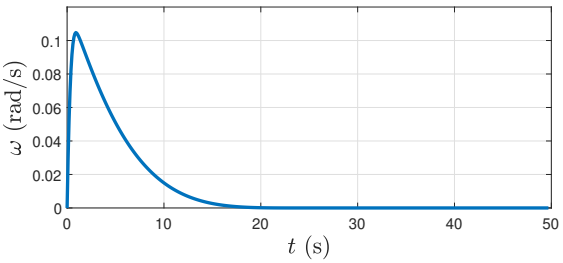

(C) Angular velocity error

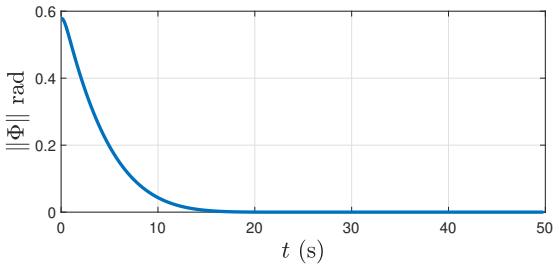

(D) Attitude tracking error function

FIGURE 3.8: Tracking errors for discrete-time FTS tracking control scheme for $\Delta t = 0.1$ and $t_f = 50s$.

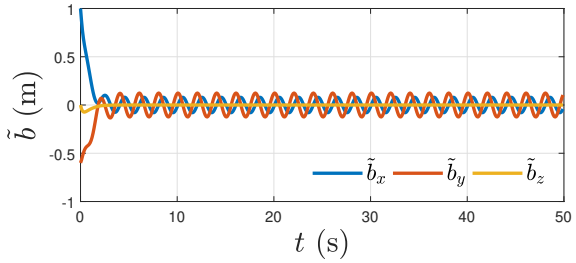

(A) Position tracking error

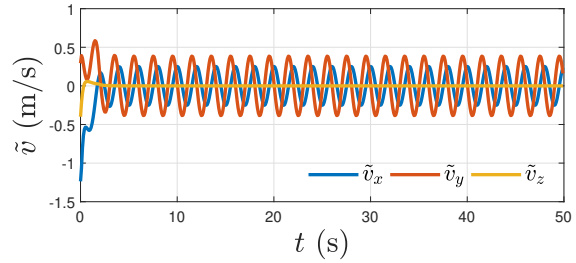

(B) Velocity tracking error

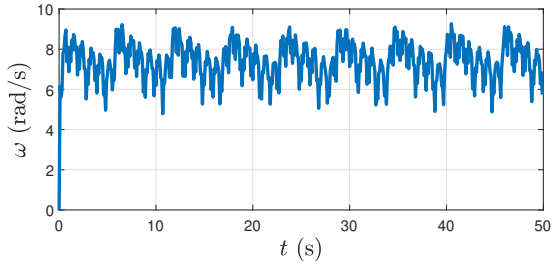

(C) Angular velocity error

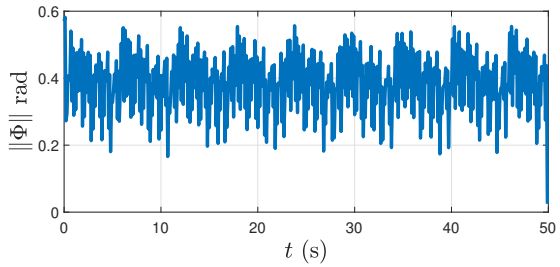

(D) Attitude tracking error function

FIGURE 3.9: Tracking errors for sampled FTS continuous tracking control scheme for $\Delta t = 0.1$ and $t_f = 50s$.

3.8 Conclusion

This research work proposes a discrete-time stable tracking control scheme with finite-time stability for unmanned vehicles that can be modeled as rigid bodies with one degree of freedom of translational motion and three degrees of freedom of rotational motion actuated. This control scheme is designed with two loops: an inner loop for attitude control and an outer loop for position control. In the outer loop, given a desired position trajectory in an inertial coordinate frame, the desired control force vector is obtained in discrete time to stabilize the desired trajectory in finite time. This control force vector expressed in the body-fixed frame is then used to generate a desired attitude trajectory. In the inner loop to track this desired attitude trajectory, a discrete-time finite-time stable (FTS) attitude tracking scheme is developed and utilized. The outer loop for position tracking also uses a discrete-time FTS control scheme. The finite-time stability of the overall tracking control scheme is proved using a discrete-time Lyapunov analysis, which results in discrete-time error dynamics in terms of translational and rotational motion tracking errors. A two-step method is proposed for each of the two control loops here, designed using a Lyapunov function that is quadratic in vector-valued functions linear in velocity and angular velocity tracking errors. Then, it is shown that position and attitude tracking errors converge to zero when this vector-valued function vanishes. This analysis results in discrete-time control laws that guarantee the convergence of the position and attitude states to the desired position and attitude trajectories in a finite time interval. Analysis of robustness to bounded disturbance torque is also presented. Moreover, a comparison between the performance of the proposed scheme and that of a sampled continuous FTS scheme is studied here, and numerical results show that a discrete-time FTS tracking control scheme is more reliable for onboard computer implementation when we need to

work with a variety of input data frequencies.

Chapter 4

Stable Nonlinear Attitude Estimation with Finite-Time Convergence

This chapter is adapted from the paper (Sanyal, Warier, and Hamrah, 2019) published in Proceeding of the 18^{th} European Control Conference (ECC 2019). The author gratefully acknowledges Dr. Amit Sanyal, and Dr. Rakesh R. Warier for their participation.

Abstract This research work presents a nonlinear finite-time stable attitude estimation scheme for a rigid body with unknown dynamics. Attitude is estimated from a minimum of two linearly independent known vectors measured in the body-fixed frame, and the angular velocity vector is assumed to have a constant bias in addition to measurement errors. Estimated attitude evolves directly on the special Euclidean group $\mathrm{SO}(3)$, avoiding any ambiguities. The constant bias in angular velocity measurements is also estimated. The estimation scheme is proven to be almost globally finite time stable in the absence of measurement errors using a Lyapunov analysis. The robustness of the scheme in the presence of bounded measurement errors is analytically shown. For digital implementation, the estimation scheme is discretized as a geometric integrator. Numerical simulations

demonstrate the robustness and convergence properties of the estimation scheme.

4.1 Mathematical Preliminaries

Any square matrix $A \in \mathbb{R}^{n\times n}$ can be written as the sum of unique symmetric and skew-symmetric matrices as follows:

$$A = \text{sym}(A) + \text{skew}(A), \tag{4.1}$$

where the symmetric and skew-symmetric components are defined as,

$$\text{sym}(A) = \frac{1}{2}(A + A^{\mathrm{T}}), \text{skew}(A) = \frac{1}{2}(A - A^{\mathrm{T}}). \tag{4.2}$$

Additionally, the following property holds. If $A_1 \in \mathbb{R}^{n\times n}$ is a symmetric matrix and $A_2 \in \mathbb{R}^{n\times n}$ is a skew symmetric matrix, then,

$$\langle A_1, A_2 \rangle = 0. \tag{4.3}$$

In other words, symmetric and skew matrices are orthogonal under the trace inner product. For all $a_1, a_2 \in \mathbb{R}^3$,

$$\left\langle a_1^{\times}, a_2^{\times} \right\rangle = 2a_1 \cdot a_2 \tag{4.4}$$

With these definitions, we proceed to lay out the attitude estimation problem.

4.2 Static Attitude Determination From Vector Measurements

The aim of this section is to formulate the problem of attitude determination from vector measurements. Let $\mathcal{I}$ denote an inertial frame that is spatially fixed. A body-fixed frame is fixed to the rigid body with its origin at the center of mass of the body, and is denoted $\mathcal{B}$. We denote the attitude of the rigid body by $R \in \mathrm{SO}(3)$, which transforms vectors in the body frame $\mathcal{B}$ to their counterparts in the inertial frame $\mathcal{I}$.

4.2.1 Vector Measurements

The attitude of the rigid body is determined from body-fixed measurements of k known inertial vectors. Let $e_1, e_2, \cdots e_k$, $k \in \mathbb{N}$ be the known inertial vectors and $u_1^m, u_2^m, \cdots u_k^m$ be the corresponding body-fixed measurements. The i^{th} vector measurement in the body-fixed frame $\mathcal{B}$ satisfies,

$$u_i^m = R^{\mathrm{T}} e_i + \sigma_i \tag{4.5}$$

where $\sigma_i \in \mathbb{R}^3$ is the noise in the i^{th} vector measurement, for all $i \in 1, 2, \cdots k$. The attitude of the rigid body can be calculated from the vector measurements provided the following assumption is satisfied.

Assumption 4.2.1. *There are at least two non-collinear vectors in the set $\{e_1, \cdots, e_k\}$ for attitude determination at all times. If $k = 2$, $e_3 = e_1 \times e_2$ is selected as the third non-collinear vector.*

Define the matrix consisting of k known inertial vectors e_i as column vectors,

$$E = \begin{cases} [e_1 \; e_2 \; e_1 \times e_2] \in \mathbb{R}^{3\times 3} & \text{when } k = 2, \\ [e_1 \; e_2 \; \ldots e_k] \in \mathbb{R}^{3\times k} & \text{when } k > 2. \end{cases} \tag{4.6}$$

The assumption 4.2.1 can be alternatively specified as follows: matrix E should have rank equal to 3. The corresponding matrix composed of body-fixed measurements as column vectors can be defined as,

$$U^m = \begin{cases} [u_1^m \; u_2^m \; u_1^m \times u_2^m] \in \mathbb{R}^{3\times 3} & \text{when } k = 2, \\ [u_1^m \; u_2^m \; \ldots \; u_k^m] \in \mathbb{R}^{3\times k} & \text{when } k > 2. \end{cases} \tag{4.7}$$

The matrix consisting of inertial vectors E and the matrix containing the body frame vectors U^m are related by:

$$U^m = R^{\mathrm{T}} E + \Xi, \tag{4.8}$$

where the columns of matrix Ξ correspond to the measurement errors σ_i. Let the true vectors in body frame be denoted by $u_i = R^{\mathrm{T}} e_i$, then the matrix of the actual body vectors corresponding to the inertial vectors e_i is given by

$$U = R^{\mathrm{T}} E, \tag{4.9}$$

in the absence of measurement errors.

The static attitude determination problem is formulated in the next subsection.

4.2.2 Cost Function For Attitude Determination

The objective is to obtain an estimate of the attitude denoted by $\widehat{R} \in \mathrm{SO}(3)$ from k known inertial vectors $e_1, \ldots, e_k$ and corresponding measured vectors $u_1^m, \ldots, u_k^m$. The static attitude estimation can be formulated as an optimization problem as follows,

$$\text{Minimize}_{\widehat{R}} \mathcal{U} = \frac{1}{2} \sum_{i}^{k} w_i (e_i - \widehat{R} u_i^m)^{\mathrm{T}} (e_i - \widehat{R} u_i^m), \tag{4.10}$$

where $w_i > 0$ are weight factors. This is referred to as Wahba's problem as in (Wahba, 1965). The cost function is re-expressed as,

$$\mathcal{U} = \frac{1}{2} \left\langle E - \widehat{R} U^m, (E - \widehat{R} U^m) W \right\rangle, \tag{4.11}$$

where $W = \mathrm{diag}([w_1,\ w_2,\ \ldots,\ w_k])$ and E and U^m are given by equations (4.6) and (4.7) respectively. The cost function can be generalized such that W is a symmetric positive semi-definite matrix satisfying some special conditions. This is described in the next subsection. The structure of the generalized cost function in the absence of measurement errors, is detailed in the following lemma.

Lemma 4.2.1. *Define $Q = R\widehat{R}^T$ as the attitude estimation error. Let $E \in \mathbb{R}^{3\times k}$ be as defined as in (4.6) with $\mathrm{rank}(E) = 3$. Let the gain matrix W of the generalized Wahba cost function be given by,*

$$W = E^T \left(EE^T\right)^{-1} K \left(EE^T\right)^{-1} E, \tag{4.12}$$

where $K = \mathrm{diag}([k_1, k_2, k_3])$ *and* $k_1 > k_2 > k_3 \geq 1$. *Then, in the absence of measurement errors,*

$$\mathcal{U} = \frac{1}{2}\left\langle E - \widehat{R}U^m, (E - \widehat{R}U^m)W \right\rangle = \langle K, I - Q \rangle, \tag{4.13}$$

which is a Morse function on $\mathrm{SO}(3)$ *whose critical points are given by the set,*

$$\begin{aligned} \mathcal{C} = \{&I, \mathrm{diag}([-1,-1,1]), \mathrm{diag}([1,-1,-1]), \\ &\mathrm{diag}([-1,1,-1])\}. \end{aligned} \tag{4.14}$$

In addition, $\mathcal{U}$ *has a global minimum at* $Q = I$.

Proof. Utilizing the properties of the inner product we can arrive at the following simplification:

$$\begin{aligned} \mathcal{U} = &\frac{1}{2}\mathrm{tr}\Big((E^{\mathrm{T}}E + (U^m)^{\mathrm{T}}U^m)W\Big) \\ &- \frac{1}{2}\mathrm{tr}\Big(((U^m)^{\mathrm{T}}\widehat{R}^{\mathrm{T}}E - E^{\mathrm{T}}\widehat{R}U^m)W\Big). \end{aligned} \tag{4.15}$$

Substituting W as given by (4.12) and defining

$$L = EW(U^m)^{\mathrm{T}}, \tag{4.16}$$

the expression (4.15) can be further simplified to:

$$\mathcal{U} = \frac{1}{2}\mathrm{tr}\Big(K + U^m W(U^m)^{\mathrm{T}} - \widehat{R}^{\mathrm{T}}L - L^{\mathrm{T}}\widehat{R}\Big). \tag{4.17}$$

In the absence of measurement noise in the vector measurements, $U^m = U = R^{\mathrm{T}}E$ and $L = KR$. Substituting $U^m = R^{\mathrm{T}}E$ in equation (4.17) and $\mathrm{tr}(AB) = \mathrm{tr}(BA)$, we get

$$\begin{aligned}\mathcal{U} =& \mathrm{tr}(K - L^{\mathrm{T}}\widehat{R}) = \mathrm{tr}\left(K - \widehat{R}R^{\mathrm{T}}EWE^{\mathrm{T}}\right) \\ &= \langle K, I - Q\rangle \text{ , where } Q = R\widehat{R}^{\mathrm{T}}. \end{aligned} \tag{4.18}$$

The choice of W given in eq. (4.12) ensures that $K = EWE^{\mathrm{T}}$. Next it is shown that $\langle K, I - Q\rangle$ is a Morse function with four isolated non-degenerate critical points on $\mathrm{SO}(3)$ given in (4.14). A Morse function is a function that has isolated non-degenerate critical points, which can be classified as minimum, maximum or saddle points by examining the Hessian of this function as in (Milnor, Spivak, and Wells, 1969). The proof that shows (4.13) is a Morse function is presented in detail in Lemma 2.1 in (Izadi and Sanyal, 2014) and is omitted here for brevity.

A first variation of $Q \in \mathrm{SO}(3)$ is given by,

$$\delta Q = Q\Sigma^{\times}, \tag{4.19}$$

where $\Sigma \in \mathbb{R}^3$. The first variation of $\langle K, I - Q\rangle$ with respect to Q is given by

$$\partial_Q \langle K, I - Q\rangle = \langle K, -\delta Q\rangle = tr(-KQ\Sigma^{\times}). \tag{4.20}$$

KQ can be written as sum of skew and symmetric matrices i.e., $KQ = \mathrm{sym}(KQ) +$

skew(KQ). Exploiting the linearity of the trace inner product and utilizing the identities given by Eq. (4.3) and Eq. (4.4), the following expression is obtained.

$$\begin{aligned}\partial_Q \langle K, I - Q\rangle &= \langle \text{skew}(KQ), \Sigma\rangle \\ &= \text{vex}(KQ - Q^{\mathrm{T}}K)^{\mathrm{T}}\Sigma = s_K(Q)^{\mathrm{T}}\Sigma,\end{aligned} \tag{4.21}$$

where $s_K(Q)$ is given by,

$$s_K(Q) = \text{vex}(KQ - Q^{\mathrm{T}}K), \tag{4.22}$$

and vex$(.)$ is as defined in Section 4.1. The critical points of $\langle K, I - Q\rangle$ on SO(3) are where the variation vanishes. Since Σ is arbitrary, the critical points satisfy, $s_K(Q) = 0$, which implies,

$$KQ = Q^{\mathrm{T}}K. \tag{4.23}$$

Due to the properties of K, the critical points of $\langle K, I - Q\rangle$ are therefore given by,

$$\begin{aligned}Q \in \{&I, \text{diag}([-1, -1, 1]), \text{diag}([1, -1, -1]), \\ &\text{diag}([-1, 1, -1])\}.\end{aligned} \tag{4.24}$$

By taking the second variation it can be shown that $\langle K, I - Q\rangle$ achieves a minimum at $Q = I$. Similar results are available in prior literature, e.g., (Izadi and Sanyal, 2014; Bullo and Lewis, 2004). ■

The static estimation problem outlined here can be solved by computing $\widehat{R}$ that will

minimize the $\mathcal{U}$ at any given instant. However, static methods often under perform when measurements have noise and bias. The following section considers dynamic attitude estimation under unknown attitude dynamics and with biased angular velocity measurements.

4.3 Preliminary Results for Attitude State and Angular Velocity Bias Estimation

4.3.1 Dynamic Attitude Estimation

The kinematics of rigid body rotation is given by Poisson's equation:

$$\dot{R} = R\Omega^{\times}, \tag{4.25}$$

where $\Omega \in \mathbb{R}^3$ is the true angular velocity of the rigid body represented in the body-fixed coordinate frame. Let the measured angular velocity, denoted by Ω^m, be given by

$$\Omega^m = \Omega + \beta + \nu, \tag{4.26}$$

where $\beta \in \mathbb{R}^3$ is a constant bias in angular velocity measurements that also has to be estimated, and $\nu \in \mathbb{R}^3$ is the vector of additive noise in angular velocity components. Let $(\widehat{R}, \widehat{\Omega}) \in \mathrm{SO}(3) \times \mathbb{R}^3$ be the estimated attitude and angular velocity states provided by the estimation scheme, satisfying the following kinematic relation:

$$\dot{\widehat{R}} = \widehat{R}\widehat{\Omega}^{\times}. \tag{4.27}$$

In addition, let

$$\widehat{\Omega} = \Omega^m - \widehat{\beta} - \omega, \tag{4.28}$$

where $\widehat{\beta} \in \mathbb{R}^3$ is the estimate of the bias in angular velocity measurements, and $\omega \in \mathbb{R}^3$ is the "excess" or error in estimating the angular velocity and the bias.

The objective is to obtain estimates of the attitude, angular velocity, and bias ($\widehat{R}$, $\widehat{\Omega}$ and $\widehat{\beta}$) in real time, from the matrix of known inertial vectors E, the corresponding vector measurements made in the body-fixed frame U^m, and the biased angular velocity measurement Ω^m. The moment of inertia and other parameters that occur in the dynamics of the rigid body are unknown. Note that the (number of) measured vectors may be varying over time, as long as at least two non-collinear vectors are measured at all times. The observer design given in the following section is shown to provide almost global finite-time stable (AGFTS) estimates $\widehat{R}$, $\widehat{\Omega}$ and $\widehat{\beta}$, where these estimates converge to the respective true values R, Ω and β in finite time, in the absence of measurement noise. Section 5.3 shows the robustness of this observer in the presence of measurement noise. The following result, relating the attitude estimation error to the angular velocity estimation error, is used in the next section to prove the main result.

Lemma 4.3.1. *Let K be as defined in Lemma 4.2.1. Then, in the absence of the measurement errors, the time derivative of $\mathcal{U}$ along the trajectories satisfying the kinematic equations (4.25)-(4.27), is given by:*

$$\frac{\mathrm{d}}{\mathrm{d}t}\mathcal{U} = \frac{\mathrm{d}}{\mathrm{d}t}\langle K, I - Q\rangle = s_K(Q) \cdot \left(\widehat{R}\widetilde{\Omega}\right) \tag{4.29}$$

$$= \frac{\mathrm{d}}{\mathrm{d}t}\mathrm{tr}(K - L^T\widehat{R}) = -s_L(\widehat{R}) \cdot \widetilde{\Omega}, \tag{4.30}$$

where

$$\widetilde{\Omega} = \Omega - \widehat{\Omega}, \;\; s_L(\widehat{R}) = \text{vex}(L^T\widehat{R} - \widehat{R}^T L). \tag{4.31}$$

Proof. Since $R_e = R\widehat{R}^{\mathrm{T}}$, we obtain from eqs. (4.25)-(4.27):

$$\begin{aligned} \dot{Q} = \frac{\mathrm{d}}{\mathrm{d}t}Q &= \dot{R}\widehat{R}^{\mathrm{T}} + R\dot{\widehat{R}}^{\mathrm{T}} \\ &= R\Omega^{\times}\widehat{R}^{\mathrm{T}} - R\widehat{\Omega}^{\times}\widehat{R}^{\mathrm{T}} \\ &= R\widehat{R}^{\mathrm{T}}\big(\widehat{R}(\Omega - \widehat{\Omega})\big)^{\times} \\ &= Q(\widehat{R}\widetilde{\Omega})^{\times}. \end{aligned} \tag{4.32}$$

Further, from the definition of L in eq. (4.16), we see that in the absence of measurement noise $U^m = U = R^{\mathrm{T}}E$ and

$$\dot{L} = EW\dot{U}^{\mathrm{T}} = EWU^{\mathrm{T}}\Omega^{\times} = L\Omega^{\times}. \tag{4.33}$$

From eq. (4.32), we obtain

$$\frac{\mathrm{d}}{\mathrm{d}t}\langle K, I - Q\rangle = \langle K, -Q(\widehat{R}\widetilde{\Omega})^{\times}\rangle.$$

From eq. (4.33), we get

$$\frac{\mathrm{d}}{\mathrm{d}t}\text{tr}(K - L^{\mathrm{T}}\widehat{R}) = \text{tr}(\Omega^{\times}L^{\mathrm{T}}\widehat{R} - L^{\mathrm{T}}\widehat{R}\widehat{\Omega}^{\times}).$$

As in the proof of Lemma 4.2.1, (4.3) and (4.4) are utilized to obtain,

$$\begin{aligned}\frac{\mathrm{d}}{\mathrm{d}t}\langle K, I-Q\rangle &= -\frac{1}{2}\mathrm{tr}\big((KQ-Q^{\mathrm{T}}K)(\widehat{R}\widetilde{\Omega})^{\times}\big)\\ &= \mathrm{vex}(KQ-Q^{\mathrm{T}}K)\cdot(\widehat{R}\widetilde{\Omega})\end{aligned} \tag{4.34}$$

and

$$\frac{\mathrm{d}}{\mathrm{d}t}\mathrm{tr}(K-L^{\mathrm{T}}\widehat{R}) = -\mathrm{vex}(L^{\mathrm{T}}\widehat{R}-\widehat{R}^{\mathrm{T}}L)\cdot\widetilde{\Omega}. \tag{4.35}$$

As (4.34) is identical to (4.29) and (4.35) is identical to (4.30), we conclude the result. ■

4.3.2 Some Preliminary Results

The following four lemmas are used to prove the main result on finite time stable attitude, angular velocity and bias estimation scheme given in Section 4.4.

Lemma 4.3.2. *Let x and y be non-negative real numbers and let $p \in (1,2)$. Then*

$$x^{(1/p)} + y^{(1/p)} \geq (x+y)^{(1/p)}. \tag{4.36}$$

Moreover the above inequality is a strict inequality if both x and y are non-zero.

Proof. The proof of this result is given in (Bohn and Sanyal, 2014; Bohn and Sanyal, 2015), and is omitted here for brevity. ■

Lemma 4.3.3. *Let K be as defined in Lemma 4.2.1 and $s_K(Q)$ be as given in the equation (4.22). Let $\mathcal{S} \subset \mathrm{SO}(3)$ be a closed subset containing the identity in its interior, defined by*

$$\begin{aligned}\mathcal{S} = \{ Q \in \mathrm{SO}(3) \ : \ & Q_{ii} \geq 0 \text{ and } Q_{ij}Q_{ji} \leq 0 \\ & \forall i,\ j \in \{1,2,3\},\ i \neq j\}. \end{aligned} \tag{4.37}$$

Then for $Q \in \mathcal{S}$, we have

$$s_K(Q)^T s_K(Q) \geq \mathrm{tr}(K - KQ). \tag{4.38}$$

Proof. The proof of this result is given in (Bohn and Sanyal, 2015), and is omitted here for brevity. ■

Lemma 4.3.4. *Let $s_L(\widehat{R})$ and $s_K(Q)$ be as defined earlier. Then following holds:*

$$s_L(\widehat{R})^T s_L(\widehat{R}) = s_K(Q)^T s_K(Q) \tag{4.39}$$

Proof. From the definition of L, it can be seen that $L = KR$. $s_L(\widehat{R})$ and $s_K(Q)$ can be rewritten as,

$$s_L(\widehat{R}) = \mathrm{vex}(R^{\mathrm{T}} K \widehat{R} - \widehat{R}^{\mathrm{T}} K R) =: \mathrm{vex}(A_1), \tag{4.40}$$

$$s_K(Q) = \mathrm{vex}(KR\widehat{R}^{\mathrm{T}} - \widehat{R}R^{\mathrm{T}} K) := \mathrm{vex}(A_2), \tag{4.41}$$

where A_1, A_2 are used to represent the skew symmetric matrices inside the $\mathrm{vex}(.)$ operator. From the identity given in Eq.(4.4), it is clear that Eq.(4.39) is equivalent to following

expression,

$$tr(A_1 A_1) = tr(A_2 A_2). \tag{4.42}$$

The RHS turns out to be,

$$tr(A_1 A_1) = tr\big((R^{\mathrm{T}} K \widehat{R} - \widehat{R}^{\mathrm{T}} K R)(R^{\mathrm{T}} K \widehat{R} - \widehat{R}^{\mathrm{T}} K R)\big) \tag{4.43}$$

The LHS is obtained as,

$$tr(A_2 A_2) = tr\big((K R \widehat{R}^{\mathrm{T}} - \widehat{R} R^{\mathrm{T}} K)(K R \widehat{R}^{\mathrm{T}} - \widehat{R} R^{\mathrm{T}} K)\big) \tag{4.44}$$

The identity in Eq. (4.42) can be obtained by expanding and simplifying the above two expressions using the properties of trace inner product. ■

The design and stability result of the finite-time stable estimator are given in the following section. Note that the attitude estimation error $Q = R\widehat{R}^{\mathrm{T}}$ is defined on the group of rigid body rotations, $\mathrm{SO}(3)$, which is not a vector space. The angular velocity estimation error, $\widetilde{\Omega}$, and bias estimation error, $\widetilde{\beta}$, are expressed on the vector space $\mathbb{R}^3$. Therefore, for Lyapunov stability analysis of the observer designed on $\mathrm{SO}(3) \times \mathbb{R}^3 \times \mathbb{R}^3$, a suitable Lyapunov function is required. This comes in the form of a Morse-Lyapunov function, as defined later in Theorem 4.4.1 in Section 4.4, where the Morse function $\mathcal{U} = \langle K, I - Q \rangle$ on $\mathrm{SO}(3)$ is used as the component of the Morse-Lyapunov function that depends on the attitude component of the full state. The Morse-Lyapunov function is subsequently shown to guarantee convergence of state estimation errors $(Q, \widetilde{\Omega}, \widetilde{\beta})$ to $(I, 0, 0)$ in finite-time.

4.4 Finite-time Stable Attitude State and Angular Velocity Bias Estimation

In this section we give the main result; a finite-time stable observer for estimation of rigid body attitude, angular velocity, and a constant bias in angular velocity measurements. A Hölder-continuous Morse-Lyapunov function is utilized to show the finite-time stability of the resulting closed-loop system. For rigid body attitude, we assume that at least two non-collinear but known inertial vectors are measured in a body-fixed frame, as described earlier in section 4.2.

Theorem 4.4.1. *Consider the attitude kinematics and angular velocity measurements given by* (4.25)-(4.28) *in the absence of measurement noise (i.e., $\sigma = 0$, $\nu = 0$). Let $p \in]1,2[$ and $\kappa > 0$ be scalar observer gains, and define the following quantities:*

$$\widetilde{\beta} = \beta - \widehat{\beta}, \tag{4.45}$$

$$z_L(\widehat{R}) = \frac{s_L(\widehat{R})}{\left(s_L(\widehat{R})^T s_L(\widehat{R})\right)^{1-1/p}}, \tag{4.46}$$

$$\Psi(L, \widehat{R}, \omega) = \omega - \kappa z_L(\widehat{R}), \text{ and} \tag{4.47}$$

$$\begin{aligned} w_L(\widehat{R}, \widehat{\Omega}, \Omega^m, \widehat{\beta}) = \frac{\mathrm{d}}{\mathrm{d}t} s_L(\widehat{R}) = \operatorname{vex}\left(L^T \widehat{R} \widehat{\Omega}^\times + \widehat{\Omega}^\times \widehat{R}^T L\right) \\ - \operatorname{vex}\left(\widehat{R}^T L (\Omega^m - \widehat{\beta})^\times + (\Omega^m - \widehat{\beta})^\times L^T \widehat{R}\right). \end{aligned} \tag{4.48}$$

Let Assumption 4.2.1 be satisfied and let μ, k_p, k_v be positive scalar observer gains such that $\mu \leq 1$. Thereafter, consider the following observer equations:

$$\dot{\widehat{R}} = \widehat{R}\widehat{\Omega}^{\times} = \widehat{R}(\Omega^m - \widehat{\beta} - \omega)^{\times}, \tag{4.49}$$

$$\dot{\widehat{\beta}} = \frac{k_p}{2-\mu} s_L, \text{ and} \tag{4.50}$$

$$\mu\dot{\omega} = k_p s_L - k_v \frac{\Psi}{\left(\Psi^T\Psi\right)^{1-1/p}} + \frac{\mu\kappa}{\left(s_L^T s_L\right)^{1-1/p}} H(s_L) w_L, \tag{4.51}$$

where the functional dependencies of s_L, w_L and Ψ have been suppressed for notational convenience, and where $H : \mathbb{R}^3 \to Sym(3)$, the space of symmetric 3×3 real matrices, is defined by

$$H(x) = I - \frac{2(1-1/p)}{x^T x} x x^T. \tag{4.52}$$

Then the attitude and angular velocity estimation errors (Q, ω) converge to $(I, 0) \in \mathrm{SO}(3) \times \mathbb{R}^3$ and the bias estimation error $\widetilde{\beta}$ converges to $0 \in \mathbb{R}^3$ in a finite time stable manner, from almost all initial conditions except those in a set of measure zero.

Proof. Consider the following Morse-Lyapunov function:

$$\begin{aligned} \mathcal{V}(L, \widehat{R}, \Omega, \widehat{\Omega}, \widetilde{\beta}) = \frac{\mu}{2}\Psi^{\mathrm{T}}\Psi + k_p\, \mathcal{U}(\widehat{R}, U^m, E) \\ + \frac{2-\mu}{2}\widetilde{\beta}^{\mathrm{T}}\widetilde{\beta}, \end{aligned} \tag{4.53}$$

where $\mathcal{U}(\cdot,\cdot,\cdot)$ is as defined in Lemma 4.2.1. In the following analysis, we suppress the functional dependencies of $\mathcal{U}$ and $\mathcal{V}$ for notational ease. Taking the time derivative of this Lyapunov function, we get

$$\dot{\mathcal{V}} = \mu\Psi^{\mathrm{T}}\dot{\Psi} - k_p s_L^{\mathrm{T}}\widetilde{\Omega} - (2-\mu)\widetilde{\beta}^{\mathrm{T}}\dot{\widehat{\beta}}$$

where we used eq. (4.30) to substitute for the time derivative of $\mathcal{U}$ in the second term, and the fact that β is a constant bias (therefore $\dot{\widetilde{\beta}} = -\dot{\hat{\beta}}$) in the third term on the right side of the above expression. Substituting from eq. (4.50) for $\dot{\hat{\beta}}$ into the third term, we get

$$\dot{\mathcal{V}} = \mu \Psi^{\mathrm{T}} \dot{\Psi} - k_p s_L^{\mathrm{T}} (\widetilde{\Omega} + \widetilde{\beta}). \tag{4.54}$$

From (Bohn and Sanyal, 2014; Bohn and Sanyal, 2015), we know that

$$\frac{d}{\mathrm{d}t} z_L = \frac{1}{\left(s_L^{\mathrm{T}} s_L\right)^{1-1/p}} H(s_L) w_L.$$

Now substituting for Ψ from eq. (4.47) in to eq. (4.54), using the time derivative of z_L as given by the above equation, and noting that $\omega = \widetilde{\Omega} + \widetilde{\beta}$ in the absence of measurement noise, we obtain

$$\dot{\mathcal{V}} = \mu \Psi^{\mathrm{T}} \left(\dot{\omega} - \frac{\kappa}{\left(s_L^{\mathrm{T}} s_L\right)^{1-1/p}} H(s_L) w_L \right) - k_p s_L^{\mathrm{T}} \omega. \tag{4.55}$$

Finally, substituting the observer eq. (4.51) for $\dot{\omega}$ into eq. (4.55), we get

$$\begin{aligned} \dot{\mathcal{V}} &= \Psi^{\mathrm{T}} \left(k_p s_L - k_v \frac{\Psi}{\left(\Psi^{\mathrm{T}} \Psi\right)^{1-1/p}} \right) - k_p s_L^{\mathrm{T}} \omega \\ &= k_p s_L^{\mathrm{T}} (\Psi - \omega) - k_v \left(\Psi^{\mathrm{T}} \Psi\right)^{1/p} \\ &= -k_p \kappa s_L^{\mathrm{T}} z_L - k_v \left(\Psi^{\mathrm{T}} \Psi\right)^{1/p} \\ &= -k_p \kappa \left(s_L^{\mathrm{T}} s_L\right)^{1/p} - k_v \left(\Psi^{\mathrm{T}} \Psi\right)^{1/p}. \end{aligned} \tag{4.56}$$

From Lemma 4.3.3 and Lemma 4.3.4, in a neighborhood of $I \in \mathrm{SO}(3)$, we have

$$-s_L^{\mathrm{T}} s_L \leq -\mathcal{U}(\widehat{R}, U^m, E) = -\langle K, I - Q \rangle. \tag{4.57}$$

Therefore, for the expression (4.56), we get

$$\begin{aligned} \dot{\mathcal{V}} &\leq -k_p^{1-1/p} \kappa (k_p \mathcal{U})^{1/p} - k_v \Big(\Psi^{\mathrm{T}} \Psi \Big)^{1/p} \\ &\leq -k_0 \Big(\Big(\Psi^{\mathrm{T}} \Psi \Big)^{1/p} + \big(k_p \mathcal{U} \big)^{1/p} \Big), \\ &\text{where } \; k_0 = \min(k_p^{1-1/p} \kappa, k_v). \end{aligned} \tag{4.58}$$

Finally, applying Lemma 4.3.2 to the above inequality, we have:

$$\dot{\mathcal{V}} \leq -k_0 \Big(\Psi^{\mathrm{T}} \Psi + k_p \mathcal{U} \Big)^{1/p}. \tag{4.59}$$

Considering equation (4.59), the set where $\dot{\mathcal{V}} = 0$ is:

$$\begin{aligned} \dot{\mathcal{V}}^{-1}(0) =& \{ (Q, \omega) \;\; : \;\; s_k(Q) = 0 \text{ and } \Psi = 0 \} \\ =& \{ (Q, \omega) \;\; : \;\; Q \in \mathcal{C} \text{ and } \omega = 0 \}. \end{aligned} \tag{4.60}$$

where $\mathcal{C}$ is as defined by eq. (4.14). Using the invariance-like theorem 8.4 in (Khalil, 2001), we can conclude that as $t \to \infty$, (Q, ω) converges to the set:

$$\mathrm{S} = \{ (Q, \omega) \;\; : \;\; Q \in \mathcal{C} \text{ and } \omega = 0 \in \mathbb{R}^3 \} \tag{4.61}$$

in finite time, which is equivalent to:

$$\mathbb{S} = \{(Q, \widetilde{\Omega}, \widetilde{\beta}) \in \mathrm{SO}(3) \times \mathbb{R}^3 \times \mathbb{R}^3 \quad : \quad Q \in \mathcal{C}\,, \widetilde{\Omega} = 0 \text{ and } \widetilde{\beta} = 0\}, \tag{4.62}$$

as $\omega = \widetilde{\Omega} + \widetilde{\beta}$.

This means that the resulting closed-loop system has a set of equilibria $\mathbb{S} \subset \mathrm{SO}(3) \times \mathbb{R}^3 \times \mathbb{R}^3$, to which all initial estimation errors ultimately converge. The only stable equilibrium in $\mathbb{S}$ is $(I, 0, 0)$ while the other three are unstable equilibria. The resulting closed-loop system with the estimation errors gives rise to a Hölder-continuous feedback with exponent less than one ($\frac{1}{p} < 1$), while in the limiting case of $\frac{1}{p} = 1$ the feedback system is Lipschitz-continuous. Proceeding with an analysis similar to that in (Sanyal, Izadi, and Bohn, 2014; Bohn and Sanyal, 2014; Sanyal, Bohn, and Bloch, 2013), it can be concluded that the equilibria and the corresponding regions of attraction of the Hölder-continuous FTS observer with $p \in]1, 2[$ are identical to those of the corresponding Lipschitz-continuous asymptotically stable observer with $p = 1$, and the region of attraction is almost global.

■

4.5 Robustness Analysis

The almost global finite-time stability property of the estimator given by Theorem 4.4.1 results in a guaranteed convergence of almost any bounded initial estimate errors to the true state, given by the estimation errors $(Q, \tilde{\Omega}, \tilde{\beta}) = (I, 0, 0)$, in finite time in the absence of any disturbances. In the presence of a bounded measurement noise ν in the measurement of angular velocity, all estimate errors will converge to a bounded neighborhood of

$(I, 0, 0)$. The following result gives a conservative statement relating the bound of measurement noise that can be tolerated and bounds on the neighborhood of $(I, 0, 0)$.

Corollary 4.5.1. *Consider the observer equations* (4.49)-(4.51). *Let the measured angular velocity be given by*

$$\Omega^m = \Omega + \beta + \nu \tag{4.63}$$

where ν is the time-varying noise vector. Let $\mathcal{N} \subset S \times \mathbb{R}^3 \times \mathbb{R}^3$, where S is as defined in equation (4.37), *be a closed neighborhood of $(I, 0, 0)$ defined by*

$$\mathcal{N} := \left\{ (Q, \tilde{\Omega}, \tilde{\beta}) : \|s_L\| \leq s_{L_{max}} \text{ and } \|\Psi\| \leq \Psi_{max} < 1 \right\}, \tag{4.64}$$

If the norm of the noise in angular velocity ν satisfies following inequality,

$$\|\nu(t)\| \leq \epsilon \leq \frac{k_v \left(s_{L_{max}}^{(2/p)} + \Psi_{max}^{(2/p)} \right)}{k_p \; s_{L_{max}}}, \tag{4.65}$$

then, the estimation errors $(Q, \tilde{\Omega}, \tilde{\beta})$ converge to the neighborhood $\mathcal{N}$.

Proof. The proof of this statement is based on the Lyapunov analysis used in the proof of Theorem 4.4.1. Substituting (4.26) in (4.28), we find

$$\tilde{\Omega} + \tilde{\beta} = \omega - \nu, \tag{4.66}$$

where $\tilde{\Omega}$ and $\tilde{\beta}$ are defined in (4.31) and (4.45), respectively. Substituting (4.66) into the time derivative of Lyapunov functions that is obtained and simplified as in (4.54), we have

$$\dot{\mathcal{V}} = \mu \Psi^{\mathrm{T}} \dot{\Psi} - k_p s_L^{\mathrm{T}} \omega + k_p s_L^{\mathrm{T}} \nu, \tag{4.67}$$

Then substituting for Ψ from (4.47) into (4.67) using the time derivative of z_L, in the presence of measurement noise, we obtain

$$\begin{aligned}\dot{\mathcal{V}} = \mu\Psi^{\mathrm{T}}\left(\dot{\omega} - \frac{\kappa}{\left(s_L^{\mathrm{T}}s_L\right)^{1-1/p}}H(s_L)w_L\right) \\ - k_p s_L^{\mathrm{T}}\omega + k_p s_L^{\mathrm{T}}\nu.\end{aligned} \tag{4.68}$$

Finally, substituting the expression given in (4.51) for $\dot{\omega}$ into (4.68), we get

$$\begin{aligned}\dot{\mathcal{V}} &= \Psi^{\mathrm{T}}\left(k_p s_L - k_v\frac{\Psi}{\left(\Psi^{\mathrm{T}}\Psi\right)^{1-1/p}}\right) - k_p s_L^{\mathrm{T}}\omega + k_p s_L^{\mathrm{T}}\nu \\ &= k_p s_L^{\mathrm{T}}(\Psi - \omega) - k_v\left(\Psi^{\mathrm{T}}\Psi\right)^{1/p} + k_p s_L^{\mathrm{T}}\nu \\ &= -k_p\kappa s_L^{\mathrm{T}}z_L - k_v\left(\Psi^{\mathrm{T}}\Psi\right)^{1/p} + k_p s_L^{\mathrm{T}}\nu \\ &= -k_p\kappa\left(s_L^{\mathrm{T}}s_L\right)^{1/p} - k_v\left(\Psi^{\mathrm{T}}\Psi\right)^{1/p} + k_p s_L^{\mathrm{T}}\nu.\end{aligned} \tag{4.69}$$

which has an additional term due to the measurement noise, when compared with expression (4.56) for $\dot{\mathcal{V}}$ along the noise-free observer. Considering upper bounds of the noise as defined in (4.65) on this extra term, we find

$$k_p s_L^{\mathrm{T}}\nu \leq \left\|k_p\right\|\left\|s_L\right\|\left\|\nu\right\| \leq k_p s_{L_{max}}\epsilon \tag{4.70}$$

Therefore, $\dot{\mathcal{V}}$ is upper bounded as

$$\dot{\mathcal{V}} \leq -k_p\kappa\left(s_L^{\mathrm{T}}s_L\right)^{1/p} - k_v\left(\Psi^{\mathrm{T}}\Psi\right)^{1/p} + k_p s_{L_{max}}\epsilon \tag{4.71}$$

On the boundary of the neighborhood $\mathcal{N}$ defined by (4.64), the upper bound on $\dot{\mathcal{V}}$ is given by

$$\dot{\mathcal{V}} \leq -k_v \left(s_{L_{max}}^{(2/p)} + \Psi_{max}^{(2/p)} \right) + k_p s_{L_{max}} \epsilon. \tag{4.72}$$

Therefore, $\dot{\mathcal{V}}$ is non-positive along the boundary of $\mathcal{N}$ if

$$-k_v \left(s_{L_{max}}^{(2/p)} + \Psi_{max}^{(2/p)} \right) + k_p s_{L_{max}} \epsilon \leq 0. \tag{4.73}$$

which is a sufficient condition for all trajectories starting outside this neighborhood to converge to the neighborhood of $(I, 0, 0)$. Expression (4.73) leads to (4.65) for the bound on the norm of the noise ν for which convergence of estimation errors $(Q, \tilde{\Omega}, \tilde{\beta})$ to $(I, 0, 0)$ is guaranteed. ■

4.6 Numerical results of the finite-time stable (FTS) estimator

In this section, simulation results of the proposed finite-time stable (FTS) estimator *without any measurement noise* are presented to show the finite-time convergence of all estimation errors to zero. Attitude estimation with the FTS estimator as well as the discrete VAE introduced in Section 5.2.1 are numerically implemented using a *geometric scheme*. Unlike commonly used numerical integration methods like Runge-Kutta, geometric integration schemes preserve the geometry of the state space without any projection or parameterization.

Let $\dot{\omega} = \chi$ where χ is the right-hand side of (4.51) divided by μ, and let Δt be the time step size. Discretized equations that are used to numerically implement the proposed FTS estimation scheme are as follows:

$$\widehat{R}_{i+1} = \widehat{R}_i \exp\left(\Delta t(\Omega_i^m - \widehat{\beta}_i - \omega_i)^\times\right), \tag{4.74}$$

$$\omega_{i+1} = \omega_i + \Delta t \chi_i, \tag{4.75}$$

$$\widehat{\beta}_{i+1} = \widehat{\beta}_i + \frac{\Delta t\ k_p}{2-\mu} s_{L_i}(\widehat{R}_i). \tag{4.76}$$

where

$$\chi_i = \mu^{-1}\Big(k_p s_{L_i} - \frac{k_v \Psi_i}{\left(\Psi_i^{\mathrm{T}}\Psi_i\right)^{1-1/p}} + \frac{\mu\kappa H(s_{L_i}) w_{L_i}}{\left(s_{L_i}^{\mathrm{T}} s_{L_i}\right)^{1-1/p}}\Big) \tag{4.77}$$

The matrix exponential map in (4.74) guarantees that each attitude estimate belongs to $\mathrm{SO}(3)$.

The estimator is simulated with a time step size of $\Delta t = 0.01$ s for a time duration of $T = 30$ s. The rigid body is assumed to have the following initial attitude and angular velocity:

$$R_0 = \exp\Big(\pi\big([1,\ 0,\ 0]^{\mathrm{T}}\big)^\times\Big), \quad \Omega_0 = [1\ 0.5\ 0]^{\mathrm{T}} \mathrm{rad/s}.$$

The initial estimated states are selected to be $\widehat{R}_0 = I$, $\widehat{\Omega}_0 = [0,\ 0,\ 1]^{\mathrm{T}}$rad/s, and $\widehat{\beta}_0 = [0,\ 0,\ 0.1]^{\mathrm{T}}$. Three inertial vectors are considered to be measured at a constant rate by body-fixed sensors. There is no measurement noise in the direction vector measurements or angular velocity vector measurement. The angular velocity measurement is only assumed to have a constant bias of $\beta = [-0.1,\ -1,\ 0.2]^{\mathrm{T}}$ rad/s. The observer gains are

$k_p = 2$, $k_v = 1$, $\kappa = 0.1$, and $\mu = 0.35$. The fractional exponent is taken as $p = 1.1$.

The simulation results are illustrated in Fig. 4.1. The attitude error, Q, error in estimation of angular velocity and bias, ω, and bias estimation error itself, $\tilde{\beta}$, are shown to converge in finite time in the absence of measurement noise, which implies the finite time stability of the estimation scheme.

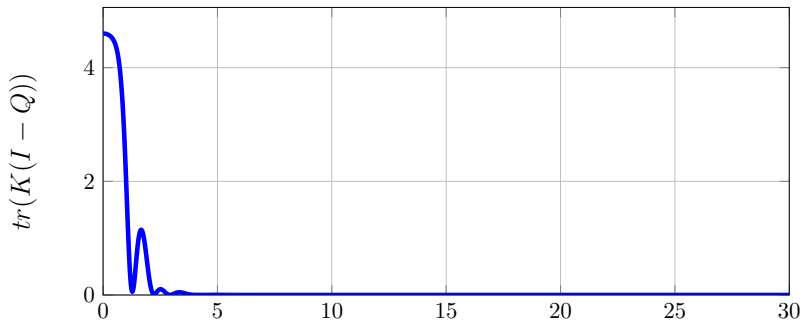

(A) Attitude Estimation Error with time

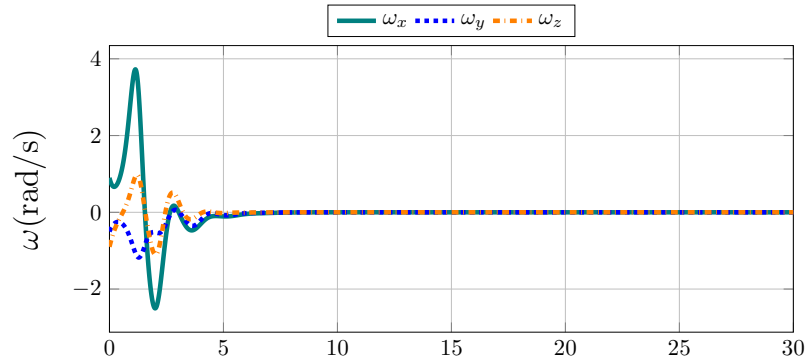

(B) Angular velocity error ω with time

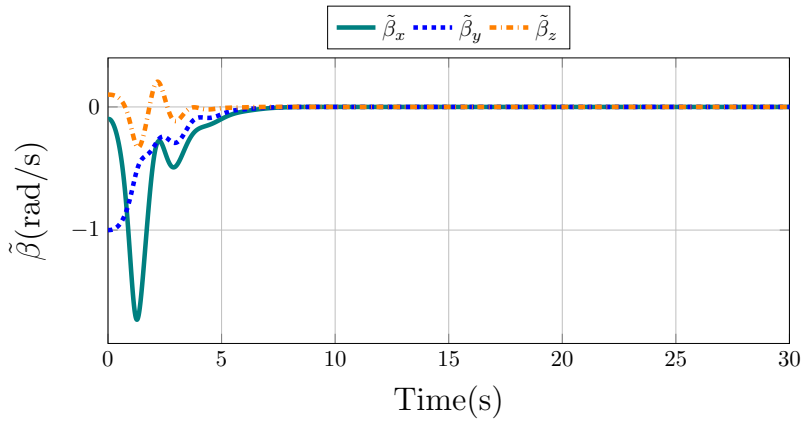

(C) Bias estimation error $\tilde{\beta}$ with time

FIGURE 4.1: Simulation results of the FTS estimator without any measurement noise

4.7 Conclusion

The chapter presented a nonlinear state estimator for rigid body rotational motion. The proposed scheme estimates the attitude and constant angular velocity bias vector from a minimum of two known linearly independent vectors for attitude, and biased angular velocity measurements made in the body-fixed frame. The rigid body's dynamics is unknown. The estimation errors including the bias estimation error are analytically proven to stabilize to zero from almost all initial conditions in the absence of measurement errors. The scheme is numerically implemented by a geometric integrator for a realistic scenario involving measurement errors. Numerical results validate the theoretical results and show the robustness of the proposed estimation scheme.

Chapter 5

Comparison of A Geometric Finite-Time Stable Observer with Some State-of-the-Art Filters

This chapter is adapted from a journal paper submitted in Automatica on July 2019 and is still under review. The author gratefully acknowledges Dr. Amit Sanyal, and Dr. Rakesh R. Warier for their participation.

Abstract This research work presents a nonlinear finite-time stable attitude estimation scheme for a rigid body with unknown dynamics and with unknown bias in angular velocity measurements. The attitude and angular velocity are estimated from a minimum of two linearly independent known vectors measured in the body-fixed frame, and the measured angular velocity vector is assumed to have a constant bias in addition to measurement errors. The estimated attitude evolves directly on the special orthogonal group $SO(3)$ of rigid body rotations, avoiding any ambiguities and singularities. The constant bias in angular velocity measurements is also estimated. The estimation scheme is proven

to be almost globally finite time stable in the absence of measurement errors using a Lyapunov analysis. The estimation scheme is discretized as a geometric integrator for digital implementation. Numerical simulations demonstrate the finite time stability properties of the estimation scheme. Robustness of this estimation scheme is also demonstrated through a numerical comparison against some state-of-the-art nonlinear attitude estimation schemes.

5.1 Introduction

This chapter presents a numerical comparison between the proposed attitude estimation scheme in Chapter 4 and existing results from the literature including the discrete-time variational estimator (VAE) given in (Izadi et al., 2016), the geometric approximate minimum-energy (GAME) of (Zamani, Trumpf, and Mahony, 2011), and the constant gain observer (CGO) given in (Mahony, Hamel, and Pflimlin, 2008). As mentioned in previous chapter, the main contributions of the work are: (1) the proposed attitude estimation scheme evolves on the special orthogonal group $\mathrm{SO}(3)$ and does not suffer from singularities or unwinding; (2) the estimation scheme is model-free in the sense that no assumptions are made on the attitude dynamics model including knowledge of the moment of inertia or the measurement noise model; (3) the estimation scheme is continuous and almost globally finite time stable in the absence of measurement errors even when the angular velocity measurement has an unknown constant bias; (4) the angular velocity bias estimate is also stabilized to the true value in finite time; and (5) the robustness of the proposed scheme under time-varying noise in angular velocity measurements is analytically shown.

5.2 Other State-of-the-Art Filters on $\mathrm{SO}(3)$

Three estimation schemes are used in comparisons with the finite-time stable variational estimator (FTS): The discrete-time variational estimator (VAE), the geometric approximate minimum-energy (GAME) estimator, and a constant gain observer (CGO).

5.2.1 Discrete-time Variational Attitude Estimator

This estimator appeared in (Izadi et al., 2016) and obtained by applying the (discrete) Lagrange-d'Alembert principle of variational mechanics to a (discrete) Lagrangian constructed from residuals between measurements and state estimates with a dissipation term that is linear in the angular velocity measurement residual. This discrete-time estimator is based on the earlier (continuous-time) variational attitude estimator (VAE) that appeared in (Izadi and Sanyal, 2014). Here, we generalize the discrete-time VAE to include angular velocity measurements that have a constant bias in addition to measurement noise. The filter equations in discrete-time for a rigid body with the attitude kinematics (4.25) and with measurements of vectors and angular velocity in a body-fixed frame, are given by

$$\widehat{R}_{k+1} = \widehat{R}_k \ \exp\ \big(\Delta t(\Omega_k^m - \omega_k - \widehat{\beta}_k)^\times\big), \tag{5.1}$$

$$\widehat{\beta}_{k+1} = \widehat{\beta}_k + \Delta t \Phi'\big(\mathcal{U}^0(\widehat{R}_k, U_k^m)\big) P^{-1} s_{L_k}(\widehat{R}), \tag{5.2}$$

$$\widehat{\Omega}_k = \widehat{\Omega}_k^m - \omega_k - \widehat{\beta}_k, \tag{5.3}$$

$$\begin{aligned} m\omega_{k+1} = \exp(-\Delta t \widehat{\Omega}_{k+1}^\times)\{(m\ I_{3\times 3} - \Delta t\ D)\omega_k \\ + \Delta t \Phi'\big(\mathcal{U}^0(\widehat{R}_{k+1}, U_{k+1}^m)\big) s_{L_{k+1}}(\widehat{R}_{k+1})\}, \end{aligned} \tag{5.4}$$

where $\Delta t = t_{k+1} - t_k$ is the time step size for $k = 1, 2, ..., N$, $s_{L_k}(\widehat{R}) = \text{vex}(L_k^{\text{T}}\widehat{R}_k - \widehat{R}_k^{\text{T}}L_k) \in \mathbb{R}^3$, L_k is as defined in (4.16) and evaluated at time t_k, m is a positive scalar, D is a positive definite filter gain matrix, and $\mathcal{U}^0(\widehat{R}_k, U_k^m)$ and $\Phi\big(\mathcal{U}^0(\widehat{R}, U^m)\big)$ are as defined in (Izadi et al., 2016).

5.2.2 GAME Filter

This estimator is a near-optimal filter proposed in (Zamani, Trumpf, and Mahony, 2011) by generalizing Mortensen's maximum-likelihood filtering scheme to $\text{SO}(3)$. The geometric approximate minimum-energy (GAME) filter in continuous form is as given below:

$$\dot{\widehat{R}} = \widehat{R}(\Omega^m - \widehat{\beta} + P_a l)^\times, \tag{5.5}$$

$$\text{where } \; l = \sum_{i=1}^{j} \big(\mathscr{D}_i(\widehat{u}_i - u_i)\big) \times \widehat{u}_i$$

$$\dot{P}_a = \mathcal{Q}_\Omega + 2\mathbb{P}_s\big(P_a(2(\Omega^m - \widehat{\beta}) - P_a l)^\times\big) \tag{5.6}$$

$$\quad + P_a(\mathbb{E} - \mathbb{S})P_a - P_c^{\text{T}} - P_c,$$

$$\dot{P}_c = -(\Omega^m - \widehat{\beta} - P_a l)^\times P_c + P_a(\mathbb{E} - \mathbb{S})P_c - P_b, \tag{5.7}$$

$$\dot{P}_b = \mathcal{Q}_b + P_c(\mathbb{E} - \mathbb{S})P_c, \tag{5.8}$$

$$\dot{\widehat{\beta}} = P_c^{\text{T}}\, l, \tag{5.9}$$

where

$$\mathbb{S} = \sum_{i=1}^{j} (\widehat{u}_i^{\times})^{\mathrm{T}} \mathscr{D}_i \widehat{u}_i^{\times}, \tag{5.10}$$

$$\mathbb{E} = \mathrm{trace}(C) I - C, \tag{5.11}$$

$$C = \sum_{i=1}^{j} \mathbb{P}_s\big(\mathscr{D}_i (\widehat{u}_i - u_i) \widehat{u}_i^{\mathrm{T}}\big). \tag{5.12}$$

Here u_i is the true vector observed in body frame, $\hat{u}_i = \widehat{R}^{\mathrm{T}} e_i$, $\mathcal{Q}_\Omega = BB^{\mathrm{T}}$ where $B \in \mathbb{R}^{3\times 3}$ allows for different weights for the components of the vector of additive noise in angular velocity components, $Q_b = I_{3\times 3}$, $\mathbb{P}_s(X) = \frac{1}{2}(X + X^{\mathrm{T}})$ for $X \in \mathbb{R}^{3\times 3}$, $\mathscr{D}_i = (\mathcal{D}_i \mathcal{D}_i^{\mathrm{T}})^{-1}$ where $\mathcal{D}_i \in \mathbb{R}^{3\times 3}$ allows for different weights for the vector measurement noise, $\widehat{R}(0) = I_{3\times 3}$, $P_c(0) = 0_{3\times 3}$, $P_a(0) = \frac{1}{\varphi^2} I_{3\times 3}$ where φ^2 is the variance of the principal angle corresponding to the initial attitude estimate, and $P_b(0) = \frac{1}{\psi^2} I_{3\times 3}$ where ψ^2 is the standard deviation of an initial bias.

5.2.3 The Constant Gain Observer

The Constant Gain Observer (CGO) presented in (Mahony, Hamel, and Pflimlin, 2008) in continuous form is also represented as

$$\dot{\widehat{R}} = \widehat{R}\Big(\Omega^m - \widehat{\beta} + K_P \bar{\ell}\Big)^{\times}, \ \bar{\ell} = \sum_{i=1}^{j} \big(u_i \times \widehat{u}_i\big), \tag{5.13}$$

$$\dot{\widehat{\beta}} = K_I \ \ell. \tag{5.14}$$

where K_P and K_I are constant gains and $\widehat{R}(0) = I_{3\times 3}$. Note that the discrete-time versions of this filter and the GAME filter as presented in (Zamani, 2013) use the unit quaternion

representation, and are implemented as such in the following numerical simulations.

5.3 Numerical Simulation Results

This section presents numerical simulation results of a comparison between this scheme and three other state-of-the-art estimators. The performance of the finite-time stable estimator *in the presence of vector measurement noise, σ_i, and angular velocity noise, ν_i, and unknown bias in angular velocity measurements* is compared to that of the three estimators presented in Section 5.2, under identical conditions. To do so, all the estimation schemes are applied to the same rigid-body dynamics, with the same initial estimate errors, equal time steps, and identical measurement noise. The sampling period and the total simulation time are $\Delta t = 0.01s$ and $T = 30s$, respectively. Three known inertial directions are measured by the sensors in the body frame, and these measurements include known levels of noise, and rate gyro sensors for angular velocity measurement are assumed to be biased with a constant bias of $\beta = [-0.01,\ -0.005,\ 0.02]^{\mathrm{T}}$ rad/s for all schemes. The initial estimate of the bias is set to be $\widehat{\beta}_0 = [0,\ 0,\ 0.1]^{\mathrm{T}}$, the initial estimated rotation matrix is set equal to identity, and the initial rotation matrix is selected such that its principal angle has zero mean and a standard deviation of 60°. The rigid body simulated has the following angular velocity profile:

$$\Omega(t) = \left[\sin\frac{2\pi}{15}t \quad -\sin\frac{2\pi}{18}(t+\frac{\pi}{20}) \quad \cos(\frac{2\pi}{17}t)\right]^{\mathrm{T}} \tag{5.15}$$

The initial angular velocity estimates are also set to be identical, as follows. According to (5.5), the initial angular velocity estimation error is given by $P_a(0)l(0)$ for the GAME filter. For the FTS and discrete-time VAE estimators, choosing $\omega_0 = P_a(0)l(0)$ and for the

CGO, choosing $K_P = P_a(0)$ satisfies this condition. For this comparison in simulations, the scalar "inertia-like" gain for the VAE estimator is selected as $m = 0.5$, the constant gain K_I of CGO filter is set equal to 0.3, and the positive definite dissipation matrix as

$$D = \text{diag}\Big(\begin{bmatrix} 2.4 & 2.6 & 2.8 \end{bmatrix}^{\text{T}} \Big). \tag{5.16}$$

As in (Zamani, 2013), the GAME and CGO estimators utilize unit quaternions for attitude representation when implemented numerically. We compare the performance of these two estimators as well as the discrete VAE scheme with the FTS attitude estimator for two different cases, as described in the rest of this section.

5.3.1 CASE I: High Noise Levels

In this case, both direction vector measurement noise vectors σ_i and angular velocity measurement noise vector ν are random zero mean signals whose probability distributions are normalized bump functions. It is assumed that the standard deviation of the direction measurement noise and angular velocity measurement noise are 30° and 25°/s, respectively. In order to have a fair comparison between the different estimation schemes that may have different gains (and gain update scheme in the case of the GAME filter), the (initial) gains are selected such that all estimators have the same initial attitude and initial angular velocity estimates. Moreover, all estimators simulated here are provided the same set of measurements with the same (constant) bias added to the angular velocity measurements. The time profiles of the attitude estimate error for each estimator are plotted and compared in Fig. 5.1.

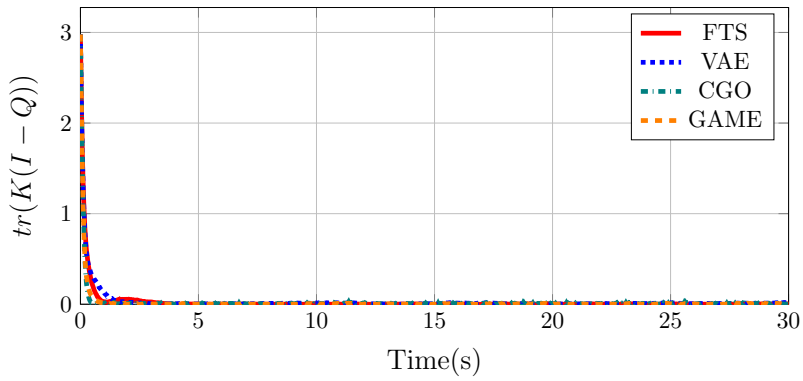

FIGURE 5.1: Attitude estimation error for noise levels similar to that in (Zamani, 2013).

Fig. 5.1 shows some transient behavior in the attitude estimation error with the FTS estimator. However, there are no remarkable differences in the steady state behavior of all four schemes compared, and in fact the constant gain observer performs somewhat better than the other schemes. The FTS estimator shows finite-time convergence of attitude estimate error to zero, and the settling time for this estimator is comparable to that of the other filters.

5.3.2 CASE II: Low Noise Levels, with Estimator Gains as Before

In this case, the noise signals are considered to be of the same type as in the previous case (random zero mean bump functions), but with much smaller amplitudes. The standard deviations in the attitude measurement noise and angular velocity measurement noise signals are 0.95° and $2.5^\circ/s$, respectively. This corresponds to having more accurate sensor measurements than in case I. In order to compare the estimator performances when the estimator gains are not designed for known sensor noise properties, all the gains are kept the same as in case I. The attitude estimation errors from all estimators are plotted

in Fig. 5.2.

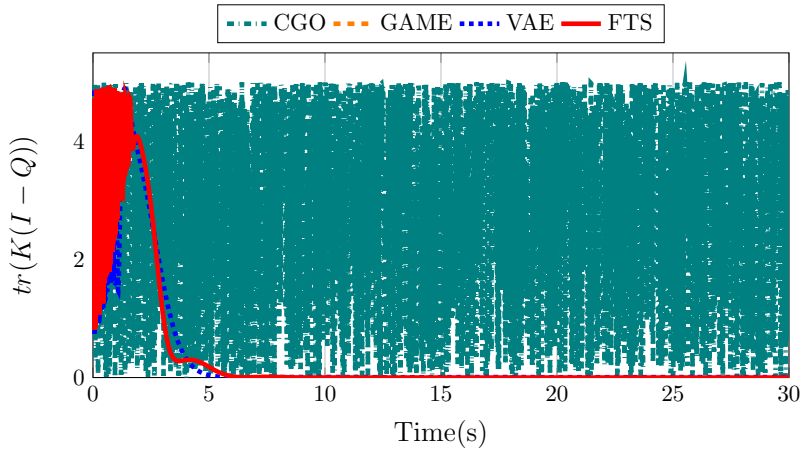

FIGURE 5.2: Attitude estimation error for low noise levels, with estimator gains unchanged.

A magnified view of the initial transient behavior of these observers is depicted in Fig. 5.3. In this case, as is shown in Fig. 5.3, the GAME filter becomes singular after a few time steps, and the CGO is not able to converge and filter out noise from the measurements. On the other hand, the FTS and VAE estimators are stable and very effective at filtering out noise. Moreover, the FTS estimator guarantees convergence of estimation errors to small bounds in finite-time. The settling times are also sufficiently small. Looking at these two cases, one can conclude that although the GAME and CGO filters perform nicely in the presence of measurement noise with known noise level, they may not be stable and their initial gains need to be reset when the noise signal changes. Therefore, one major downside to these filters is their dependence on the knowledge of the measurement noise level. On the contrary, the variational estimators (FTS and VAE) are robust with guaranteed stability, regardless of the statistics and level of the noise. Moreover, because of the almost global finite-time stable property of the FTS estimator, it is robust to bounded measurement noise in attitude states, as shown in this research work.

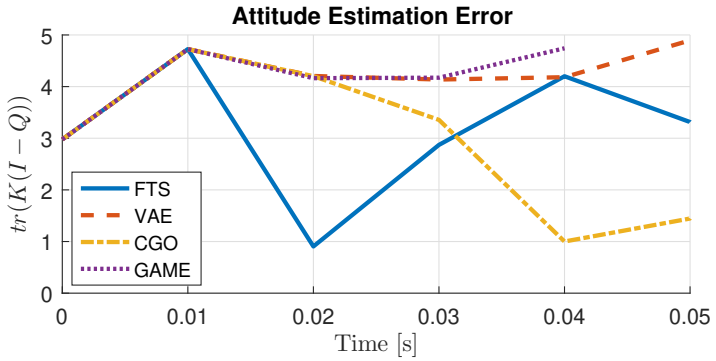

FIGURE 5.3: Zoomed-in view of the initial transient response of the attitude estimation error as plotted in Fig. 5.2.

5.4 Conclusion

This chapter presents a nonlinear finite-time stable state estimator for rigid body rotational motion. The proposed scheme estimates the attitude and constant angular velocity bias vector from a minimum of two known linearly independent vectors for attitude, and biased angular velocity measurements made in the body-fixed frame. The estimation errors including the bias estimation error are analytically proven to stabilize to zero from almost all initial conditions in the absence of measurement errors. The scheme is numerically implemented by a geometric integrator for a realistic scenario involving measurement errors. Numerical results validate the theoretical results given in previous chapter and show the robustness of the proposed estimation scheme. The behavior of this estimation scheme is compared with three state-of-the-art filters for attitude estimation. Using a realistic set of data for a rigid body, numerical simulations show that the FTS and variational attitude estimator (VAE), unlike the GAME filter and CGO, are always stable and their convergence is not dependent on the type and level of measurement noise. Moreover, finite-time stability guarantees a faster convergence of estimation errors $(Q, \tilde{\Omega}, \tilde{\beta})$ to $(I, 0, 0)$ in finite-time, and robustness to measurement noise.

Chapter 6

Experimental Results

We developed an experimental platform with quadrotor UAVs to validate our derivations and simulations. Two quadrotor UAVs are built from scratch for indoor and outdoor flights by designing every parts followed by developing a software for real-time experiments. The hardware and software development for the experimental part of this dissertation is presented in the following section of this chapter.

6.1 Building a quadrotor

The quadrotor UAVs developed at the Autonomous Unmanned Systems laboratory (AUS-Lab) at the Syracuse Center of Excellence are shown at Fig. 6.1a and Fig. 6.1b. The quadrotor platforms are equipped with a Pixhawk Cube autopilot shown in Fig. 6.3b. The Cube flight controller (previously known as Pixhawk 2.1) is a flexible autopilot intended primarily for manufacturers of commercial systems. It is based on the Pixhawk-project FMUv3 open hardware design and runs PX4 on the NuttX OS.

Cube includes vibration isolation on two of the IMU's, with a third fixed IMU as a reference/Backup. The UAV shown in Fig. 6.1a is built for outdoor flight experiments

(A) Quadrotor UAV built for outdoor flights

(B) Quadrotor UAV built for indoor flights

FIGURE 6.1: UAVs for experiments

and uses an external combined compass/GPS module mounted as far away from the motor/ESC power supply lines as possible. The angular velocity is measured from inertial measurement unit (IMU) built in the Pixhawk and the attitude is also obtained from IMU data. The UAV in Fig. 6.1b uses a Raspberry Pi as the on-board computer with ROS (Robot Operating System) that is built to fly autonomously in GPS-denied environments. The indoor flight test area includes eight Vicon Motion Capture cameras as shown in Figure 6.2 that detect the UAV's position and orientation off-board. Position of the UAV is measured from motion capture system (Vicon) and the velocity is estimated from the measurement. The Ground desktop system as a server receives the Vicon data and the UAV's companion computer can collect the data by sharing IP with that server.

FIGURE 6.2: Motion capture system including 8 Vicon cameras in AUSLab

A list of the hardware components that are used in building our quadrotor UAVs is

given bellow. The motors are connected directly to the power distribution board, and are connected to the flight controller via speed controllers and PWM ports.

- Pixhawk running the customized PX4 code stack based on our developed control algorithms, and communicating with the on-board computer through Mavlink/Mavros.
- Raspberry Pi Model B+, connected to Pixhawk via UART communicating with the desktop computer via WiFi (Figure 6.3a).
- AIR2216 KV880 brushless motors (Figure 6.3c).
- AIR 20A ESCs, connected to Pixhawk via PWM (Figure 6.3c).
- Here GNSS GPS (M8N) module for the UAV built to fly outdoor (Figure 6.3d).
- For safety and to avoid crashes when the UAV is flying autonomously, we use a Radio Controller (RC) with a FrSky telemetry module (Figure 6.3e) that allows us to access vehicle telemetry/status information.

Finally, these parts are all connected and two quadrotors are prepared for the experiments as shown in Figure 6.3.

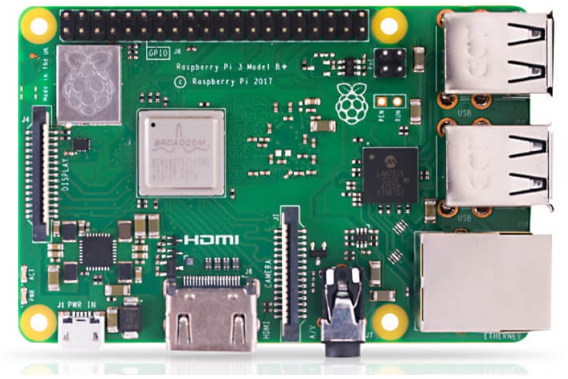

(A) Raspberry Pi 3 model B+

(B) Cube Flight Controller

Motor and ESC

(D) GPS module

(E) Telemetry module

FIGURE 6.3: Hardware components for a quadrotor UAV

6.2 Software Development

As mentioned in the previous section, Pixhawk flight controllers run PX4, which is an open source flight control software for drones and other unmanned vehicles. PX4 consists of two main layers: the flight stack is an estimation and flight control system, and the middleware is a general robotics layer that can support any type of autonomous robot, providing internal/external communications and hardware integration. The flight stack is a collection of guidance, navigation and control algorithms for autonomous drones. It includes controllers for fixed wing, multirotor and VTOL airframes as well as estimators for attitude and position (PX4-Dev, 2017).

The following diagram shows an overview of the blocks of the PX4 flight stack. It contains the full pipeline from sensors, RC input and autonomous flight control, down to the actuators.

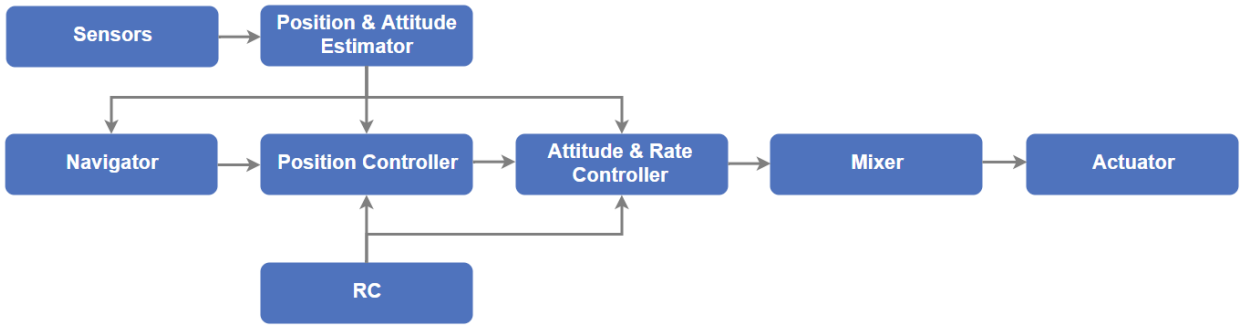

FIGURE 6.4: PX4 flight stack diagram

To verify the performance of our proposed discrete-time FTS (dFTS) control scheme in experiments, the attitude and rate control module of the PX4 (Meier, Honegger, and Pollefeys, 2015) is replaced with the attitude controller presented in Chapter 3. Multiple codes in C/C++ were modified to build a new version of the PX4 stack that runs our developed

attitude control scheme on the Pixhawk flight control module and handles several tasks. In addition, we use ROS to communicate with the flight controller for sending our desired trajectory to the flight controller instead of using the PX4's Navigator module. There are two steps to carry out the experiments:

- Software-in-the-Loop (SITL) Simulation
- Real flight experiments

Software-in-the-Loop (SITL) Simulation:

Simulators allow PX4 flight code to control a computer modeled vehicle in a simulated "world". We can interact with this vehicle just as we do with a real vehicle. Simulation is a quick, easy, and most importantly, safe way to test *changes* to PX4 code before attempting to fly in the real world. PX4 supports both Software In the Loop (SITL) simulation, where the flight stack runs on a computer, and Hardware In the Loop (HITL) simulation using a simulation firmware on a real flight controller board. All simulators communicate with PX4 using the Simulator MAVLink API. This API defines a set of MAVLink messages that supply sensor data from the simulated world to PX4 and return motor and actuator values from the flight code that will be applied to the simulated vehicle. The figure below shows the message flow.

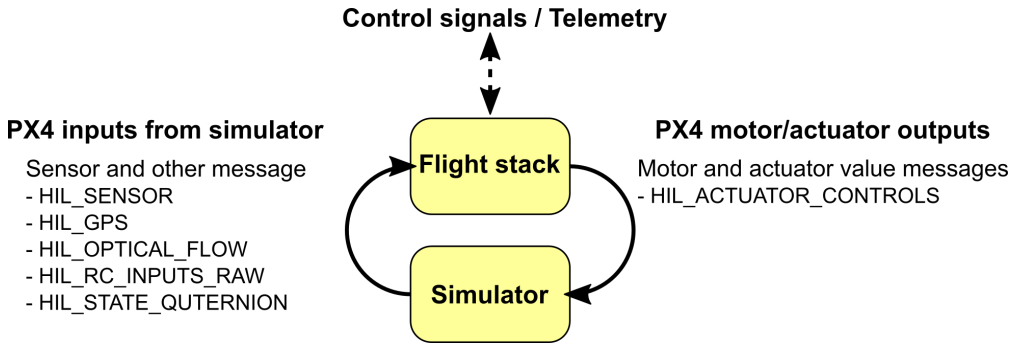

FIGURE 6.5: PX4's SITL message flow

Gazebo is a powerful 3D simulation environment that is particularly suitable for testing object-avoidance and computer vision. It can also be used for multi-vehicle simulation and is commonly used with ROS, a collection of tools for automating vehicle control (PX4-Dev, 2017).

In this step, a SITL simulation of the proposed dFTS attitude controller is carried out to show its performance in a realistic autonomous flight scenario. The 3DR-Solo quadrotor UAV is simulated in Gazebo, and several ROS nodes are written in Python to send the desired trajectory to the flight control module. The simulation is carried out for two different trajectories; a circular trajectory and a helical trajectory similar to the desired trajectory in Fig. 3.2. During the simulation, the 3DR solo is in autonomous flight mode and assigned to follow the given trajectory. These trajectories are designed in such a way that the UAV flies to the point $(0, 0, 2)$ first, and then completes its flight in the circular or spiral part of the trajectory, and then starts to land. The inertia information of the simulated 3DR Solo quadrotor, is shown as follows (PX4-Dev, 2017):

$$J = \text{diag}(0.011, 0.015, 0.021)\ \text{kg-m}^2; \quad m = 1.5\ \text{kg}. \tag{6.1}$$

The gains used for the proposed control scheme are:

$$k_l = 1,\ \kappa = 0.025,\ \Gamma = 0.006 \tag{6.2}$$

Figures 6.7, and 6.9 show the performance of the proposed control scheme in the SITL simulation.

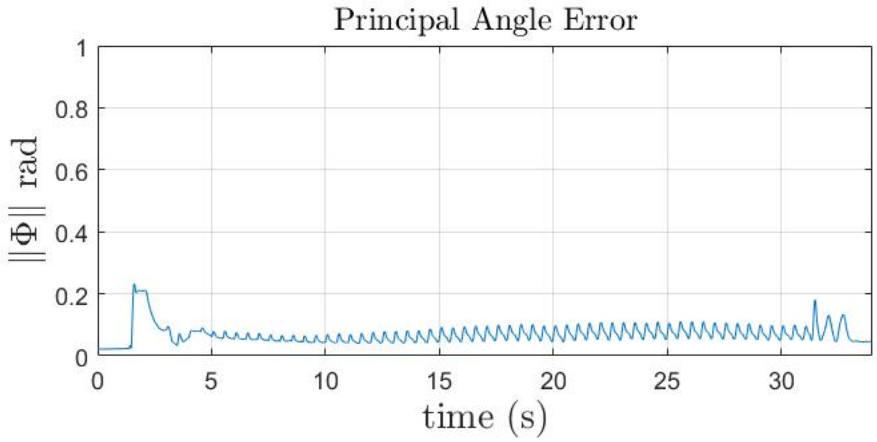

FIGURE 6.6: Principal angle error in SITL simulation for circular trajectory.

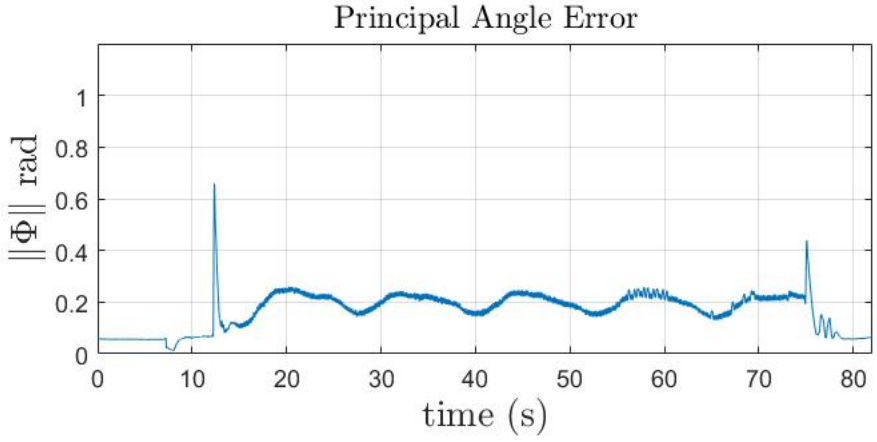

FIGURE 6.7: Principal angle error in SITL simulation for helical trajectory.

The magnitude of the attitude tracking error is given by the principal angle Φ of the attitude tracking error Q, defined by (3.89) and shown in Figures 6.6 and 6.7 for flights in the circular and helical phase of the trajectory, respectively. It can be clearly seen that the proposed geometric control scheme has a good attitude tracking control performance. In Figures 6.8 and 6.9, it can be seen that the angular velocity tracking performance of the proposed control scheme is acceptable but has some high-frequency oscillations in the angular velocity error.

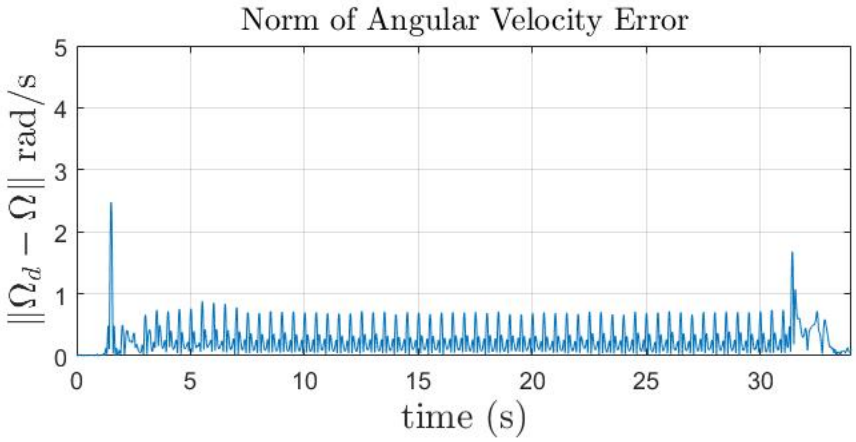

FIGURE 6.8: Angular velocity error in SITL for circular trajectory.

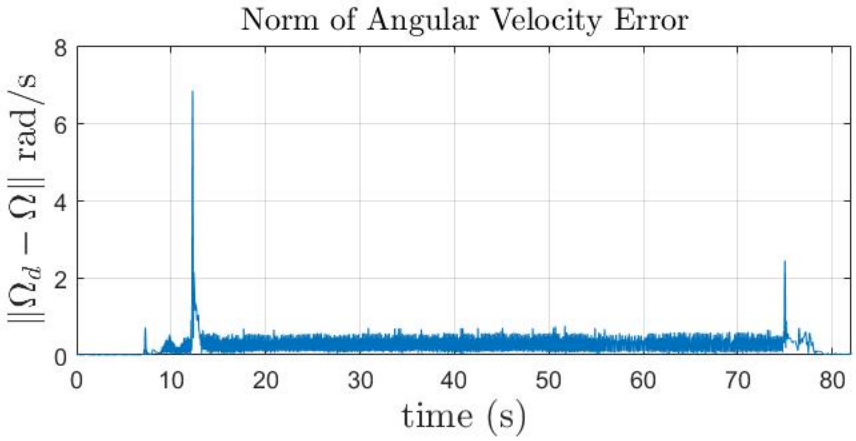

FIGURE 6.9: Angular velocity error in SITL for helical trajectory.

6.3 Real Autonomous Flight Experiment

For real autonomous flight experiments, a framework is designed that utilizes visual and inertial feedback. The framework is designed for technology and capability demonstration, particularly for autonomous trajectory tracking applications in GPS-denied environments. In addition to a standard flight controller (Pixhawk), the framework includes a companion computer (Raspberry Pi) that is utilized to receive position and attitude data retrieved via WiFi from a motion capture system (Vicon cameras). In this framework, the flight controller is utilized for low-level tasks such as attitude control, generating actuator commands and sensor data acquisition and fusion. On the other hand, the companion computer is used for high-level tasks such as trajectory generation and optimization. To establish communications between the companion computer and the motion capture system, a ROS network is used. The companion computer on the UAV operates as the ROS Master that can be used to modify the desired trajectory online and during the flight. The commands of position set-points are published on a set-point ROS node, and MAVROS sends the set-points to the flight controller. MAVROS provides a plugin to relay a visual estimate from the motion capture system to the flight controller using a vision-pose ROS node. Based on the feedback data from the motion capture system, the flight controller generates appropriate actuator commands for the quadrotor UAV to track a desired trajectory. The custom-made quadrotor UAV platform built to carry out the indoor experiments is as shown in Fig. 6.1b, and the flow diagram of this framework is given in Fig. 6.10.

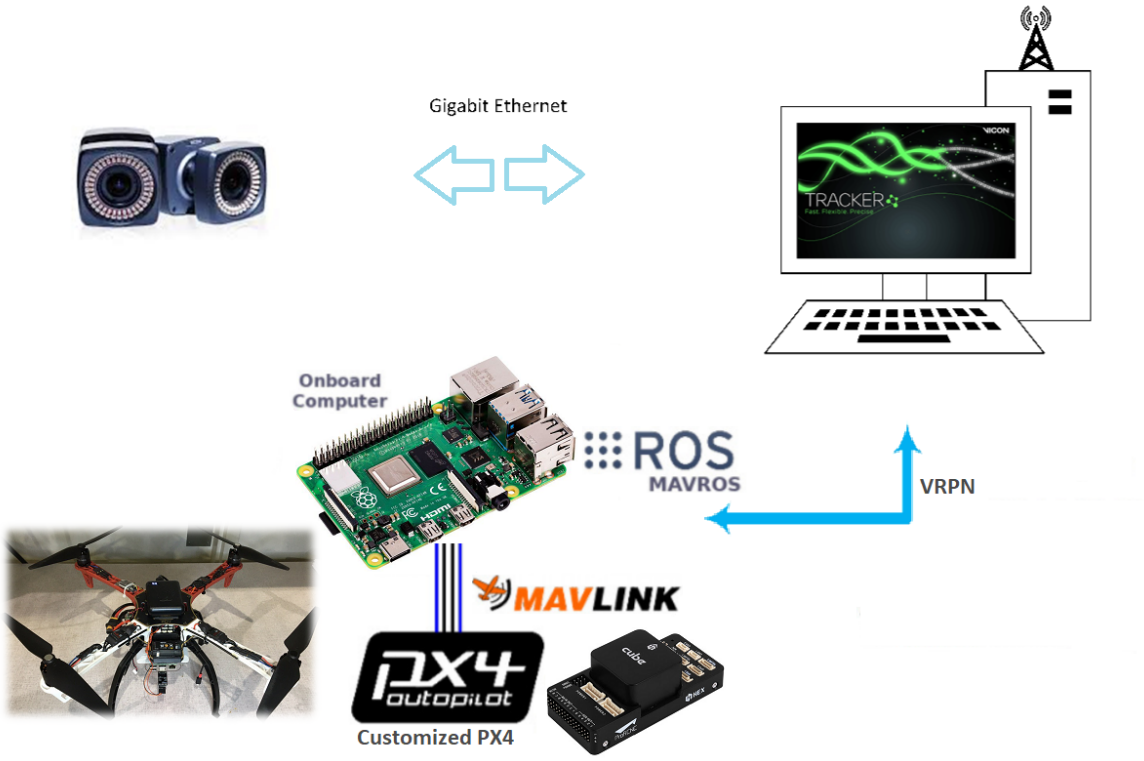

FIGURE 6.10: On-board implementation process flow diagram

Experimental results are shown in Figures 6.12 and 6.13. These two figures show the snapshots for two autonomous flight experiments by implementing the dFTS tracking control scheme as presented in Chapter 3. Fig. 6.11 indicates x, y, and z directions of the Vicon system coordinate frame in the lab.

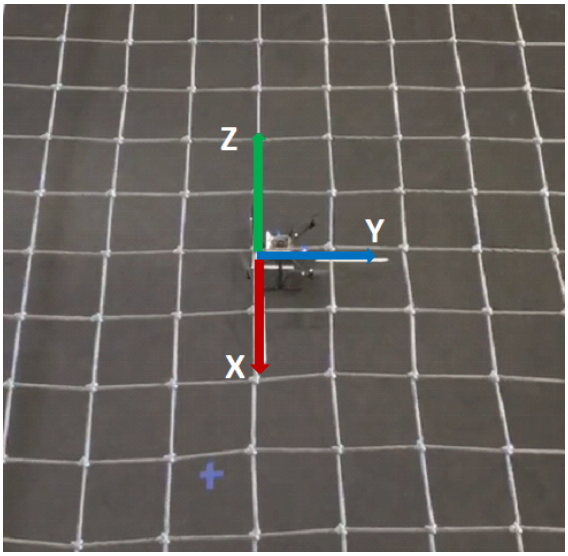

FIGURE 6.11: Coordinate frame of Vicon System

In Fig. 6.12, snapshots for an autonomous hovering is given, in which the UAV first hovers at $1.5m$ and then flies from the hovering point $(0, 0, 1.5)$ to the point $(1, 1, 1)$. Fig. 6.13 shows the snapshots of a flight in a circular trajectory given to the same UAV through a ROS node. In this scenario, UAV takes off at $(0, 0, 0)$ and flies to hover at the point $(0, 0, 1.5)$. Then, it flies to the point $(0, 1.5, 1.5)$ to start following the circular trajectory with radius $1.5m$. In both tests, the UAV lands autonomously and becomes disarmed (motors stop spinning) when the given mission is accomplished. Both Vicon and flight control module work at $30Hz$, and no delay is expected unless there is a communication failure. Therefore, due to the robustness and stability properties of the proposed controller, position and attitude tracking performance show satisfactory results.

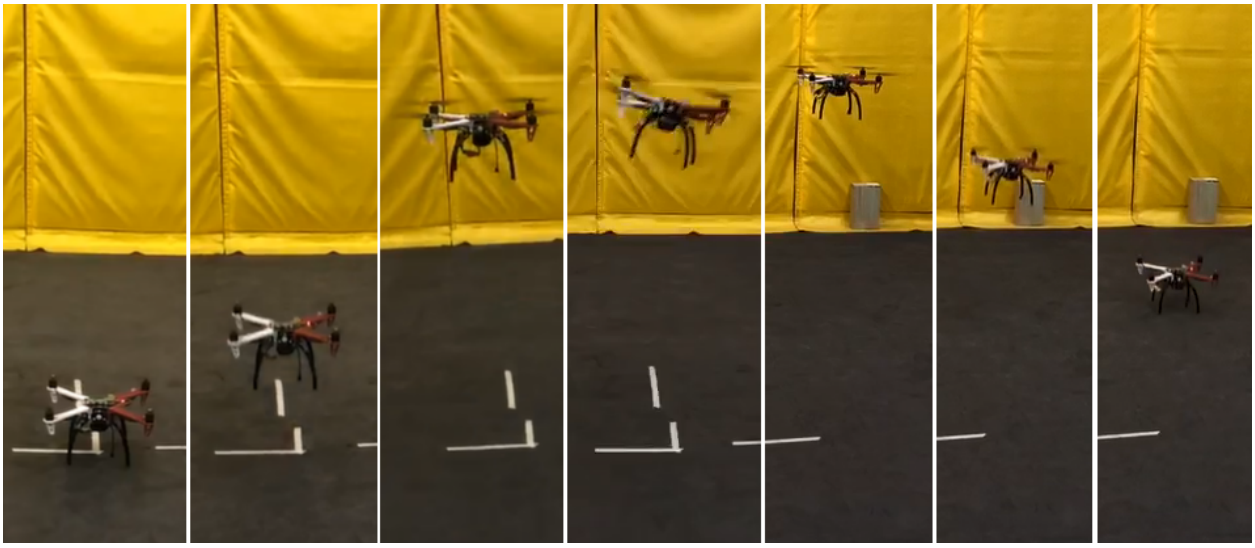

FIGURE 6.12: Snapshots for an autonomous hovering at 1.5m and flight from (0 0 1.5) to (1 1 1)

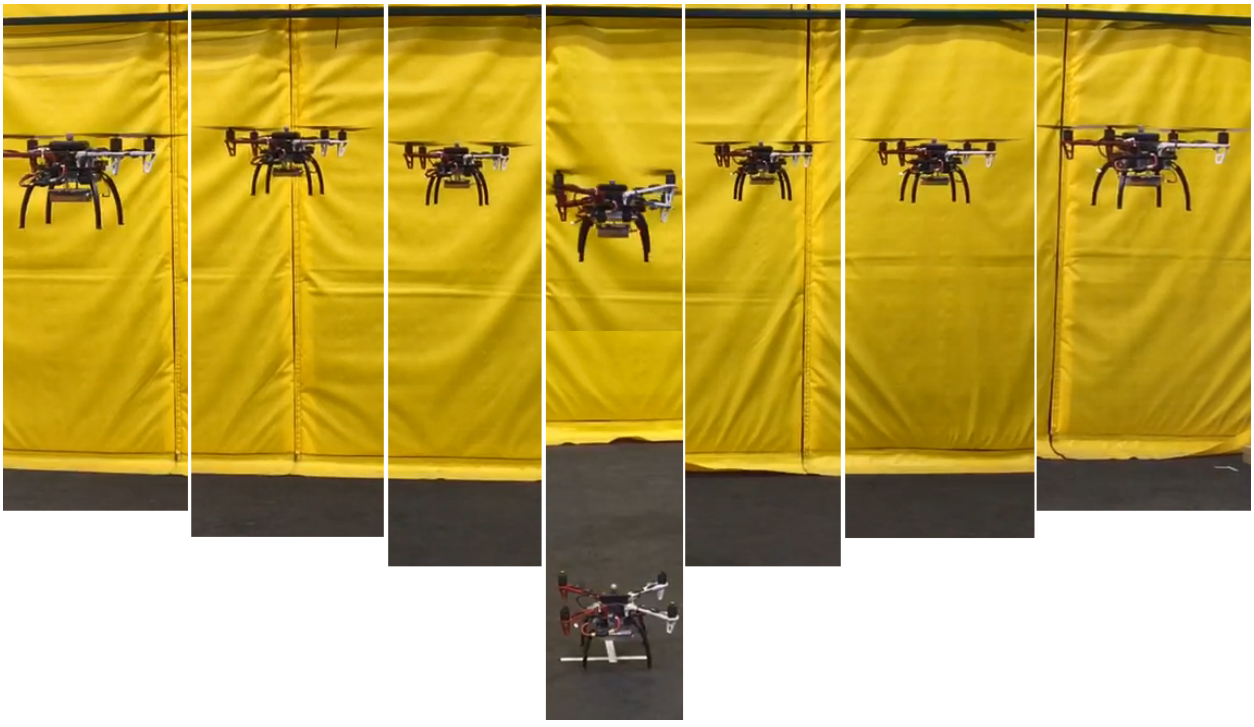

FIGURE 6.13: Snapshots for an autonomous flight in a circular trajectory with radius of 1.5m starting at (0 1.5 1.5)

There are also several limitations, and important hardware challenges for the presented experimental platform that has to be always considered for current and future experimental platforms. In real-time experiments, establishing a stable communication is very important, and so high speed update rate is required to maintain an aggressive maneuver. In some experiments, we experienced failure in communication that caused instability of the system and led to UAV crashing. Lipo Batteries used for the experiment can play an important role in a successful maneuver, since they can be drained very soon which affects the performance of the hardware. Different sensors used in real-time experiments may provide noisy data which has to be filtered to obtain smooth data. We also experienced delay in receiving the data using the Vicon system.

Chapter 7

Conclusion and Future Work

7.1 Conclusion

We conclude this dissertation by providing a summary of the research presented here, followed by a discussion on related future work.

In Chapter 2, a discrete-time stable tracking control scheme for a rigid body with one actuated translational degree of freedom and three actuated rotational degrees of freedom is presented. In this research, a discrete-time energy-based tracking control scheme is designed to obtain the desired discrete-time control force vector that asymptotically stabilizes the desired translational motion. In order to track the desired attitude trajectory, a discrete-time attitude tracking control law is developed. Discrete-time Lyapunov analysis shows that the tracking control scheme obtained provides stable asymptotic convergence of actual states to desired states. This results in discrete-time tracking error dynamics that behaves as a dissipative system, and state tracking errors are dissipated in discrete time. The stable discrete-time control laws are then obtained from these discrete-time error dynamics equations as well. The discrete-time stable tracking control algorithm utilizes a

trajectory generation scheme that selects the desired trajectory for the translational motion that passes through the given waypoints and generates an attitude trajectory to follow the desired thrust direction. Numerical simulation confirms the stable performance of the the overall tracking control scheme as well as discrete-time stability of the resulting control laws.

Chapter 3 proposes a discrete-time stable tracking control scheme with finite-time stability for unmanned vehicles. The finite-time stability of the overall tracking control scheme is proved using a discrete-time Lyapunov analysis, which results in discrete-time error dynamics in terms of translational and rotational motion tracking errors. This analysis results in discrete-time control laws that guarantee the convergence of the position and attitude states to the desired position and attitude trajectories in a finite time interval. Analysis of robustness to bounded disturbance torques is also presented. In addition, a comparison between the performance of the proposed scheme and that of a sampled continuous FTS scheme is studied here, and numerical results show that a discrete-time FTS tracking control scheme is more reliable for onboard computer implementation when we need to work with a variety of input data frequencies.

In Chapter 4, a nonlinear state estimator for rigid body rotational motion is presented. The proposed scheme estimates the attitude and constant angular velocity bias vector from a minimum of two known linearly independent vectors for attitude, and biased angular velocity measurements made in the body-fixed frame. This attitude estimation scheme is considered under unknown attitude dynamics. The estimation errors including the bias estimation error are analytically proven to stabilize to zero from almost all

initial conditions in the absence of measurement errors. The scheme is numerically implemented by a geometric integrator for a realistic scenario involving measurement errors. Numerical results validate the theoretical results and show the robustness of the proposed estimation scheme.

In Chapter 5, the behavior of the nonlinear state estimation scheme presented in Chapter 4 is compared with three state-of-the-art filters for attitude estimation. Using a realistic set of data for a rigid body, numerical simulations show that the FTS and variational attitude estimator (VAE), unlike the GAME filter and CGO, are always stable and their convergence is not dependent on the type and level of measurement noise. Moreover, FTS guarantees a faster convergence of estimation errors $(Q, \tilde{\Omega}, \tilde{\beta})$ to $(I, 0, 0)$ in finite-time, and robustness to measurement noise.

The rigorous mathematical stability proofs that are given in this dissertation are verified by mathematical analysis, numerical simulations, and in Chapter 6 they are also implemented and verified by experiments in both SITL and real autonomous flights.

7.2 Ideas for Future Work

The following are ideas to extend the research presented in this PhD dissertation:

- More comprehensive comparison of the proposed discrete-time stable tracking control scheme with other state-of-the-art sampled continuous-time tracking control schemes through hardware-in-the-loop (HITL) experiments.

- Developing the discrete finite-time stable attitude estimation from intermittent measurements at different rates, and design of state-varying or time-varying filter gains for faster convergence of state estimates.

- Combining and implementing the discrete FTS controller and a discrete FTS estimator in a flight control module for unmanned aerial and ground vehicles.

- Developing the finite-time stable model-free filter in $\mathrm{SE}(3)$. The comparison of the proposed FTS observer with the variational estimator and other state-of-the-art filters presented in Chapter 5 can also be verified numerically.

- Experimental validation of model-free FTS filter in $\mathrm{SO}(3)$ or $\mathrm{SE}(3)$ in the presence of bias in angular velocities; gyroscopes are used in practice to provide angular velocities. The output of such sensors usually contain constant or variable drift, which harms the performance of the filter. The estimator presented in Chapter 4 is designed in such a way that it could be robust to bias in the sensor readings.

- Developing an analytical approach to design a delayed stable feedback system in the presence of an unknown time delay in feedback measurement using delay differential equations and Morse–Lyapunov–Krasovskii or Morse-Lyapunov-Razumikhin techniques. This approach can be developed to deal with the delay limitation outlined in the last paragraph of Chapter 6. A related research is presented in (Samiei, Sanyal, and Butcher, 2017).

- Modeling the "hidden" dynamics of the actuators at the Motor-ESC level in the design of a robust control system, and studying the effects of actuator dynamics, control-structure interaction, and the impact of the mechanical design of the actuators on it.

- Extending the experimental research work in an outdoor environment to identify the wind effects and verifying the performance of the controller in various weather situations.

Bibliography

Aguiar, A. P. and J. P. Hespanha (2006). "Minimum-energy state estimation for systems with perspective outputs". In: *IEEE Transactions on Automatic Control* 51.2, pp. 226–241.

Barrau, Axel and Silvère Bonnabel (2017). "The invariant extended Kalman filter as a stable observer". In: *IEEE Transactions on Automatic Control* 62.4, pp. 1797–1812.

Bhat, S. P. and D. S. Bernstein (1998). "Continuous finite-time stabilization of the translational and rotational double integrators". In: *IEEE Transactions on Automatic Control* 43.5, pp. 678–682. ISSN: 0018-9286. DOI: 10.1109/9.668834.

Bhat, Sanjay P and Dennis S Bernstein (2000a). "A topological obstruction to continuous global stabilization of rotational motion and the unwinding phenomenon". In: *Systems & Control Letters* 39.1, pp. 63–70.

— (2000b). "Finite-time stability of continuous autonomous systems". In: *SIAM Journal on Control and Optimization* 38.3, pp. 751–766.

Black, Harold D (1964). "A passive system for determining the attitude of a satellite". In: *AIAA journal* 2.7, pp. 1350–1351.

Bloch, A.M. et al. (2003). *Nonholonomic Mechanics and Control, ser. Interdisciplinary Applied Mathematics.* Springer, Verlag.

Bohn, J. and A. K. Sanyal (2014). "Almost global finite-time stable observer for rigid body attitude dynamics". In: *2014 American Control Conference*, pp. 4949–4954.

Bohn, Jan and Amit K Sanyal (2015). "Almost global finite-time stabilization of rigid body attitude dynamics using rotation matrices". In: *International Journal of Robust and Nonlinear Control*.

Bonnabel, Silvere, Philippe Martin, and Pierre Rouchon (2009). "Non-linear symmetry-preserving observers on Lie groups". In: *IEEE Transactions on Automatic Control* 54.7, pp. 1709–1713.

Bullo, Francesco and Andrew D. Lewis (2004). *Geometric Control of Mechanical Systems, ser. Texts in Applied Mathematics.* Springer, Verlag.

Bullo, Francesco and Richard M. Murray (1999). "Tracking for fully actuated mechanical systems: a geometric framework". In: *Automatica* 35, pp. 17–34.

Chaturvedi, N. A., A. K. Sanyal, and N. H. McClamroch (2011). "Rigid-Body Attitude Control". In: *IEEE Control Systems Magazine* 31.3, pp. 30–51. ISSN: 1066-033X. DOI: 10.1109/MCS.2011.940459.

Choukroun, Daniel, Itzhack Y Bar-Itzhack, and Yaakov Oshman (2006). "Novel quaternion Kalman filter". In: *IEEE Transactions on Aerospace and Electronic Systems* 42.1, pp. 174–190.

Crassidis, John L, F Landis Markley, and Yang Cheng (2007). "Survey of nonlinear attitude estimation methods". In: *Journal of guidance, control, and dynamics* 30.1, pp. 12–28.

Dorato, Peter (2006). "An Overview of Finite-Time Stability". In: *Current Trends in Nonlinear Systems and Control: In Honor of Petar Kokotović and Turi Nicosia*. Boston, MA: Birkhäuser Boston, pp. 185–194.

Fernando, T. et al. (2011). "Robust adaptive geometric tracking controls on SO(3) with an application to the attitude dynamics of a quadrotor UAV". In: *2011 50th IEEE Conference on Decision and Control and European Control Conference*, pp. 7380–7385. DOI: 10.1109/CDC.2011.6161306.

Gamagedara, K., T. Lee, and D. E. Chang (2019). "Attitude Observer on SO(3) with Time-Varying Reference Directions". In: *2019 18th European Control Conference (ECC)*, pp. 4034–4039.

Goodarzi, Farhad A., Daewon Lee, and Taeyoung Lee (2015). "Geometric control of a quadrotor UAV transporting a payload connected via flexible cable". In: *International Journal of Control, Automation and Systems* 13, pp. 1486–1498.

Haddad, Wassim M., Sergey G. Nersesov, and Liang Du (2008). "Finite-time stability for time-varying nonlinear dynamical systems". In: *2008 American Control Conference*, pp. 4135–4139. DOI: 10.1109/ACC.2008.4587141.

Haddad, Wassim Michael and VijaySekhar Chellaboina (2008). *Nonlinear Dynamical Systems and Control: A Lyapunov-Based Approach*. Princeton University Press.

Hamrah, R., A. K. Sanyal, and S. Prabhakaran (2020). "Discrete Finite-time Stable Attitude Tracking Control of Unmanned Vehicles on SO(3)". In: *2020 American Control Conference (ACC)*, pp. 824–829.

Hamrah, Reza and Amit K. Sanyal (2020). "Finite-time stable tracking control for an underactuated system in SE(3) in discrete time". In: *International Journal of Control*, pp. 1–16. DOI: 10.1080/00207179.2020.1841299. eprint: https://doi.org/10.1080/00207179.2020.1841299. URL: https://doi.org/10.1080/00207179.2020.1841299.

Hamrah, Reza, Amit K. Sanyal, and Sasi Prabhakaran (2019). "Discrete Finite-time Stable Position Tracking Control of Unmanned Vehicles". In: *58th IEEE Conference on Decision and Control (CDC), Nice, France, December 11-13, 2019*. IEEE.

Hamrah, Reza, Rakesh R. Warier, and Amit K. Sanyal (2018). "Discrete-time Stable Tracking Control of Underactuated Rigid Body Systems on SE(3)". In: *57th IEEE Conference on Decision and Control, CDC 2018, Miami, FL, USA, December 17-19, 2018*, pp. 2932–2937.

Harshavarthini, S., Sakthivel Rathinasamy, and Choon Ki Ahn (2019). "Finite-time reliable attitude tracking control design for nonlinear quadrotor model with actuator faults". English. In: *Nonlinear Dynamics*. ISSN: 0924-090X. DOI: 10.1007/s11071-019-04952-4.

Hashim, H. A., L. J. Brown, and K. Mcisaac (2019). "Guaranteed Performance of Nonlinear Attitude Filters on the Special Orthogonal Group SO(3)". In: *IEEE Access* 7, pp. 3731–3745.

Hussein, I. I. et al. (2006). "A discrete variational integrator for optimal control problems on SO(3)". In: *IEEE Conference on Decision and Control (CDC)*, 6636—6641.

Invernizzi, Davide and Marco Lovera (2017). "Geometric tracking control of a quadcopter tiltrotor UAV". In: *IFAC-PapersOnLine* 50.1. 20th IFAC World Congress, pp. 11565 – 11570. ISSN: 2405-8963.

Izadi, M. et al. (2015a). "GPS-Denied Relative Motion Estimation For Fixed-Wing UAV Using the Variational Pose Estimator". In: *54th IEEE Conference on Decision and Control (CDC)*, pp. 2152–2157.

Izadi, M. et al. (2015b). "Rigid Body Motion Estimation based on the Lagrange-d'Alembert Principle". In: *54th IEEE Conference on Decision and Control (CDC)*, pp. 3699–3704.

Izadi, M. et al. (2016). "The Variational Attitude Estimator in the Presence of Bias in Angular Velocity Measurements". In: *American Control Conference, 2016*, pp. 4065–4070.

Izadi, Maziar (2015). *Stable Estimation of Rigid Body Motion using Geometric Mechanics*. arXiv: 1510.05294 [math.OC].

Izadi, Maziar and Amit K. Sanyal (2014). "Rigid body attitude estimation based on the Lagrange-d'Alembert principle". In: *Automatica* 50.10, pp. 2570–2577.

— (2016). "Rigid body pose estimation based on the Lagrange-d'Alembert principle". In: *Automatica* 71, pp. 78–88.

Izadi, Maziar et al. (2015c). "Comparison of an Attitude Estimator based on the Lagrange-d'Alembert Principle with some State-of-the-Art Filters". In: *2015 IEEE International Conference on Robotics and Automation (ICRA)*.

Karthikeyan, K. P., H. Simha, and H. Priyadarshan (2016). "A linear discrete time controller for spacecraft attitude dynamics on Lie group". In: *2016 Indian Control Conference (ICC)*, pp. 165–169. DOI: 10.1109/INDIANCC.2016.7441123.

Khalil, Hassan K. (2001). *Nonlinear Systems (3rd Edition)*. Prentice Hall: Upper Saddle River, New Jersey.

Kushleyev, Aleksandr et al. (2013). "Towards a swarm of agile micro quadrotors". In: *Autonomous Robots* 35.4, pp. 287–300.

Lageman, Christian, Jochen Trumpf, and Robert Mahony (2010). "Gradient-like observers for invariant dynamics on a Lie group". In: *IEEE Transactions on Automatic Control* 55.2, pp. 367–377.

Lee, Daewon, H. Jin Kim, and Shankar Sastry (2009). "Feedback linearization vs. adaptive sliding mode control for a quadrotor helicopter". In: *International Journal of Control, Automation and Systems* 7, pp. 419–428.

Lee, H. et al. (2013). "Backstepping Control on SE(3) of a Micro Quadrotor for Stable Trajectory Tracking". In: *2013 IEEE International Conference on Systems, Man, and Cybernetics*, pp. 4522–4527. DOI: 10.1109/SMC.2013.769.

Lee, T., M. Leok, and N. H. McClamroch (2005). "A Lie group variational integrator for the attitude dynamics of a rigid body with applications to the 3D pendulum". In: *IEEE Conference on Control Applications*. IEEE, 962—967.

Lee, T., M. Leok, and N. H. McClamroch (2012). "Nonlinear robust tracking control of a quadrotor UAV on SE(3)". In: *2012 American Control Conference (ACC)*, pp. 4649–4654. DOI: 10.1109/ACC.2012.6315143.

Lee, Taeyoung, Melvin Leok, and N. Harris McClamroch (2010). "Geometric tracking control of a quadrotor UAV on SE(3)." In: *49th IEEE Conference on Decision and Control (CDC)*. IEEE, pp. 5420–5425.

Li, Fanbiao et al. (2015). "State estimation and sliding mode control for semi-Markovian jump systems with mismatched uncertainties". In: *Automatica* 51, pp. 385–393.

Mahony, Robert and Tarek Hamel (2017). "A geometric nonlinear observer for simultaneous localisation and mapping". In: *Decision and Control (CDC), 2017 IEEE 56th Annual Conference on*. IEEE, pp. 2408–2415.

Mahony, Robert, Tarek Hamel, and Jean-Michel Pflimlin (2008). "Nonlinear complementary filters on the special orthogonal group". In: *IEEE Transactions on automatic control* 53.5, pp. 1203–1218.

Markley, F Landis (2006). "Attitude filtering on SO(3)". In: *The Journal of the Astronautical Sciences* 54.3-4, pp. 391–413.

Markley, F.L. (1988). "Attitude determination using vector observations and the singular value decomposition". In: *The Journal of the Astronautical Sciences* 36.3, pp. 245–258.

Marsden, J. E. and M. West (2001). "Discrete mechanics and variational integrators". In: *Acta Numerica* 10, pp. 357–514.

Meier, Lorenz, Dominik Honegger, and Marc Pollefeys (2015). "PX4: A node-based multithreaded open source robotics framework for deeply embedded platforms". In: *2015 IEEE international conference on robotics and automation (ICRA)*. IEEE, pp. 6235–6240.

Mellinger, D. and V. Kumar (2011). "Minimum snap trajectory generation and control for quadrotors". In: *2011 IEEE International Conference on Robotics and Automation*, pp. 2520–2525. DOI: 10.1109/ICRA.2011.5980409.

Mellinger, Daniel, Nathan Michael, and Vijay Kumar (2012). "Trajectory generation and control for precise aggressive maneuvers with quadrotors". In: *The International Journal of Robotics Research* 31.5, pp. 664–674.

Milnor, J. (1963). *Morse theory*. Based on lecture notes by M. Spivak and R. Wells. Annals of Mathematics Studies, No. 51. Princeton, N.J.: Princeton University Press, pp. vi+153.

Milnor, J., M. Spivak, and R. Wells (1969). *Morse Theory*. Vol. 51. Princeton University Press. ISBN: 9780691080086. URL: http://www.jstor.org/stable/j.ctv3f8rb6.

Moutinho, A., M. Figueirôa, and J.R. Azinheira (2015). "Attitude Estimation in SO(3): A Comparative UAV Case Study". In: *Journal of Intelligent & Robotic Systems* 80, 375–384. DOI: 10.1007/s10846-014-0170-2.

Murray, Richard M. (2017). *A Mathematical Introduction to Robotic Manipulation*. CRC Press.

Nordkvist, Nikolaj and Amit K. Sanyal (2010). "A Lie Group Variational Integrator for Rigid Body Motion in SE(3) with Applications to Underwater Vehicle Dynamics". In: *49th IEEE Conference on Decision and Control (CDC)*. IEEE, pp. 5414–5419.

Prabhakaran, Sasi, Amit Sanyal, and Maziar Izadi (2017). "Integrated Guidance and Nonlinear Feedback Control of Underactuated Unmanned Aerial Vehicles in SE(3)". In:

AIAA Guidance, Navigation, and Control Conference, AIAA SciTech Forum. AIAA 2017-1044. DOI: 10.2514/6.2017-1044. URL: http://dx.doi.org/10.2514/6.2017-1044.

Prabhakaran, Sasi, Amit K. Sanyal, and Ehsan Samiei (2018). "Integrated Guidance and Feedback Control of Underactuated Robotics System in SE(3)". In: *Journal of Intelligent and Robotic Systems* 89.1-2, pp. 251–263.

Prabhakaran, Sasi, Amit K. Sanyal, and Rakesh R. Warier (2017). "Finite-time stable tracking control for a class of underactuated aerial vehicles in SE(3)". In: *2017 American Control Conference, ACC 2017, Seattle, WA, USA, May 24-26, 2017*, pp. 3926–3931. DOI: 10.23919/ACC.2017.7963556.

PX4-Dev, Team (2017). *Open Source for Drones-PX4 Pro Open Source Autopilot*. URL: https://px4.io/.

Rehbinder, Henrik and Bijoy K Ghosh (2003). "Pose estimation using line-based dynamic vision and inertial sensors". In: *IEEE Transactions on Automatic Control* 48.2, pp. 186–199.

Reis, J. et al. (2018). "Nonlinear Attitude Observer on SO(3) Based on Single Body-Vector Measurements". In: *2018 IEEE Conference on Control Technology and Applications (CCTA)*, pp. 1319–1324.

Rudin, Konrad et al. (2011). "A Robust Attitude Controller and its Application to Quadrotor Helicopters". In: *18th IFAC World Congress, Milano (Italy) August 28 - September 2*, pp. 10379–10384.

Samiei, Ehsan, Amit K. Sanyal, and Eric A. Butcher (Sept. 2017). "Stabilization of rigid body attitude motion with time-delayed feedback". English (US). In: *Aerospace Science and Technology* 68, pp. 509–517. ISSN: 1270-9638. DOI: 10.1016/j.ast.2017.06.004.

Sanyal, A.K. (2006). "Optimal Attitude Estimation and Filtering Without Using Local Coordinates, Part 1: Uncontrolled and Deterministic Attitude Dynamics". In: *American Control Conference, 2006*. IEEE. Minneapolis, MN, pp. 5734–5739.

Sanyal, Amit, Nikolaj Nordkvist, and Monique Chyba (2011). "An Almost Global Tracking Control Scheme for Maneuverable Autonomous Vehicles and its Discretization". In: vol. 56. 2. IEEE Transactions on Automatic Control, pp. 457 –462.

Sanyal, Amit K. (2019). "Nonlinearly Stable Real-Time Learning and Model-Free Control". In: *arXiv preprint arXiv:1907.10840*.

Sanyal, Amit K., J. Bohn, and A. M. Bloch (2013). "Almost global finite time stabilization of rigid body attitude dynamics". In: *52nd IEEE Conference on Decision and Control*, pp. 3261–3266. DOI: 10.1109/CDC.2013.6760381.

Sanyal, Amit K. and Jan Bohn (2015). "Finite-time stabilisation of simple mechanical systems using continuous feedback". In: *Int. J. Control* 88.4, pp. 783–791. DOI: 10.1080/00207179.2014.974675.

Sanyal, Amit K. and Nalin A. Chaturvedi (2008). "Almost global robust attitude tracking control of spacecraft in gravity". In: *AIAA Guidance, Navigation and Control Conference and Exhibit*. AIAA Guidance, Navigation and Control Conference and Exhibit. American Institute of Aeronautics and Astronautics Inc. DOI: 10.2514/6.2008-6979.

Sanyal, Amit K, Maziar Izadi, and Jan Bohn (2014). "An observer for rigid body motion with almost global finite-time convergence". In: *ASME 2014 Dynamic Systems and Control Conference*. American Society of Mechanical Engineers, V003T41A006–V003T41A006.

Sanyal, Amit K., Rakesh. R. Warier, and Reza Hamrah (2019). "Finite Time Stable Attitude and Angular Velocity Bias Estimation for Rigid Bodies With Unknown Dynamics". In: *2019 18th European Control Conference (ECC)*, pp. 4047–4052.

Shi, Xiao-Ning, Yong-An Zhang, and Di Zhou (2015). "A geometric approach for quadrotor trajectory tracking control". In: *International Journal of Control* 88.11, pp. 2217–2227. DOI: 10.1080/00207179.2015.1039593.

Shuster, Malcolm D (1990). "Kalman filtering of spacecraft attitude and the QUEST model". In: *Journal of the Astronautical Sciences* 38, pp. 377–393.

Tayebi, A, A Roberts, and A Benallegue (2011). "Inertial measurements based dynamic attitude estimation and velocity-free attitude stabilization". In: *American Control Conference (ACC), 2011*. IEEE, pp. 1027–1032.

Varadarajan, V.S (1984). *Lie Groups, Lie Algebras, and Their Representations*.

Vasconcelos, José Fernandes et al. (2010). "A nonlinear position and attitude observer on SE (3) using landmark measurements". In: *Systems & Control Letters* 59.3, pp. 155–166.

Wahba, Grace (1965). "A least squares estimate of satellite attitude". In: *SIAM review* 7.3, pp. 409–409.

Wang, Lifeng et al. (2013). "Trajectory Tracking of Quadrotor Aerial Robot Using Improved Dynamic Inversion Method". In: *Intelligent Control and Automation* 4.4, pp. 343–348. DOI: 10.4236/ica.2013.44040.

Warier, Rakesh R., Amit K. Sanyal, and Sasi Prabhakaran (2019). "Finite time stable attitude estimation of rigid bodies with unknown dynamics". In: *Asian Journal of Control* 0.0. DOI: 10.1002/asjc.2089.

Xiang, Xiao jia et al. (2015). "Geometric Collocation Method on SO(3) with Application to Optimal Attitude Control of a 3D Rotating Rigid Body". In: *Mathematical Problems in Engineering* 2015, pp. 1–14.

Yan, Zheping et al. (2015). "Globally finite-time stable tracking control of underactuated UUVs". In: *Ocean Engineering* 107, pp. 132–146.

Zamani, M. (Mar. 2013). "Deterministic Attitude and Pose Filtering, an Embedded Lie Groups Approach". PhD thesis. Canberra, Australia: Australian National University.

Zamani, M., J. Trumpf, and R. Mahony (2011). "Near-Optimal Deterministic Filtering on the Rotation Group". In: *IEEE Transactions on Automatic Control* 56.6, pp. 1411–1414. ISSN: 0018-9286. DOI: 10.1109/TAC.2011.2109436.

VITA

Reza Hamrah is a Ph.D. Candidate in the Department of Mechanical and Aerospace Engineering at Syracuse University, where he has been awarded with the Research Excellence Doctoral Funding (REDF) Fellowship for 2019-20 academic year. He received his Bachelor of Science from MUT University of Technology in 2009, and got his Master of Science in Aerospace Engineering from Shahid Beheshti University in 2012. His research focuses on developing theories on discrete-time stable geometric controllers and observers for Autonomous Unmanned Vehicles and Robotic Systems. During PhD, he has been conducting research on dynamics modeling, control and estimation of Autonomous Aerial Robots and Unmanned Vehicles.